POLITECNICO
MILANO 1863

SCUOLA DI INGEGNERIA INDUSTRIALE E DELL'INFORMAZIONE

Laurea Magistrale in Ingegneria Meccanica

WIND TURBINE PERFORMANCE AND FLOW FIELD MEASUREMENTS IN A MODELED URBAN ENVIRONMENT

Supervisor: Prof. Vincenzo Dossena

ROBERTO BOLIS

928087

Academic year 2019/20

AKNOWLEDGMENTS

Poiché la gratitudine è la più grande di tutte le virtù, giunti a questo punto dei ringraziamenti sono doverosi.

Il primo e più grande ringraziamento va alla mia famiglia; ai miei genitori, che mi hanno supportato economicamente ed emotivamente durante tutto questo viaggio, e ai miei fratelli, che mi sono stati sempre vicini.

Ringrazio mia madre per essere stata da sempre la mia più grande guida in tutto e per tutto, soprattutto nei momenti di difficoltà, per essere stata sempre dalla mia parte ed aver guidato le mie scelte.

Ringrazio mio padre per avere cercato di trasmettermi tutta la sua conoscenza e tutte le esperienze di vita. Per avermi trasmesso la pragmaticità e la curiosità che mi porterò sempre con me.

Ringrazio mia sorella per essere mia sorella, per tutti i momenti condivisi che mi hanno fatto capire l'importanza e la potenza del legame fraterno. Ma più di ogni altra cosa ti ringrazio per avermi aperto il cancello tutte le volte che ho scordato il telecomando, so che la tentazione di lasciarmi tutta la notte fuori casa è stata grande.

Ringrazio mio fratello per essere da sempre un esempio e per essere sempre stato disposto ad aiutarmi in ogni momento, soprattutto quando la vale non mi apriva il cancello. Ti ringrazio per tutti confronti avuti nei più disparati argomenti.

Ringrazio i miei nonni, quelli che ci sono e quelli che purtroppo non ci sono più, per avermi cresciuto e per avermi trasmesso tanto come persone. Ringrazio mio nonno Franco, per avermi insegnato i valori di un uomo e per avermi trasmesso la passione per il Napoli. Ringrazio mia nonna Velia, per tutta la saggezza trasmessa e per avermi fatto sentire quella piccola parte partenopea dentro di me. Ringrazio mia nonna Luisa, per essere riuscita a farmi apprezzare il caratteraccio del nonno con la sua estrema gentilezza. Ringrazio mio nonno Dario, per avermi fatto assaggiare la bellezza e la soddisfazione dei lavori pratici e dell'arte di arrangiarsi.

Ringrazio Gio(vanni) per avermi liberato di mia sorella permettendomi una maggiore concentrazione, per tutti i consigli guida ricevuti nei più disparati campi e per tutti i confronti fatti e per quelli che faremo.

Ringrazio Irene per non avermi disturbato troppo durante quei momenti di baby-brother e per avermi rallegrato i pomeriggi con i suoi discorsi interminabili. Sono stato tentato di aggiungerti come co-autore ma quando te l'ho chiesto mi hai risposto "bobo", l'ho preso come un "no".

Ringrazio Vanessa per avermi fatto compagnia durante i pomeriggi di studio.

Ringrazio la Professoressa Bracchi e il Professor Dossena per avermi dato la possibilità di vivere questa esperienza all'estero, mi ha dato molto e la porterò sempre con me. Un ringraziamento doveroso anche a Yannick che mi ha guidato per tutta la durata della tesi e dal quale ho imparato e condiviso tanto. Grazie perché il confronto aperto e costruttivo nei più disparati campi mi ha permesso di crescere più di quanto abbia fatto in qualsiasi corso.

Ringrazio i miei zii, Ste e Gio(rgia), per essere stati sempre un supporto e aver sempre visto più in là di quello che mostravo. Per avermi sostenuto nei momenti critici e per avermi sempre offerto una cena per discuterne.

Ringrazio mia Zia Raffi per essersi sempre interessata ai miei progressi e ai miei stalli universitari e per avermi sempre dato supporto prima degli esami, soprattutto domiciliare.

Ringrazio mio cugino Enrico, per essere stato come un fratello minore per me da cui, come fratello maggiore, sono cresciuto tanto. Ringrazio mia cugina Vera per la sua presenza e il suo supporto morale.

Ringrazio Anna per aver accettato quella colazione, quella cena e tutti gli appuntamenti successivi, nonostante le location discutibili e una pandemia globale. Sei stata la mia motivazione per tutto il tempo.

Ringrazio Gian per tutto, i momenti di studi, i momenti di svago, i momenti di chill in questi 10 anni e quella convivenza a Foppolo durante il lockdown, essenziale per finire la tesi. Alla fine, il surströmming toccherà mangiarlo a entrambi. Là.

Ringrazio Dilu senza il quale non sarei il cors, rimarrò sempre convinto che tu sia una mente rubata all'ingegneria. Ti ringrazio per tutte le serate di svago e di confronto.

Ringrazio anche te che stai leggendo i ringraziamenti sperando di essere nominato, se arrivato in fondo non ti sei trovato…..scusami.

Ringrazio Ben per le lunghe conversazioni e lo scambio di opinioni sempre stimolante, per tutte le volte che hai appoggiato o che hai criticato le mie idee. Troveremo una grande idea da realizzare prima o poi.

Ringrazio michi e asia per tutti i momenti incredibili condivisi che due righe nei ringraziamenti in una tesi non possono descrivere. Siete da sempre delle grandi amiche.

Ringrazio Rudi e Giulia per tutti i viaggi e i momenti crinch vissuti. Ringrazio Kenyo, Iava, Vero, Bertins, Eli, Russo per avermi aiutato a smorzare la routine serrata del poli. Un ringraziamento particolare a Pippo, Ale e Pasqu per essere da sempre degli amici su cui contare.

Ringrazio Il santaLux perché……mens sana in corpore sano.

Non ringrazio il mio computer che ha sempre trovato il modo di mettermi in difficoltà, spesso riuscendoci.

Un abbraccio.

SOMMARIO

L’energia eolica può essere considerata una delle migliori soluzioni attuali per un’economia sostenibile. Le turbine eoliche solo una tecnologia all’avanguardia, tuttavia altri mercati legati all’eolico stanno emergendo, come l’offshore e l’ambiente urbano. L’ambiente cittadino, che è argomento di questa tesi, rispetto alle condizioni rurali in cui sono generalmente installate le turbine eoliche, è caratterizzato da una bassa velocità media del vento, da un’alta turbolenza e da forti variazioni del vento. Tutti questi aspetti si traducono in un flusso molto complesso che deve essere trattato caso per caso. L’ambiente cittadino non è adatto a turbine di grand dimensioni, è invece più interessante studiare la possibilità di installazioni di turbine eoliche di piccole dimensioni (SWT). L’interesse nello sviluppo di questo mercato è legato all’eliminazione di costi e perdite dovute alla distribuzione dell’elettricità, poiché la potenza viene prodotta direttamente nel luogo di consumo.

Questa tesi è focalizzata sulla comprensione di come il flusso in ambiente urbano sia influenzato dalla presenza di una turbina eolica montata sopra un edificio e di come varino le prestazioni della turbina in diverse posizioni. Gli esperimenti sono stati eseguiti nella galleria del vento e si dividono in due misurazioni principali, la caratterizzazione del flusso tramite il metodo di PIV e la misura della potenza meccanica, ottenuta dalle misure della velocità di rotazione e della coppia. Mentre la velocità di rotazione è calcolata grazie a un fototransistor post vicino all’albero della turbina, la coppia meccanica è derivata dalla misura della corrente elettrica generata da un motore a corrente continua accoppiato assialmente all’albero della turbina. La turbina è caratterizzata dalla curva caratteristica ottenuta con la regolazione della velocità di rotazione tramite l’utilizzo di un MOSFET. L’ambiente urbano è semplificato con due cubi di 10 cm di altezza (H) distanziati di 2 H e posizionati in linea rispetto alla direzione del flusso. La turbina è montata sulla facciata superiore in tre posizioni differenti (anteriore, centrale, posteriore) per ciascun cubo.

Il PIV consiste nel calcolo dei vettori di velocità sulla base della correlazione di due immagini acquisite con fotocamere ad alta risoluzione. Un laser viene emesso da sopra la galleria del vento e contemporaneamente due fotocamere scattano due foto dal lato della galleria. I due fotogrammi vengono scattati con un intervallo molto breve (μs) e nella galleria vengono aggiunte delle particelle micrometriche di fumo che servono a migliorare la correlazione dei due fotogrammi. Con questo metodo si ottiene il campo di moto della velocità, da cui si calcolano poi successivamente atre grandezze, come il contenuto di energia cinetica legata alla turbolenza (TKE) e la vorticità. Per avere una chiara comprensione di un ambiente così complesso come quello urbano, è importante utilizzare diversi metodi come la simulazione tramite CFD, gli esperimenti in galleria del vento, le misurazioni

dirette o algoritmi statistici. Questo spiega l'importanza di ottenere sia le misurazioni delle prestazioni della turbina, sia la caratterizzazione del campo di moto tramite PIV.

La turbina utilizzata negli esperimenti è una turbina ad asse verticale (VAWT) stampata 3D con un design Savonius, caratterizzato da un principio di funzionamento a Drag. La turbina è posizionata ha un'altezza di $0.3\ H$ e un diametro di $0.4\ H$ ed è elevata rispetto alla superficie del cubo di $0.1\ H$. Poiché la presenza della turbina influisce sulle condizioni del campo di moto, è stata eseguita una prima misurazione tramite PIV dei cubi senza la turbina per poter avere un campo di moto come riferimento per gli esperimenti seguenti. Questa configurazione viene utilizzata quindi come confronto per gli altri casi.

Il campo di moto di due cubi in linea è caratterizzato da una zona di "stagnazione" davanti al primo cubo, un vortice a forma di ferro di cavallo si genera tra i due cubi e uno più piccolo dietro al secondo cubo. Sopra il cubo sopravento si crea una zona di separazione a partire dallo spigolo frontale del primo cubo; questa regione è caratterizzata da un flusso in direzione contraria e da un alto livello di turbolenza. Sopra questa bolla di separazione si manifesta una zona di accelerazione del flusso dove la velocità aumenta del 10% rispetto alla velocità indisturbata.

Per la turbina posizionata sul cubo a monte, i risultati mostrano che la posizione anteriore e quella centrale sono entrambe valide. Mentre le immagini del campo di moto ottenute dal PIV suggerirebbe che la posizione d'avanti è migliore poiché la turbina non è completamente immersa nella bolla di ricircolo sopra descritta, la misura della potenza rivela che la posizione centrale è altrettanto efficiente. Ciò è dovuto al ritardo nella generazione della zona di ricircolo dovuto al blockage effect causato dalla turbina, questo ritardo si traduce in una minore turbolenza del flusso incidente sul rotore.

Per la turbina posizionata sul cubo a valle, sia il PIV che la misurazione della potenza mostrano che la posizione migliore è la più distante dal bordo anteriore del cubo, cioè la posizione posteriore. Lì, l'influenza del vortice generato tra i due cubi può essere considerata trascurabile e la turbina estrae la massima potenza. Le altre posizioni (frontale e centrale) possono essere considerate ancora nella scia del cubo a monte e quindi le prestazioni ne risentono.

Possiamo quindi affermare che in generale per un edificio, indipendentemente dalla posizione rispetto al vento, la turbina posizionata al centro può dare buoni risultati in termini di produzione di energia. Con indicazioni più precise la turbina eolica può essere posizionata sul bordo frontale se l'edificio è direttamente investito dal vento, altrimenti può essere posizionata vicino al bordo posteriore se l'edificio è in scia di un'altra costruzione a monte. Studi futuri si possono concentrare sull'uso di turbine differenti nella forma o nelle posizioni di installazione o nello sviluppo di un campo di moto tridimensionale.

SUMMARY

Wind energy is one of the best renewable sources at the present. While the exploitation of wind in open-terrain condition is a well-known technology, other markets are growing up, such as the offshore and the urban location. The urban environment, which is the argument of this thesis, in comparison with the open terrain conditions is characterized by a low mean wind speed, a high turbulence and strong fluctuations. All these aspects result in a complex flow field which is case by case dependent. Built environment is not suited for large turbines, instead it is more interesting to study the possible installation of Small Wind Turbine (SWT). The development of this market is attractive because it will delete all the drawbacks related to the distribution of electricity since the power is extracted next to the devices to supply.

This thesis focuses the attention on the understanding of how flow field in urban environment is affected by the presence of a wind turbine mounted on the top of buildings and how the turbine performances change in different positions. The experiments were performed in a wind tunnel and it is divided into two main measurements, the velocity vector map, which is obtained by means of the PIV method and the mechanical power, calculated by the measures of the rotational speed and of the torque. While the rotational speed is simply obtained with a photo-transistor located next to the turbine shaft, the mechanical torque is derived by the measurement of the current generated by a DC generator coupled axially to the turbine shaft. To obtain the power characteristic curve of the turbine a speed regulation is performed by means of a MOSFET. The urban environment is modelled with two cubes of 10 cm height (H) in tandem configuration respect the streamwise direction with a distance of $2\ H$. The turbine was mounted on the top facade in three different locations (front, centre, back) for each cube.

The PIV measurements consist in the calculation of velocity vectors based on the correlation of two images acquired with high resolution cameras. A laser is shot from above the wind tunnel and simultaneously two cameras takes the picture of a target area from the side of the tunnel. The two frames are taken with a very short time gap (μs) and inside the flow are added lots of micro particles of smoke, which helps the correlation of the two images. By this method, the velocity vector map is obtained and other information are then calculated in the post process, such as the Turbulent Kinetic Energy (TKE) content and the vorticity presence. To have a clear understanding of such a complex environment like the urban one, is important to adopt different methodology such as CFD simulation, wind tunnel experiments, direct measurements or statistical approach. That's why the measurements of the turbine performances and the flow field characterization by means of PIV technology are both essential.

The turbine adopted in the experiments was a 3D printed Vertical Axis Wind Turbine (VAWT) with a Savonius design, which is characterized by a drag-driven working principle. It was elevated of $0.1\,H$ from the top of the cube and the rotor had a height of $0.3\,H$ and a diameter of $0.4\,H$. As the turbine presence affects the flow field, a first PIV measurement was made without the turbine to have a reference flow field caused by the only presence of the cubes, this has been used as comparison for all the other cases.

The flow field of two cubes in tandem configuration is characterized by a stagnation zone in front of the upstream cube, a large horseshoe vortex in the intra-obstacle region and a smaller one behind the downstream cube. On the top of the first cube a big recirculation region is generated starting from the leading edge; this region is characterized by a reverse wind speed and a high turbulence level. Above this recirculation bubble a region of over-speed occurs, where the wind velocity reaches the 10% of increase compared to the freestream value.

For the turbine located on the upstream cube the results show that the front and the centre positions are both suitable for the installation. While the images of the velocity vector map obtained by the PIV would suggest that the front location is the better because the turbine is not fully submersed in the recirculation bubble above described, the power measurements reveal a comparable power extraction of the centre location. This is due to the delay in the recirculation zone generation caused by the blockage effect induced by the turbine, this delay results in a lower turbulence of the inflow condition of the rotor.

For the turbine mounted on the top of the downstream cube both the PIV and the power measurement show that the best location is the farther from the leading edge of the cube, thus the back position. There, the influence of the inter-cubes horseshoe vortex is considerably negligible and the turbine has the highest power output. The other locations (centre and front) can be considered still in the wake of the upstream cube and thus, the performances are affected.

We can state that for a general building independently if it is in windward or leeward condition, the turbine placed in the centre location can give good result in terms of power production. With a more specific indication the wind turbine can be placed on the leading edge if the building faces directly the wind flow, otherwise the turbine can be located next to the trailing edge if the building is in the wake of an upstream one. Further studies can be focused on the adoption of different types of turbine in shape or locations or in the development of a three-dimensional velocity vector map.

LIST OF ABBREVIATIONS

SYMBOL	MEANING	UNIT	SYMBOL	MEANING	UNIT
δ	Boundary layer thickness	-	K_M	Torque constant	mV/RPM
η	Efficiency	%	K_E	Speed constant	mNm/A
λ	Speed ratio	-	KWh	Kilo Watt hour	
ξ	vorticity	$1/s^2$	LCOE	Levelized Cost of Energy	-
ρ	Density	Kg/m^3	$\dot{m}$	Mass flow rate	Kg/s
σ_u	Longitudinal standard deviation	m/s	MRS	Multi-Rotor System	
ω	Rotational speed	RPM	O&M	Operational and Maintenance	
a	Interference factor	-	ODGV	Omni-directional guide vane	
ABL	Atmospheric Boundary Layer		p	Pressure	Pa
AC	Alternating Current		P	Power	W
AWE	Airborne Wind Energy		PAGV	Power-augmented guide vane	
BAWT	Building Augmented WT		pc	percentile	
BL	Boundary Layer		PIV	Particle Image Velocimetry	
BMWT	Building Mounted WT		Q	Torque	mNm
BWT	Building WT		R_m	Internal resistance	Ω
C_P	Power coefficient	-	Re	Reynolds number	-
C_m	Torque coefficient	-	Re_h	Cube height Reynolds number	-
DAWT	Diffuser Augmented WT		T	Acquisition time	s
DC	Direct Current		TKE	Turbulent Kinetic Energy	m/s^2
E_k	Kinetic Energy	J	TSR	Tip Speed Ratio	-
emf	Electro-magnetic field		SWT	Small Wind Turbine	
FOWT	Floating Offshore WT		U	Mean wind speed	m/s
GW	Giga Watt		u'	Wind speed fluctuation	m/s
GHG	Green House Gases		UBL	Urban Boundary Layer	
H	Cube height	cm	UCL	Urban Canopy Layer	
HAWT	Horizontal-axis Wind Turbine		V	Voltage	
I	Current	A	V_x	Horizontal velocity (streamwise)	m/s
I_u	Turbulence intensity	%	V_y	Vertical velocity	m/s
IA	Interrogation Area		VAWT	Vertical-axis Wind Turbine	
IEC	Intl. Electrotechnical Commission		WT	Wind Turbine	
K	MOSFET parameter	-	z_0	Aerodynamic roughness height	m

TABLE OF CONTENTS

1 INTRODUCTION

1.1 BACKGROUND

1.1.1 STORY

By the first decade of 21st century, wind power has increased its relevance among the renewable sources. Main advantages of wind energy compared with other renewable sources are its high availability, the wide distribution, the easy implementation, and the continuous growth. But wind energy is not something new, this source has been exploited for thousands year for several purposes such as agricultural operation, propulsion and pumping system.

Wind is a phenomenon due to a pressure gradient of air generated by a difference in temperature, this phenomenon is responsible for most of the environment around us and it was the base for all the navigation technique of the last thousands of years. The wind has been always present in the world and thus, no one can know exactly when it has started to be exploited. However, it can be supposed that sailing was one of the first use. By all these considerations, wind can be considered at the base of the human being development together with essential sources such as water, air, and fire.

In the last centuries, air has been more and more used on the land by means of windmills. Firstly, just moving machine or pumping water, then starting to produce electricity. The first appearance of a wind turbine is in Persia-Afghan around 200 b.c. [1], where a vertical axis wind turbine was used to turn grindstone for milling the grain into flour. Two thousand years later, the first case of a practical large-scale wind turbine was built for electricity production by an American scientist, Charles Brush, in 1888 [2]. From that first step, passing through well-known. Netherlands windmills, thanks to the big development in Europe by Danish and in U.S., the first case of three-blade propeller appeared in 1927 by two American farmers. Later, wind turbine's technologies were mainly developed in the old world making of Europe the cradle of wind turbines. The leader of the development of the modern wind turbines was Denmark, whereas U.S. based the design of blades on the aerospace industry, Danes exploited their knowledge of agricultural sector to generate the machines which are the foundation of the turbines we know today.

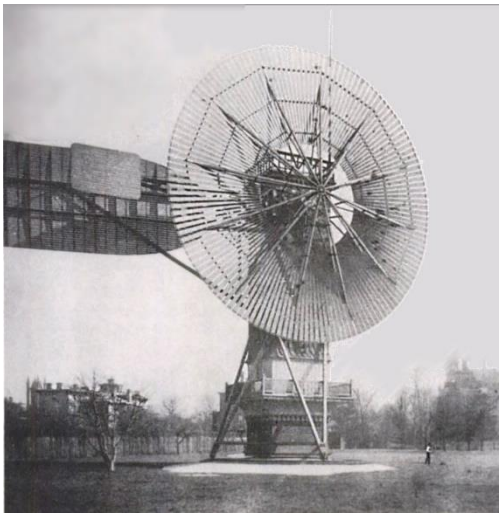

Fig. 1.1 First case of wind turbine for electricity production by Charles Brush, 1888

1.1.2 WIND ENERGY MARKET

In recent years, all over the world governments are passing through an energy transition trying to become independent by fossil fuel as main source of power production, as the scientific community concurs in considering the global warming a reality. According to Intergovernmental Panel on Climate Change (IPCC), human activities are responsible for an increase of the average temperature of 1.0 °C respect the pre-industrial period and the warming will increase of 1.5 °C more in about 2 or 3 decades [3]. International Renewable Energy Agency (IRENA) in their analysis concluded that renewable energy and energy efficiency, supported by a deep electrification, can provide over 90% of reduction in CO_2 emissions energy-related [4]. It is a widespread understanding that transition of power sources is leaded by renewables, precisely by solar and wind energy, thanks to their huge technological development and to the decrease of production costs. Renewable energies are considered main weapon against global warming and wind power is one of the best hope for a future clean energy because clean, economically competitive, socially justifiable, widely distributed, not dangerous, well-known and with a continuously developing technology. The outlook is to increase the wind power generation till 18% of the global power production by 2050 according to the international Energy Agency (IEA) [5]. For the 11th consecutive year Asia, leaded by China, was the largest market for new installation in wind power production, representing more than 50% of added capacity, much more compared to Europe (24%) and North America (16%) (Fig.1.2).

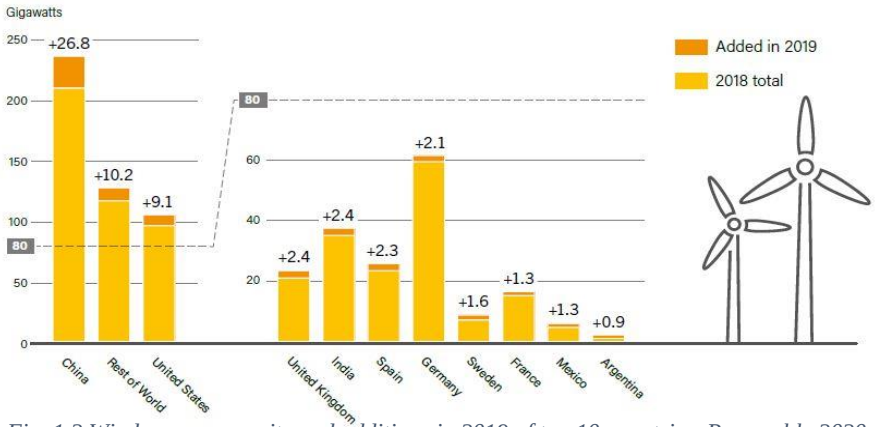

Fig. 1.2 Wind power capacity and additions in 2019 of top 10 countries, Renewable 2020 Global Status Report, REN21

According to the global wind report 2020 drawn up by Global Wind Energy Council (GWEC) [6], in 2019 new installations increase of 7% compared to the previous year, bringing to an overall wind power capacity of 645 GW (Fig.1.3).

Of the 60.4 GW of new installed capacity only the 10% is related to off-shore turbines, but the exploitation of this technology is increasing year by year. In 2019 offshore power production has increased of more than 20% respect the previous year bringing the total capacity to 29 GW [7]. According to the estimation made by GWEC (in pre-covid conditions) the offshore industries is reputed to increase of 4% per year in the next 5 years, bringing new off-shore installation in 2024 to reach 15 GW (Fig.1.3).

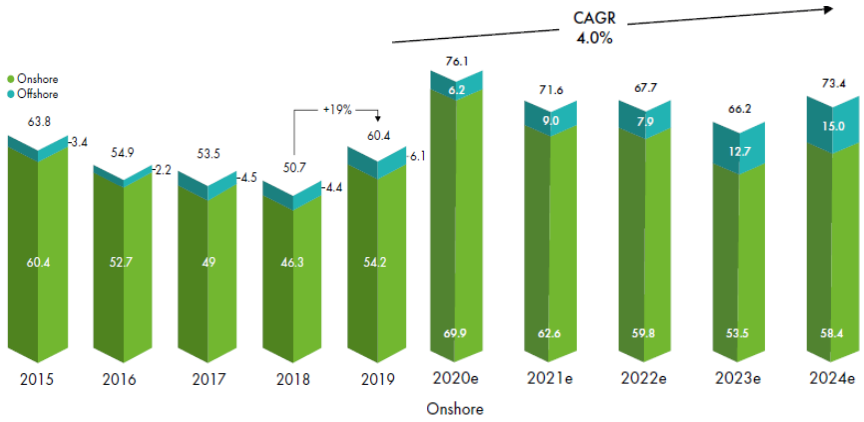

Fig. 1.3 Global new wind installation, GWEC, Global Wind Report 2020

The goal of lots of governments is to provide 20% of the global electricity demand by 2030, corresponding to 2.1 TW [6]. This forecast must be supported by many factors, such as the consistently decrease of wind system cost to make this market more and more competitive, the continuous advance in technologies, the new techniques to reach better and better performances and the development of new battery storage technologies. Promoting research and development in renewable energy has become for many countries one of the best strategies to reach the goal of being energetically independent and reducing greenhouse gases (GHG) emissions.

At present almost 80% of worldwide population has access to electricity and according to World Energy Council US, Canada and Australia are the main countries for annual household electrical consumption. Forecasts suggest us that both population and energy demand are going to increase in the following years, due to the increase in urbanization and to the development of third-world countries. To compensate this trend in the demand is required to increase power installation, starting from renewable energies [8]. According to Vargas et al. [9], wind energy production is increasing of 10% each year thanks to the huge investments supported by China government in the last years and by Europa and US in the previous decade. Despite the wind installed power is increasing each year, the on-shore turbine is still the main contribution in the new installation and the off-shore market is still below the 10% of the yearly installed capacity. The installation is estimated to have a huge increase thanks to the decrease of costs for wind turbines construction, to the new studies and to huge potential of offshore market. In the last decade, the cost of production systems for wind and solar energy was consistently decreased thanks to the development of new technologies and to the increase of this

market, which brought to a massive production of these two systems. Wind turbines cost (€/MWh) has fallen by nearly 1/3 since 2009, while PV has decreased of more than 85% (Fig.1.4) [10]. This reduction is an important factor compared with the steady cost of conventional power plant base on fossil fuel or nuclear energy, thus the pursuit of this trend can bring to have a strong advantage between renewable energies cost and other sources [6]. The falling costs per KWh of wind systems, both on-shore and off-shore, have made wind energy more competitive with conventional fossil fuel power plant, allowing the growth of wind market all over the world even without any financial support.

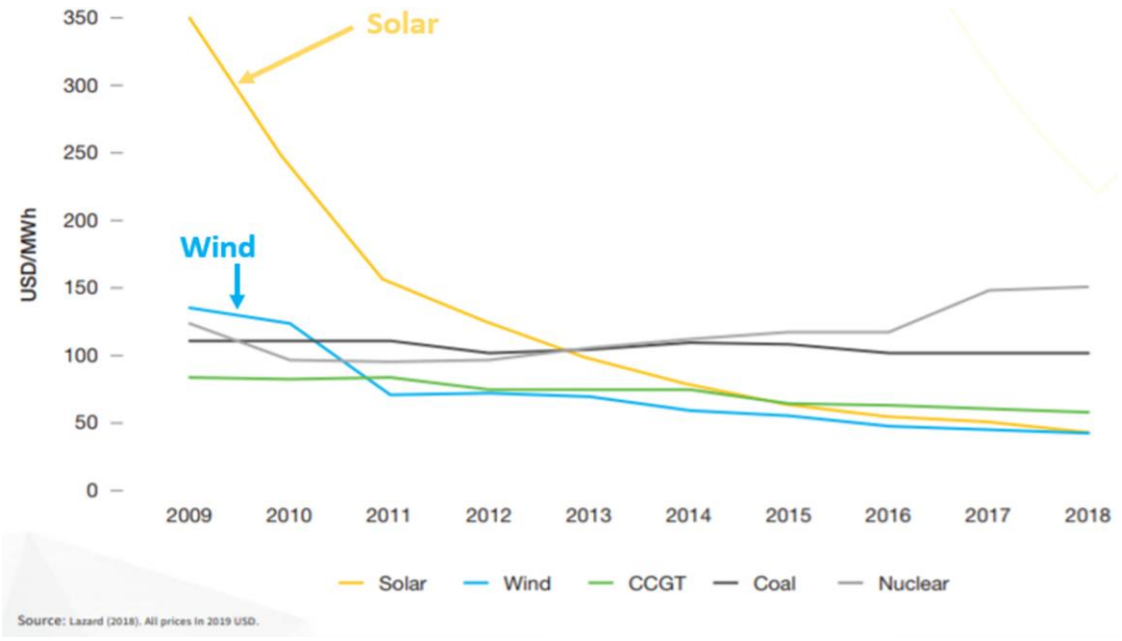

Fig. 1.4 Wind electricity generation cost in comparison with other power sources, get-invest.eu

1.2 FUTURE PROGRESSES

1.2.1 FUTURE DEVELOPMENTS

Despite the increase in the last decades of renewable energy power production, the global energy system continues to be mainly dependent on fossil fuels, with oil, natural gas and coal accounting in the world energy supply for 36%, 27% and 17% respectively [5].

Accordingly, carbon dioxide (CO_2), which are emissions associated with the use of fossil fuel in combustion, represent the largest source of greenhouse gas (GHG) emissions. Therefore a pressure over the implementation and discover of new low carbon emission technologies and renewable sources has grown. The exhaust products of combustion of fossil fuel, carbon dioxide (CO_2) methane (CH_4) and nitrous oxide (NO_x), are main cause of the environmental and public health damage, on the other hand, wind energy is characterized by very low emission. With increasing in performances of wind turbines, the impact of cost and production on installation has continuously decreased. The future of this market is going toward a larger rotor, taller towers, advanced materials, more performant monitoring techniques and more efficient transmission system [11].

While Horizontal-axis Wind Turbines (HAWT) are widespread and with an amply industrialized technology, there are other wind markets still under development. Great attention is growing around off-shore and urban locations. Different motivations push the interest in these two technologies, off-shore wind energy is promising because of the large space available and the favourable wind conditions, such as high mean wind speed, high load factor and low wind shear. Wind turbines offshore are already widespread, but the major limitation is imposed by the need of a foundation or mooring system in case of most advanced technologies. However, many researchers studied the possibility of a whole floating system, which would allow installation of turbines in very deep-sea location and will delete the cost of anchorage system. On the other hand, instead, urban environment is a good hope due to the proximity of the production to the consumers. Despite the low mean wind speed in urban areas, the interaction of flow with obstacles generates high-speed zone that can be harvested by a possible wind turbine installation. In addition to these two categories, many other technologies are growing.

Airborne Wind Energy (AWE) is a modern technology under development which harvest high wind speed at high altitudes by means of a light weight and a lift-support device, all the system is tethered to the ground (fig.1.5a). This technology has several advantages compared to the common wind turbines, first it avoids the construction of the tower, which results in lower cost and less material consumption [12]. In additions working at higher altitudes the wind turbine harness stronger and

steadier winds, that means more wind energy available. The main feature to choose for this technology is the location of the generator, ground-gen concept perform the conversion from mechanical to electrical power at the ground, by contrast fly-gen converts the power in the air, onboard the airborne [13]. Although this technology is not even fully developed, a future scenario sees an installation of AWEs in off-shore conditions. Compared to conventional off-shore wind turbines, the tethered AWE system needs only to withstand tension instead of bending loads of common offshore wind turbines [13].

Another technology under development is multi-rotor wind turbine, it consists in the substitution of a large single rotor with multiple smaller rotors. This configuration improve efficiency and reduce overall load, it allows also to have high power system (up to 20MW), which is way more than any common wind turbine. Scaling up is seen as key factor in power production, thus can be important to have a so high-power production despite the number of rotors.

MRS can have several advantages starting from the overall cost reduction due to the shared construction, but it is also less dependent by failure, every single rotor is standardised and can be easily substituted without affecting efficiency of other rotors. The development of MSR must be studied in deep to have a clear understanding of the concepts behind. At present, most promising European project about is a 900 kW four-rotor turbine developed by Vestas (fig.1.5b).

(a) **(b)**

Fig. 1.5 (a) First example of Ariborne wind system (AWS) with lifting balloon configuration by Altaeros, (b) Multi-Rotor System (MRS) by Vestas

1.2.2 OFFSHORE WIND ENERGY

In the last decades governments all over the world try to push a conversion toward a more clean energy in order to reduce CO_2 emissions and other pollutants, which increase the global warming and have a significant incidence in the population health. International protocols, such as Kyoto in 1998 or Paris agrrement in 2015, as well as regional protocols, as the European 2030 climate&energy framework, are trying to mitigate the climate change effect. In these regards, to achieve the target quota of renewable power production or the desidered decrement of GHG emissions, offshore wind energy appears to be a good option for some countries, thanks mainly to technological advance and wind turbine industry growth. To sustain the increase of energy demand, due to the increment of world population and to the third world countries modernisation, the global development of sustainable energy sector is a key factor to lie on the targets of those protocols. Therefore it is important to focus the attention to the renewable energy source with higher potentiality. Off-shore wind energy at present can be considered in a continuous progressive state and is expected to grow faster in the next years making this technology more and more relevant.

The social advantage of offshore location is the almost complete absent visual and noise impact due to the natural distance to the shore. Nevertheless, the influence on marine ecosyste must still be analyzed deeply to understand the impact and the consequences. The evolution of mega offshore wind projects will lead to a revolution in current energy production scenario since they are much more competitive than common wind turbines, despite the important capital investment, which is appoximately 50% higher than on-shore counterpart [11]. According to BNEF [14], the global offshore wind average LCOE (levelized cost of energy) has dropped of more than 65% and this trend is expected to continue.

As said, Wind energy represents at the moment one of the most promising hopes among the renewable sources and off-shore technology can drag this hope thanks to its favourable characteristics. Compared to on-shore turbines, off-shore location have high wind avaiability, high social acceptability, high load factor, due to a more constant mean wind speed and lower fluctuations. Off-shore wind turbines are already a common reality but the major limitation is imposed by the need of catenary or tensioned mooring system to keep the machines in position. Nevertheless, it is evident the need to enhance wind resource far offshore where water depth is high, this requires the development of floatinf support structure to make the installation in deep water economicaly viable. At present, in water with depth higher than 50 meters, bottom fixed support structures is not a economically competitive solution, as mooring system can represent a significant percentage on the whole system cost. This technology is instead used in the off-shore oil&gas industry where it is not a significant issue because the cost of anchorage system is marginal compared to the overall cost and to the profit margin. For floating off-

shore wind turbines (FOWTs), where the achievement of a cost effective and profitable system is one of the main purpose, the cost of mooring system must be taken into account [15].

In the last years the development of floating structure for FOWT has come up, this could bring a big innovation in wind energy increasing the available locations in sea indipendent by the water depth. This technology will result in a more expensive support system, but it will economize on the mooring system [16]. Alternate current trasmission lines are preferred to operate in off-shore park due to the low cost of transformation and to the use of more compact converter stations, nevertheless, with large distance, in case of off-shore farm far from coast, energy losses caused by shore disturbance become a critical issue. Direct current trasmission becomes more efficient at distance larger than 80 Km, even considering larger converter stations and higher installation costs. To overcome this problem, one recent solution can involv the work of off-shore wind plant in synergy with other plant to convert renewable power in chemical energy in-situ [16].

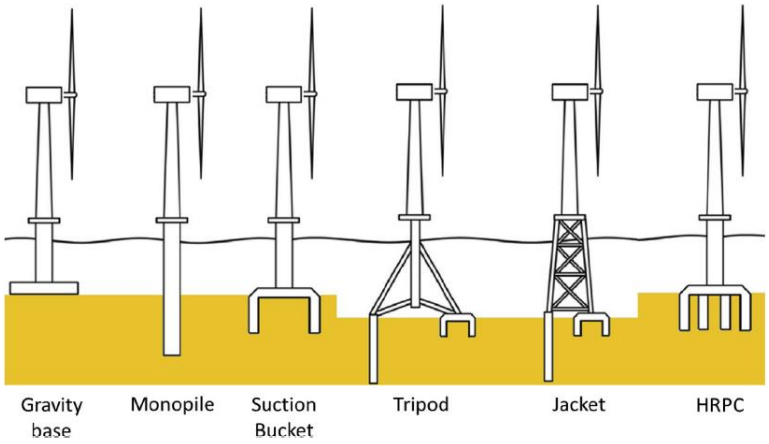

Fig. 1.6 Offshore wind turbine foundation types [11]

Crivellari and Cozzani [17] analyzed the development of this solution focusing in the comparison between power to gas (P2G) system and power to liquid (P2L) system. Caglayan et al. [18] made a techno-economic analysis of off-shore wind energy market along Europe maritime boundaries with a set of socio-technical constrains, their study revealed that 31.5% of areas within the European maritime zone are available for offshore plant installations. The analysis also revealed that it is not convinient to keep the same turbine design everywhere, but it is favourable to use rotor design based on specific site conditions. As expected, in zones with relative low mean wind speed is preferred a machine with low specific power; on the other hand, larger rotors are more suitable for locations with high specific wind power. This result depends on the fact that higher cost related to large turbine rotors is not balanced in low wind speed zones by the only increase of full load hours.

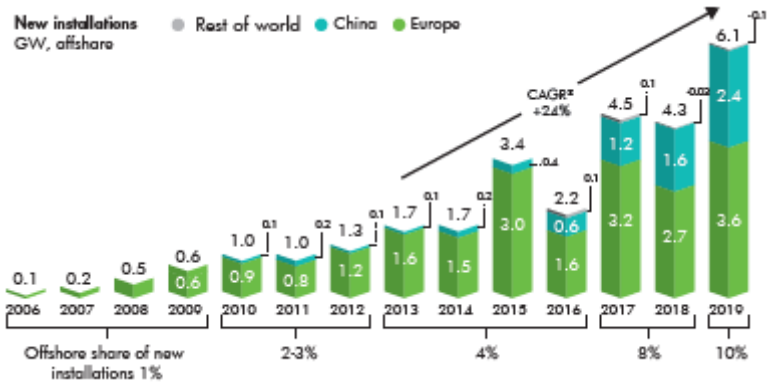

Fig. 1.7 New offshore power installation from 2006 to 2019 by GWEC

According to GWEC [14] offshore wind market has been developed in the last decade passing from 1% of global new wind installation in 2009 to over 10% in 2019. This rapid growth is due to the high potential seen by the governments all over the world in offshore locations, in 2019 was added 6.1 GW of new capacity, which is the highest increase ever had in offshore industry. This market grew on average by 24% each year since 2013, reflecting the high trust putted in this technology. UK and Germany lead the investments in offshore projects in Europe, with almost 81% of all actual investments, which reach 60 billions euros, while in Asia the projects are mainly supported by China, with the 92% of total asiatic investments. At present Europe is the largest market in off-shore with 75% of total installation capacity.

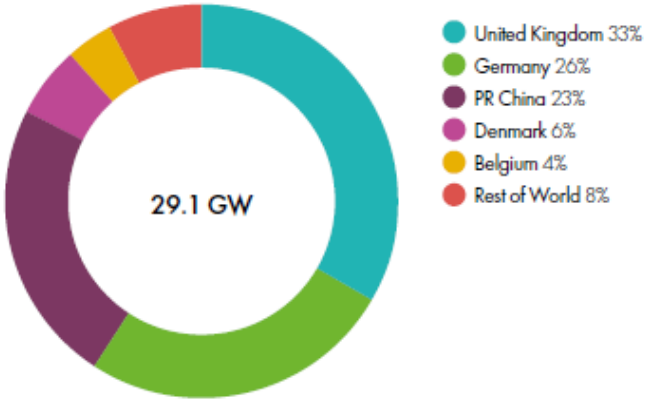

Fig. 1.8 Total installation of offshore wind power

GWEC Market Intelligence [14] expects that over 205 GW of new offshore wind capacity will be added over the next decade, contributing with more than 20% of total new installation. The forecast estimates that only in 2030 new installation in offshore locations will be of more than 30 GW, leaded for half by Europe, mainly by UK and Germany. Progress made over the next 10 years will lay the basis of how far and fast offshore market will grow in decades beyond. Further estimation forecast an overall installation of 1.4 TW of offshore power production by 2050, one third of which will be in Europe [14].

Mean wind speed and wind profile are key factors in deciding the power capacity of wind turbine. On seas and oceans, mean wind speed is much higher than on land considering the same height since the shear stress on water surface is lower than on ground. The main competitor against offshore wind investment is the onshore technology, which is still more convenient. Obstacles that slow down offshore market growth are up-front capital cost, O&M cost, harsh and unpredictable environment. All these drawbecks are expected to decrease in future and they will be offset by great advantages, such as higher mean wind speed and lower fluctuations, that result in higher efficiency and lifespan.

2 THEORY

2.1 WIND ENERGY

The wind energy is converted into electricity by means of a turbine. Wind transfers power to the turbine blades under form of mechanical power, which is then converted into electricity by means of a generator.

Wind kinetic energy inside a control volume of mass m is defined as:

$$E_k = \frac{1}{2} m V^2 \tag{2.1}$$

Thus, power can be expressed as function of mass flow rate

$$P_{wind} = \frac{1}{2} \dot{m} V_1^2 \tag{2.2}$$

Knowing that mass flow rate can be expressed as function of fluid density and volumetric flow rate, equation 2.2 can be rewritten as:

$$P_{wind} = \frac{1}{2} \rho A V_1^3 \tag{2.3}$$

Where ρ is the air density, A is the cross-sectional area and V is the free-stream wind velocity.

To calculate the power extracted by a turbine is used Betz Theory. This theory is valid under the assumptions of:

- Turbine rotor considered as an actuator disk with an infinite number of blades
- No mass flow rate crossing the control volume
- Parallel streamlines
- Negligible pressure difference between upstream and downstream conditions
- Steady state conditions
- Air considered as an uncompressible fluid; thus density is constant.

Since power turbine extracts energy from the wind, the wind speed interacting with the rotor must decrease in order to transfer energy to the blades. Applying continuity equation (eq. 2.4), as mass flow rate must be constant, section increase with the decreasing of wind velocity (fig. 2.1)

$$\rho A_1 V_1 = \rho A_2 V_2 \tag{2.4}$$

As pressure has a drop across the section A, which corresponds to the section of the turbine rotor, is defined a section just before the rotor (3) and a section just after (4).

Under hypothesis of constant potential energy and no heat exchange, Bernoulli equation can be written for the first part of control volume.

$$P_1 + \rho \frac{V_1^2}{2} = P_3 + \rho \frac{V_3^2}{2} \tag{2.5}$$

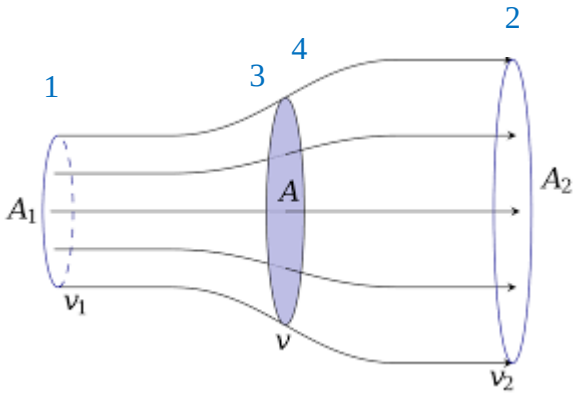

Fig. 2.1 schematic of a stream-tube and an actuator disk

Same equation can be written between section 4 and 2, second part of control volume. So, pressure drop across the actuator disk can be expressed as function of velocities.

$$\Delta p = p_3 - p_4 = \rho \frac{V_1^2 - V_2^2}{2} \tag{2.6}$$

Axial force at the rotor section is then defined as the pressure gap across the section A.

$$F = \Delta p\, A \tag{2.7}$$

Combining equation 2.6 and equation 2.7, the axial force become:

$$F = \rho A \frac{V_1^2 - V_2^2}{2} \tag{2.8}$$

According to impulse theorem, axial force can be also described by air momentum.

$$F = \dot{m}(V_1 - V_2) \tag{2.9}$$

With a simple system of equation 2.8 and equation 2.9, it results that wind speed at rotor section is the average of upstream and downstream velocities.

$$V = \frac{V_1 + V_2}{2} \tag{2.10}$$

This result means that half of wind deceleration occurs upstream and half downstream the rotor. Hence is defined a ‘’interference factor’’:

$$a = \frac{V_1 - V}{V_1} = 1 - \frac{V}{V_1} \tag{2.11}$$

This factor represents the decrease of wind velocity on the windward zone. Thanks to the addition of this factor is possible to define V and V_2 as function of upstream velocity just combining equation 2.11 and equation 2.10, it results:

$$V = (1 - a)V_1 \tag{2.12}$$

$$V_2 = (1 - 2a)V_1 \tag{2.13}$$

As in most applications, power is defined as the product of force$F$ and velocity V. Combining equation 2.8 of axial force and equation 1.10 that link the velocities, wind power results:

$$P = F\,V = \rho A V^2 (V_1 - V_2) \tag{2.14}$$

Now, everything can be written as function of interference parameter and upstream velocity

$$P = 2\rho A V_1^3 a(1 - a)^2 \tag{2.15}$$

The expression of variables as function of upstream velocity and interference factor is useful not only to apparently reduce variables, but mainly because these quantities are controllable. Upstream velocity can be easily measured, while it is more complex the measure V or V_2. As power has a quadric dependence with the interference factor, Interference factor is controllable since it has an optimal condition for which power extracted reach the maximum. To find this optimal value is differentiated the power respect a.

$$\frac{\partial P}{\partial a} = 0 \tag{2.16}$$

With simple math calculations it results that optimal interference factor is 1/3, that means an upstream velocity V_1 three times higher than the output velocity V_2. By this value of a, can be calculated the maximum power extractable:

$$P = \frac{8}{27}\rho A V_1^3 \tag{2.17}$$

POWER COEFFICIENT

Generally, to compare different machine and conditions in most of scientific study fields are used non-dimensional values, such as indices, coefficients, parameters. This is helpful to compare different system by means of similarity approach. In wind turbine theory, to evaluate power is defined a power coefficient C_P as the ratio between extracted power and available power inside wind

$$C_P = \frac{P}{P_{wind}} = \frac{P}{\frac{1}{2}\rho A V_1^3} = 4a(1 - a)^2 \tag{2.18}$$

As previously said, most theoretical power is obtained with $a = 1/3$, thus the maximum power coefficient is:

$$C_{P,max} = \frac{16}{27} = 0.59 \tag{2.19}$$

Although it can seem to be a low value for an efficiency, must be considered that a C_P equal to 1 correspond to the complete blockage of the wind at the turbine rotor, that is impossible because it

means wind is not flowing. This value is the theoretical limit of power coefficient of every wind turbine and is called ‘’Betz limit’’.

As this is a theoretical approach, this value can’t never be reached in reality. Main effects that decrease this value in real conditions are:

- The streamline deflection due to the interaction with the blades
- The finite number of blades
- The air viscosity which generate shear stress between air flow and blade surfaces and between faster and slower air flows.

Every turbine is described by a proper working curve that describes the power at varying of the operational conditions. Thus, power coefficient is expressed as function of tip-speed ratio λ_{tip} (TSR). TSR is defined as the ratio between the tangential speed of blades at tip and the incoming wind speed.

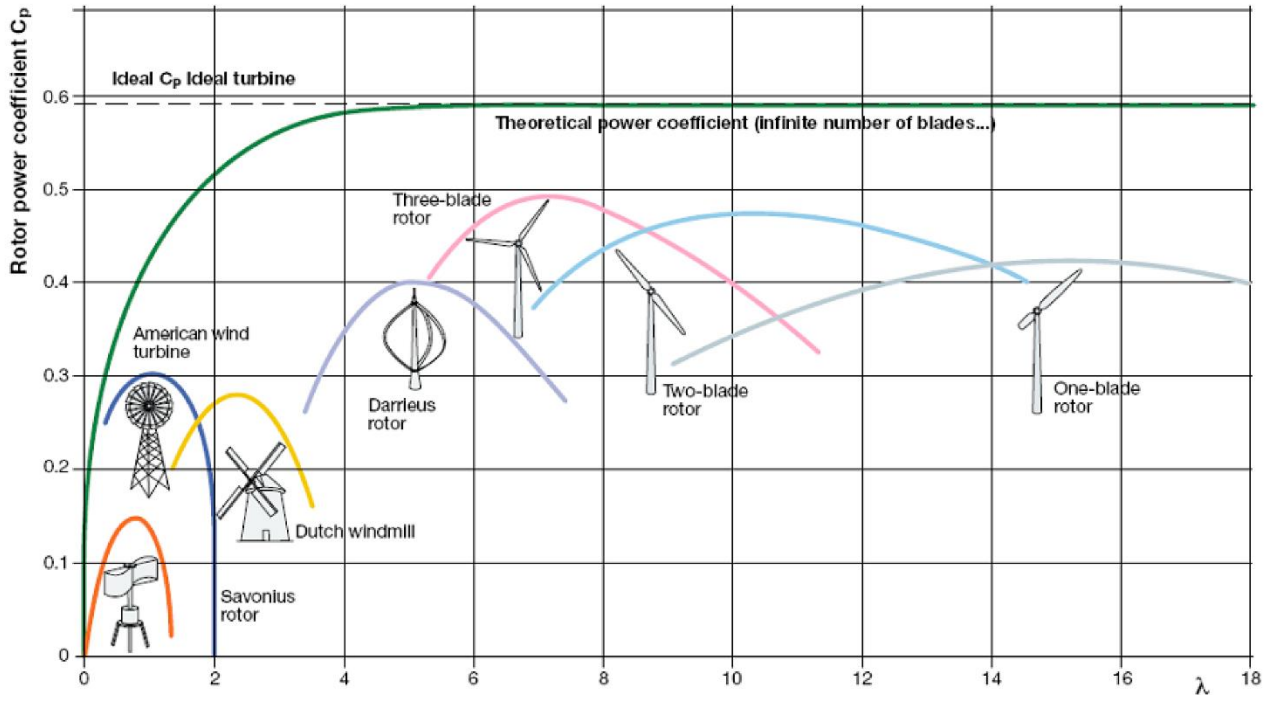

Fig. 2.2 C_P curve of different wind turbines

As previously said, the measurement of velocity in proximity of actuator disk is complex. Thus, for simplicity, is used the upstream velocity to calculate TSR:

$$\lambda_{tip} = \frac{\omega R}{V_1} \tag{2.20}$$

With power coefficient curves are compared different wind turbines (fig 2.2). In fig. 2.2 is seen that there is an optimum value of λ_{tip} for which C_P reach the maximum, this value is called optimal TSR.

Since the theoretical maximum value is lower than 100%, a second principle efficiency, which relates power coefficient of turbine and Betz limit, can give a clearer understanding of the performance o f a machine.

$$\eta = \frac{C_P}{C_{P,betz}} \tag{2.21}$$

A common three-blades HAWT, which is nowadays the most efficient wind turbine, can reach a maximum power coefficient of 50%, corresponding to an efficiency of 85% according to equation 2.21.

By equation (2.18), power extracted by turbine can be expressed as:

$$P = \frac{1}{2} C_P \rho A V_1^3 \tag{2.22}$$

P is the power transferred from the wind to the turbine rotor as mechanical power. The electrical power is then obtained considering electrical efficiency of the generator and organic efficiency of mechanical system.

$$P_{el} = \eta_O \eta_{el} P \tag{2.23}$$

By equation 2.22 is clear that to increase the power of a wind turbine is possible to act on different variables, such as the rotor size, the wind speed and the power coefficient. Velocity is the most influent parameter since P depends on the third power of V. In last years, rotor size has increased more and

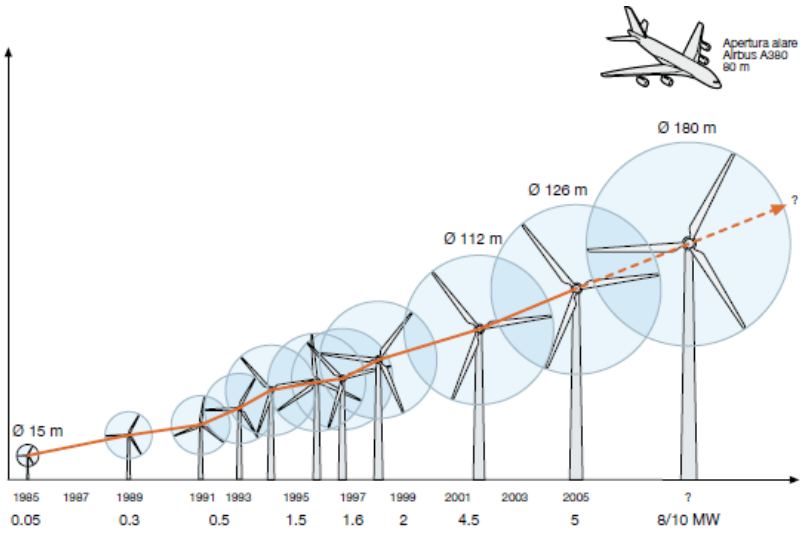

Fig. 2.3 Turbine rotor diameter development from 1995 to now

more (fig. 2.3) with the actual biggest onshore wind turbine with a rotor diameter of 164 meters and a power production at nominal conditions of 10MW. Considering offshore wind turbines, rotors are even bigger, reaching over 200 meters.

Wind turbines extract power thanks to the interaction of wind with blades. Blades are shaped with airfoil in order to generate lift, which results in torque that makes the blade rotate. All the mechanical

power generated is transferred to the drive-train and in turn to the generator. A simple schematic of a common wind turbine system is reported in fig. 2.4.

Gearbox presence depends on the generator used and on rotor rotational speed. The reduction of RPM is necessary to make the generator works at optimal condition, where efficiency is high. Despite gearbox influence, it is always present a disk-brake that avoid the turbine to work in extreme conditions, where too high wind speed can damage the system, while too low wind speed can be not

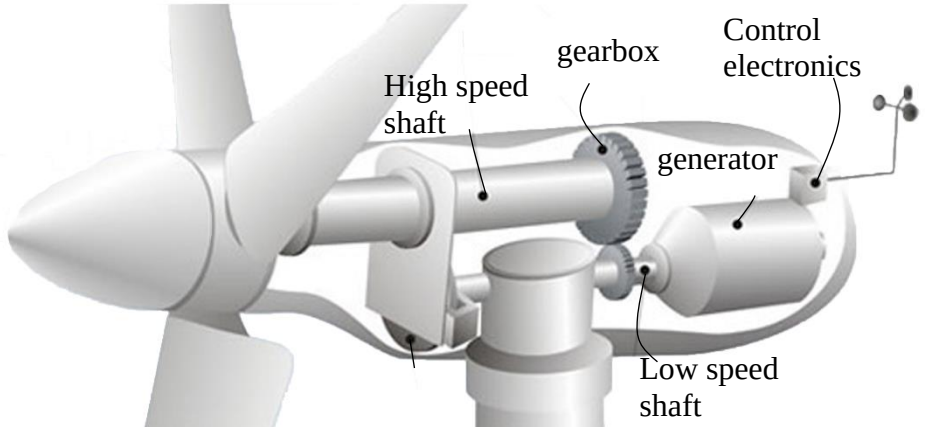

Fig. 2.4 wind turbine nacelle drive-train

economically favourable. Therefore, for every wind turbine is defined a nominal, a cut-in and a cut-off wind speed, to optimize operational conditions and avoid damages. Rotor brake for HAWTS is also useful to dissipate excess of energy induced by the gusts that could cause the damaging of some component.

Main part of wind turbine system can be considered the generator, which transform mechanical into electrical energy under form of voltage and AC current. All these components are placed inside the nacelle at several meters above the ground for HAWTs, while they are placed on the ground for VAWTs. To perform the grid connection of the electrical energy in output of the generator a rectifier and an inverter added, their position depends how far is the wind turbine from the grid. These two devices help the frequency control of the current that is mandatory for a proper grid connection. The AC current produced by the generator is transformed into DC by the rectifier, the inverter varies the DC current frequency to match the grid frequency and convert the current back to AC.

2.2 URBAN ENVIRONMENT

2.2.1 URBAN FLOW FIELD

A built environment is defined as an area with densely built-up settlements. The understanding of the aerodynamic in this kind of environment is complex and thus, it is still under investigation. Studies are focus on the looking for the most suitable methodology to forecast the wind flow conditions.

Buildings provide a kind of frictional drag to the flow that decreases the wind speed, indeed, mean wind velocity in built environment is much lower than in open-terrain. This frictional drag creates gradients of pressure which induce turbulence, which in turn produces local wind speed variation in magnitude and direction [19].

Urban and semi-urban wind flow fields are characterized by rapid fluctuations and turbulent condition, which makes exploitation of built environment complex. This turbulent behaviour of flow field in urban area can be the result of different factors, such as a high surface roughness, the interaction of wind with obstacles, atmospheric instabilities.

Therefore, major challenge of urban exploitation is associated with the complexity of aerodynamic that govern urban flow field. Wind turbine performances are highly influenced by the inflow conditions, thus a so fluctuating wind can strongly affect efficiency of power production.

Unfortunately, urban energy has many a time been motivated by a need to highlight and sponsor the energy consciousness of private, bringing turbine design to be driven by aesthetics rather than functionality. These failures brought public opinion to reject this new market. Despite this, scientific community has been very active in providing knowledge accessible to industry for a future development of urban wind market [20].

Surface roughness is main parameter of urban environment that affects characteristics of flow field, such as turbulence intensity, mean wind seed and wind profile. A precise configuration of wind flow field is essential for a depiction and prediction of wind turbine behaviour.

To estimate surface roughness there are mainly three approaches [21]:

- Davenport roughness classification (Table 1), which classifies urban roughness based on an assorted list of different surface types.
- Morphometric method, which adopts empirical equation for aerodynamic characteristic estimation.
- Micro-meteorological method.

No.	Class Name	Roughness length (m)	Landscape description
1	Sea	0.0002	Open water, featureless flat plain, fetch > 3 km
2	Smooth	0.005	Obstacle-free land with negligible vegetation, marsh, ridge-free ice
3	Open	0.03	Flat open grass, tundra, airport runway, isolated obstacles separated by >50 obstacle heights H;
4	Roughly Open	0.10	Low crops or plant cover, occasional obstacles separated by = 20 H
5	Rough	0.25	Crops of varying height, scattered obstacles with separation x ˜ 12-15 H if porous (shelterbelts) and x ˜ 8-12 H if solid (buildings)
6	Very Rough	0.5	Intensively cultivated landscape with large farms, orchards, bush land, x ˜ 8 H; low well-spaced buildings and no high trees (x ˜ 3-7 H)
7	Skimming	1.0	Full similar-height obstacle cover with interspaces ˜ H, e.g. mature forests, densely-built town area
8	Chaotic	=2	Irregular distribution of very large elements: high-rise city centre, big irregular forest with large clearings

Table 1 Davenport classification [89]

Atmospheric Boundary Layer (ABL) next to urban areas is usually divided into two main layers: Urban Boundary Layer (UBL) and Free atmosphere, where there is no more influence of urban buildings presence.

Arnfield [22] makes an important distinction between Urban Canopy Layer (UCL) and Urban Boundary Layer (UBL), the former is considered the distance between the ground and the roof level, while the latter is all the zone influenced by the presence of urban constructions (fig.2.5).

UBL is then partitioned into four main sublayers: Urban Canopy Layer (UCL), Roughness sublayer, Inertial Sublayer and Mixed Layer [23]. UCL extends generally from the ground to the rooftop level, in this layer flow is very complex and highly influenced by the ground obstacles and the canyon geometries. UCL follows the urban profile and can be characterized by a thickness equal to the average buildings, H. Roughness sublayer is the zone where flow is highly influenced by the urban roughness and has a thickness of 2-5 H. In the Inertial Sublayer the effect of urban roughness has been completed blended and wind velocity profile follows a logarithmic relation according to equation (2.23). The Outer Layer, also called Mixed Layer, is the zone where wind profile is no longer logarithmic.

In general, most of the focus in urban studies is on the first two layers, as there is no possibility for installation of so tall structures (turbine or meteorological towers) to reach the others. While for open-terrain condition is specified that stations have to be placed 10 meters above ground for a representative wind measurements and 2 meters for the humidity and the temperature measurements, in case of urban areas there are not any guidelines for proper assessment [24]. A specified procedure for the data acquisition of flow characteristics is important to define a universal methodology.

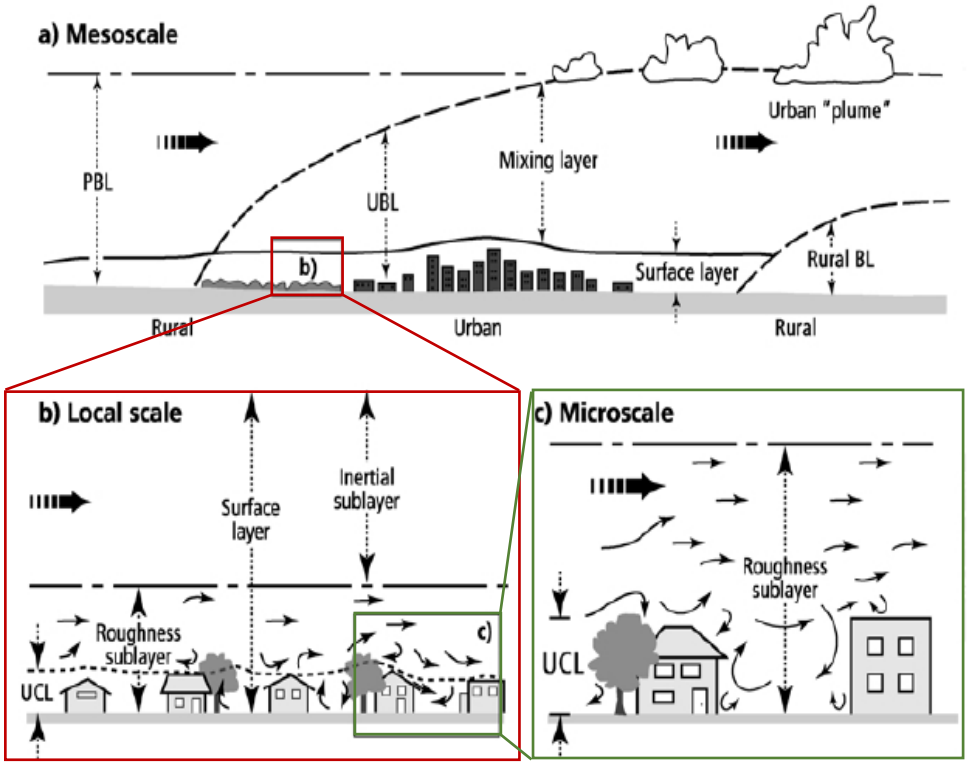

Fig. 2.5 Urban Boundary Layer breakdown in (a) Mesoscale (b) Local scale (c) Microscale [24]

Mean wind speed profile for the atmospheric boundary layer under neutrally stable conditions is defined by a logarithmic equation (fig.2.6) [25]:

$$U(z) = \frac{u_*}{k} \ln\left(\frac{z-d}{z_0}\right) \tag{2.24}$$

Where u_* is the friction velocity at the ground surface, k is the Von Karman constant (~40), z is the height above the ground, z_0 is the aerodynamic roughness height, which depends on the ground roughness, and d is the zero-plane displacement defined where the wind velocity is 0 m/s. z_0 is the key parameter that differentiate onshore, offshore and urban locations since it evaluates the surface roughness, which affects the wind shear and in turn the wind profile (table 1 [26]).

Urban wind energy is still far to be exploited efficiently due to the lack of detailed studies and data about. One of the main constrains in understanding the flow field is the complexity to obtain adequate

Type of terrain	z_0 (m)
Sand	0.0001–0.001
Sea surface	0.005
Grass	0.01–0.1
Pine forest	0.90–1.0
Suburban areas	0.20–0.40
Centers of cities	0.35–0.80

Table 2 aerodynamic roughness height for different type of terrain [92]

field measurements, which are essential to characterized urban wind and the relative influence on the turbines.

Kesby et al. [27], in WINEUR project report about wind energy integration in urban environment, recognized the direct measurements of wind characteristics as the most dependable method for accurate prediction of annual energy production. Nevertheless, it doesn't exist a monitoring methodology for urban wind source, therefore it is used the same procedure in resource assessment for large-scale wind farms installed in open terrain.

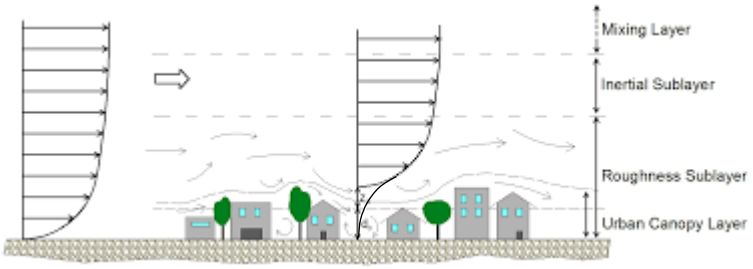

Fig. 2.6 approximative wind velocity profile in urban environment [90]

Prediction of wind speed in a built environment is complex, due to the continuously varying of the roughness and the influence of the surface-mounted obstacles. In addition, all the adjacent buildings influence the flow with each other. The complexity of the flow field limits the assessment of wind speed in urban areas slowing down the development of micro-scale energy urban market.

2.2.2 ANALYSIS APPROACHES

Several methods have been implemented for the initial assessment of wind resources based on data measured by meteorological stations. We can differentiate methods into three categories [19]:

- Probabilistic mathematical function, such as Weibull and Rayleigh
- Indirect methods, such as wind tunnel tests
- Numerical simulation by means of CFD tools

At present the best anemological campaign for urban application to quantify the wind resource is considered the onsite atmospheric measurements, although it is a challenging and expensive option due to the natural difficulties of built environment. In case of large-scale wind turbines or wind farms the anemological campaign has a small contribution on the whole system cost. By contrary, in case of installation in urban environment, where the overall cost is much lower, such a big acquisition of data has a relevant impact on the final cost [28]. This is the reason why, as said by Fields et al. [29], specific assessment of wind resource and wind classification by means of in-situ measurements is not a common practice urban area application. Additionally, data acquisition of wind is difficult in complex terrain due to the stochastic nature of wind, which does not follow any statistical distribution and thus, it is hard to be characterized.

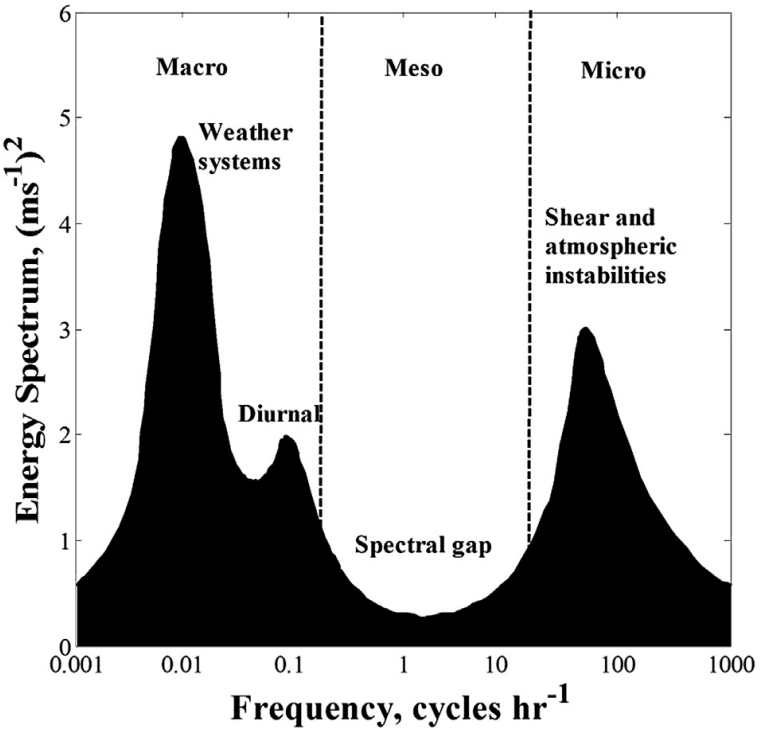

Fig. 2.7 Frequency distribution of fluctuating wind energy within the internal sub-layer [88]

Since data analysis provides useful information about installation, design and wind turbine performance, several methods have been developed to have a reliable prediction of wind flow field. Weibull and Rayleigh frequency distribution functions have been widely adopted for a precise estimation of wind conditions [20].

The complex characteristic of urban flow field makes hard the tracking of wind fluctuations. While in rural area gusts' energy inside wind flow is considered negligible respect the main wind energy, in built environment a significant amount is stored within the higher frequency components of gusts (fig.2.7). Therefore, the extraction of this excess of energy through advanced turbine controls could partially offset the low mean wind speed that characterize urban conditions.

The monitoring at high temporal resolution of wind characteristic within urban areas is not widespread, despite it can lead to a high level of accuracy in the assessment of installation. A precise evaluation of turbulence can bring to a good estimation of the energy available inside wind flow, this is essential to be able to relate the turbulence intensity and the excess of energy inside gusts, which is the key factor to make urban turbine profitable [30].

Gusts are defined as sudden fluctuations in wind speed that may bring an increase of mean velocity of about 30-50% [31].Gusts cause sudden rise and drops of wind speed, largely caused by the high surface roughness of urban areas; these speed variations occur in a relative short time (milliseconds), which explains the difficulty in their understanding and exploitation. Since gusts are predominant in urban areas and they own a big portion of the whole flow field energy, for a HAWT a gust tracking system is essential to keep the turbine operation within the region of peak aerodynamic efficiency and maximise the energy extraction.

The lack of site-specific measurements in urban environment causes an high level of uncertainty for a wind turbine installation, hence, numerical simulation by means of CFD tools and wind tunnel experiments have become more and more relevant to determine the effectiveness of urban installation [28]. Although high resolution models can estimate flow field for large-scale turbine in urban environment, the small-scale ones are harder due to the high dependence on boundary conditions and computational parameters set by the users. Because of these obstacles, a numerical result coming from a CFD tool is suggested to be compared with measured data, to validate the results.

Ledo et al. [25] and Lu and Ip [32] analysed the influence of buildings on wind speed and turbulence intensity with CFD simulations, both studies considered different roof types. Former study concluded that flat roof is the most attractive for urban wind turbine installation, while latter determined that sloped roof are interesting as well when turbine is located on top edge, where wind flow is accelerated and the turbulence intensity is low. These types of analysis are essential to determine the optimal

location for a wind turbine and the design that better perform in that location, both factors are relevant in increasing performance and decreasing issues, such as loads, noises and vibrations. Toja-Silva et al. [33] showed how a vortex is generated on the building roof even at very low wind velocities. With increasing of incident velocity both dragging and dispersion of this vortex are observed. However, the installation of a turbine in that location can completely change the flow field since the rotor spinning influence the flow field.

As underlined by Balduzzi et al. [34] in their work, the CFD tools are not able to quantify accurately the flow field around individual buildings due to the difficult in characterize conditions with so high turbulence. The difficulty on estimating the flow field in urban environment can be quickly understood by looking at the complexity generated by the interaction of a flow with a simple cube (fig.2.8). Over

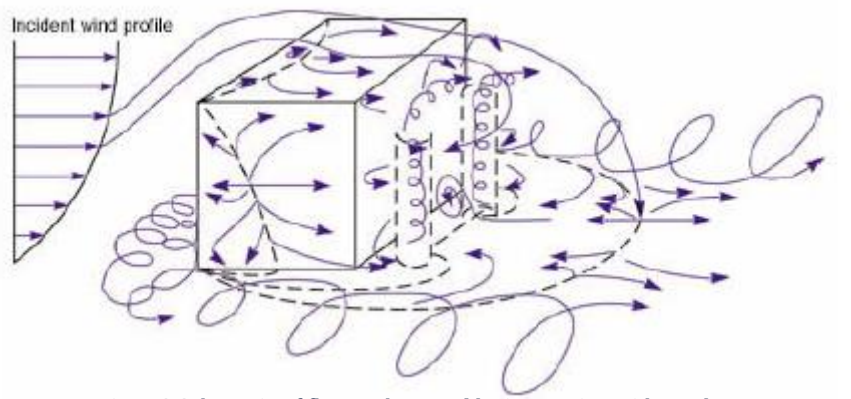

Fig. 2.8 Schematic of flow path caused by interaction with a cube

the sides of the buildings (including the roof) a separation zone is generated, the difference of pressure locally generated causes the formation of vortical structure. The estimation of wind flow field in built environment is complex and different case by case, it requires the synergy between analytical correlation, in-situ measurements and CFD tools. All these methods used together have still limitation when it comes to more detailed flow.

Regarding experimental tests, for large scale wind energy studies, relative wind tunnel tests are performed on small-scale rotors, therefore the Reynolds number equivalence can't be satisfied. Actually, this kind of studies are carried out with Re number in the order of hundred thousand, while full-scale turbine operate in the range of few millions of Re. Accordingly, most of real experiments assume Re independent behaviour of the blades. Al-Quarann et al. [35] proposed the combination of meteorological and wind tunnel measurements to find the velocity field at the roof of buildings. They suggested that an appropriate utilization of wind tunnel technology can provide a realistic estimation of urban wind energy potential in urban areas with a reasonable accuracy. Thanks to wind tunnel tests, they found the ratio between the velocity at the building roof and the upstream velocity, which is then used to find the actual velocity they are interested in just with the on-site measure of the upstream speed. This method is quite simple and validated by the application to two case studies: homogeneous

and non-homogeneous upstream terrain. The error in the estimated wind energy is calculated to be less than 5% for open-terrain conditions and less than 20% for the heterogeneous terrain.

At present, the most common methodology to study the flow field at the building roof makes use of probability distributions. A good representation of the wind spectrum allows to have a good estimation of design loads. In turbulence model is suggested by the standard to use Von Karman or Kaimal spectral density of functions to simulate wind flow field [36]. Both spectra are based on observations of wind conditions over open and uniform terrain: Von Karman spectrum is used for isotropic turbulence, while Kaimal spectrum derives from atmospheric parameters. Von Karman spectrum gives a good representation of turbulence flow field inside the wind tunnel and thus, is often used for consistency with analytical expression.

Mertens [37] used Weibull and Rayleigh probability distributions to estimate the energy yield from a turbine in built environment. This method takes into account the height above the roof level where turbine is placed, energy yield is then found by the equation

$$E = T \int_{u_i}^{u_0} f(u_s) P(u_s) du_s \tag{2.25}$$

Where E is the energy, T is the time of operation, which depends on the integration extremities, u_i is the cut-in wind speed, u_0 is the cut-out wind speed, $f(u_s)$ is the probability of wind speed u_s and $P(u_s)$ is the power produced at that wind speed. Mertens adopted a CFD tool to estimate the wind speed variations at different location on the building roof.

2.3 WIND TURBINE IN URBAN ENVIRONMENT

2.3.1 SMALL WIND TURBINE (SWT)

Wind sector has had a strong increase in the last years, that makes this market the second for the share in renewable source and the first as prospective of growth. Main barrier to the large-scale wind farms is the availability of sites, impact of grid power quality and distribution of electricity to the consumers. One alternative that climbs over these barriers is the development of small wind turbine (SWT) technology. SWTs are not suited for massive production of energy, such as the large-scale one, but are ideal to produce energy for household use. Recently, this technology has had an increase in research and studies act to detect the turbine design and the wind characteristic. SWTs can easily blend into the city through the incorporation with tall buildings, in high rise city centres, or on the ground, in semi-urban region.

The development of this market would lessen the losses experienced within the electricity supply system [38] and would create greater public awareness in renewable energy options. To exploit wind energy in the urban environment is important to face up with three main issues: wind flow assessment and characterization, building integration and system design suited for urban requirements.

Lakeman et al. [39] calculated that the potential market in Netherlands of wind turbines in urban areas can give around 50 and 60 MW of power production; considering an average machine capacity of 3/5 kW, it results 10-20 thousand turbines. The development of this market only depends on the economic competitivity of urban wind turbine technology, which is in turn related to the flow conditions understanding

In contrast with rural conditions, in urban and sub-urban areas space is limited and so large power plants are not feasible. By this consideration, the concept of on-site micro wind turbine installation is

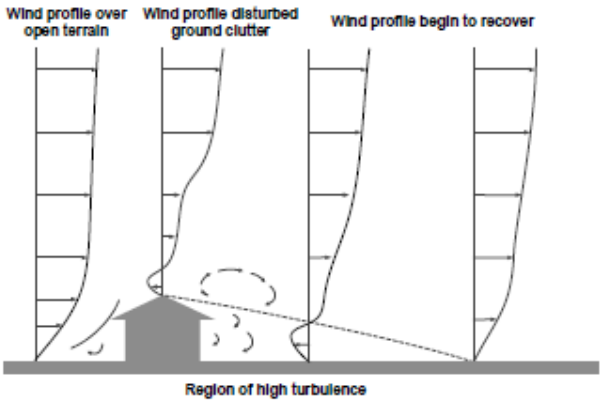

Fig. 2.9 wind velocity profile development during interaction with a single building

interesting because it allows to produce energy close to the application, deleting all the losses and cost related to electricity distribution. Urban wind turbine characteristics required can be grouped into good performance in highly turbulent flow, safe operation, low noise emissions, low visual disturbance and small dimensions.

Urban wind regime, compared to rural open-terrain areas, is characterized by low annual mean wind speed and high turbulence level. Turbulence is caused by the interaction of wind with buildings that modify both magnitude and direction of velocity. In Fig.2.9 [28] is shown a schematic representation of how wind flow in influenced by a single building, real urban field is much more complex and three dimensional, thus wind flow is extremely intricate. Due to this complexity of the problem, most of SWTs installed in built environment are sited with a limited understanding of wind conditions of the candidate location. Atmospheric turbulence generated by the morphology of the site is superimposed to wind average motion, causing a difficulty in forecasting the power production, A lack in understanding can cause an improper installation with the consequent inconstant work of the wind turbine, which can bring to early failure [40]. The wrong characterization of flow field due to its stochastic behaviour can result in a unsuited operation which affects the safety, lifetime and performance. An adequate knowledge of the flow field in a complex environment supported by more research is mandatory to develop a massive new market for the introduction of SWTs.

As it is well-know, the mean wind speed in built environment is much lower than the wind speed in open-terrain, however there are spots where flow is accelerated by the interaction with buildings and ground obstacles. Since the wind turbine power generation is proportional to the wind speed at third power, even a small increase in the wind speed can have a high influence in the feasibility of urban locations. The research of an optimal location for wind turbine installation is in contrast with normal engineering approach in building, that searches the place with lower wind speed to minimize wind-induced loads against the building.

Different papers, [41] [42] compared real wind conditions in different built environments, showing that NTM (normal turbulence model) underestimates both magnitude and fluctuations, especially at high wind speeds. By literature it is evident that urban flow field has high turbulence intensity in the range between 20% and 30%, which leads to higher fatigue loads and lower performance compared to the open-terrain conditions [29].

2.3.2 BUILDING INTEGRATION

Wind turbines installed in built environment can be either vertical-axis wind turbines (VAWT) or horizontal-axis wind turbines (HAWT). Thus, urban turbines are divided into three categories: built-environment wind turbines (BWT), built-integrated or built-augmented wind turbines (BIWT or BAWT), building-mounted wind turbines (BMWT) [28]. Sharpe and Proven [43] collect most of the earlier installation of wind turbines in urban context, which were generally stand-alone HAWT mounted on the top of masts (BWT) with a battery for energy storage.

(a) **(b)** **(c)**

Fig. 2.10 (a) Bahrain World Trade Center, (b) Strata Tower in London, (c) Pearl River Tower in Guangzhou

One of the most promising solution for the exploitation of wind energy in cities is the full integration of wind turbines (BAWT), this solution involves the wind turbine project during the building design. So, shape of structure can be designed to guide the flow in order to increase the wind speed, as result performance and power output of turbine increase as well. Usually large-scale building integrated HAWTs have problems of safety, noise, vibrations and visual disturbance; all these issues are minimized with the adoption of VAWTs.

Three well-known examples of BAWTS are Bahrain World Trade Center (2008), the Strata Tower in London (2010) and the Pearl River Tower in Guangzhou, China (2011) (fig.2.10). While the first two examples have adopted HAWTs integrated in between two towers or at the top of the building, the third tower installed two rows of VAWTs with Savonius design.

All three cases have a particular building shape that acts as a nozzle to canalize the wind flow towards the turbines. This configuration is useful to better harvest the wind energy increasing performance and power extraction. There are many position in which wind turbine can be placed to exploit the acceleration of flow (fig.2.11), nevertheless the concentration effect is present only for small dimension of wind turbine respect the building size, this limit the turbine diameter up to 20% of the building characteristic length [19].

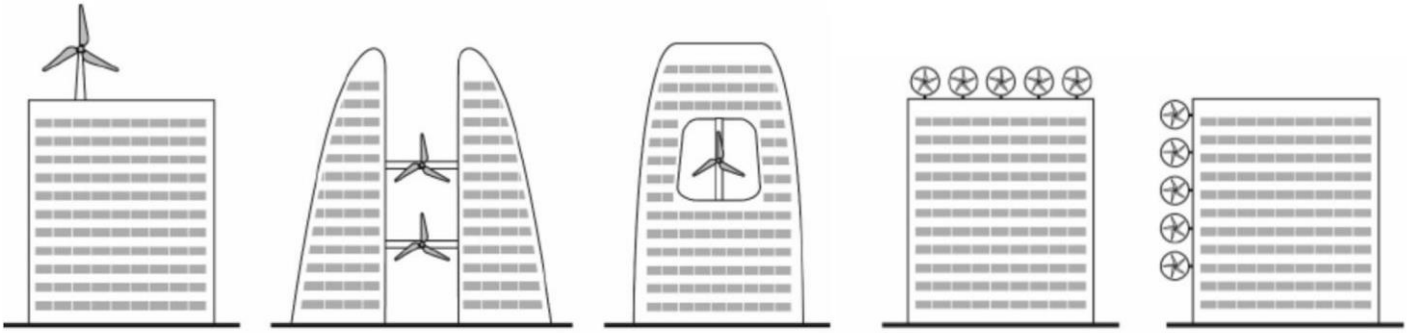

Fig. 2.11 possible Building Integrated Wind Turbine (BIWT) solutions [19]

Another choice for the urban wind turbine installation is the retrofitting onto existing buildings of micro-wind turbines for small-scale electricity generation (BMWT). As this option has a very small-scale, the power production performance can be very low and the system can be not so convenient. Hence, wind turbine can be integrated by a power augmentation guide-vane (PAGV) [44] or by an Omni-directional-guide-vane (ODGV) [45]to minimize the drawbacks of system safety, noises, vibrations and visual disturbance. Both systems are designed to increase the VAWT performances and improve self-starting behaviour, which is very important in an environment where mean wind speed is generally low. The overall performance of the retrofitted wind turbine change case by case depending on location, upwind area roughness, building size, edges and flow conditions [46].

One of the best example of retrofitting technology is the Boston Logan airport building [47] where a raw of 20 HAWT turbines designed specifically for urban environment is located next to the building parapet to take advantage of the flow acceleration (fig.2.12).

The main locations for wind turbine installation are the place where buildings acting as a nozzle accelerating the wind. Even zones with a frequent passage of fast vehicle can bring an acceleration of flow that can be exploited by a turbine, under this assumption, the Arizona State University proposed the concept of VAWTs installation horizontally above the highways in order to exploit the effect of air turbulence generated by the fast passage of vehicles and heavy trucks [21].

Another interesting solution is a diffuser structure to guide the wind flow, this results in higher power output and efficiency, this kind of solution is called Diffuser Augmented Wind Turbine (DAWT). DAWTs allow to work in flow field with lower wind speed and higher turbulence intensity. Wang et al. [48] confirms that the use of diffuser-concentrator can increase the wind speed by 1.5, thus the

power can increase with a factor of 2.2. Still the diffuser makes the system highly dependent on wind direction, which is a strong assumption in an urban flow field.

Economic analysis of traditional wind energy conversion system in urban environment, showed that the investment pay-back time is often greater than the machines life. Therefore, the enhancement of power conversion is essential to have an economically competitive technology, starting from the

Fig. 2.12 example of retrofitting technology in Bosotn Logan airport building

finding of the best installation site. So, buildings aerodynamics (governed by height, roof shape and sloping) can play an important role in finding the best location. Zanforlin and Letizia [49] in their study analysed a 2D CFD model of common urban conditions, concluding that dual-pitched roof and a diffuser-shaped wall can increase the power coefficient of a VAWT placed in the high-speed zone of about 40-50%. To get the same power output turbine should be installed several meters above the rooftop in order to catch higher wind speed. Diffuser configuration allows to mitigate the torque ripple, that implies lower fatigue loads and vibrations, which results in higher performance and lifetime.

VAWTs, respect to the HAWTs, can be considered the most suitable technology for urban wind exploitation because of their low turbulence intensity sensitivity, small dimension, absence of any yaw control, low noise. Omni-directional guide vanes with augmentation effects are an attractive alternative for VAWT and some prototypes have been designed: drag based VAWT such as Zephyr [50] or the PAGV (power augmentation guide vane) Sistan Turbine [51] or the ODGV (omni directional guide vanes) Darrieus [45]. A visual integrated turbine for urban environments is Crossflex [43], a flexible blade tropskein VAWT that can be sited on ridges and corners of buildings with advantages in terms of structural solidity, modularity, flow concentration.

2.3.3 STANDARD

Every wind turbine is design for durability, safety and performance according to the international standard IEC 61400 series. This standard describes the different possible flow fields, the turbulence, the interaction between turbines and extreme events that can occur. IEC 61400 contains the guidelines for manufacturer to design load on machines, by this legislative documentation SWTs are defined as wind turbines with swept area lower than 200 m^2 [28].

The standard (IEC 61400-2) defines SWTs design in terms of wind speed and turbulence parameters.

KC et al. [28] analysed the standards (IEC 61400-2) used to differentiate SWTs classes according to external conditions of different sites, as shown in table 1. These categories typifying a range of wind conditions that SWTs can experience in sites. Wind turbine classes are differentiate based on average and extreme wind speed and characteristic hub turbulence intensity, defined as ratio of wind speed standard deviation over mean wind speed. The characteristic turbulence intensity, I_{15}, considered in

Basic Parameters		Wind Turbine Classes				
		I	II	III	IV	S
V_{ref} (m/s)		50	42.5	37.5	30	Value to be specified
V_{avg} (m/s)		10	8.5	7.5	6	by the designer
A	I_{15} (−)	0.18	0.18	0.18	0.18	
	a	2	2	2	2	

Table 3 Basic parameters for the standard SWT (IEC 61400-2) , V_{ref} is the reference velocity averaged over 10 minutes, V_{avg} is the annual average wind speed at hub height, I_{15} is the characteristic turbulence intensity at hub height, A is turbulence class, a is the dimensionless slope parameter for turbulence standard deviation model

the standard is defined as the 90th percentile of longitudinal turbulence intensity measurements, assuming a gaussian distribution of wind fluctuations.

Based on the data reviewed by the IEC Technical Committee (TC) [52], the parameter ‘a’ represents sites turbulence. If this standard is not sufficient to reach acceptance for reliability and safety design levels, a special class ‘S’ is available to address special conditions. This same standard (IEC 61400-2) also defines wind conditions in terms of turbulent fluctuations and extreme wind events.

This standard is studied for wind turbines installed in conventional open-terrain areas, so it is necessary to expand the ranges to include the built environment. Otherwise, urban condition will always lie outside the ranging conditions causing an improper design. At present, wind turbines used in urban flow field are designed with this standard pertaining to the open terrain, thus it results in inadequacy related to performances, safety and lifetime. Unsuitable performance and failure of wind turbines in built environment may be due to inadequate design consideration coming from inconsistent statistic description of atmospheric turbulence.

As highlighted by Fields er al. [29], main factors of urban environment that affect performances are urban location morphology, low mean wind speed, wind direction variations, gusts, wind speed fluctuations, extreme conditions, unusual wind shear, atmospheric conditions; all these factors are not considered in the present standard for wind turbine design.

Wind speed is characterized by a mean value $\overline{U}$, and a random fluctuation *u'(t)* function of time, which is related to the turbulence effect. Wind speed is so defined as:

$$u(t) = \overline{U} + u'(t) \tag{2.26}$$

The estimation of turbulence strength in the time interval Δt is given by the turbulence intensity I.

$$I = \frac{\sigma_u}{\overline{U}} \tag{2.27}$$

Where σ_u is defined as the longitudinal standard deviation of wind speed variations at hub height. Turbulence intensity is main parameter for assessment of urban environment because it considers atmospheric stability, elevation and roughness length, giving a wide definition of the wind flow field.

Mertens [53] highlighted the problem of having low mean wind speed and high turbulence intensity related to power production. As reported by KC et al. [28], in the standard IEC 61400-2 suitable for SWT is given a relation to define the link between longitudinal turbulence and wind speed:

$$\sigma_{u,90pc} = \frac{I_{15}(15 + aU)}{a + 1} \tag{2.29}$$

Where $I_{15}$is the characteristic longitudinal turbulence intensity at 90th percentile, a is dimensionless slope parameter and U is the magnitude of three-dimensional wind speed at hub-heigh averaged over 10 min. All these values are found in Table 3 according to standard for different wind turbine class.

Considering standard value of characteristic turbulence intensity, $I_{15} = 0.18$, and dimensionless slope parameter, $a = 2$, equation 2.29 can be rewritten:

$$\sigma_{u,90pc} = 0.9 + 12U \tag{2.30}$$

Re-arranging equation 2.30 to explicit turbulence intensity, it results:

$$I_u = \frac{0.9}{\overline{U}} + 0.12 \tag{2.31}$$

Equation 2.30 gives an understanding of the turbulence intensity as function of average wind speed. By the standard 18% is considered as the maximum value of longitudinal turbulence intensity for siting SWTs. Still, many real installations have registered much higher values, up to 30%. As the turbulence level is used for the project of mechanical structure as well as aerodynamic efficiency, a wrong turbulence assessment can bring to the inefficiency of the turbine or to failure, in worst case, because an under-estimation of short and long-term fatigue loads. Due to this considerations, high turbulence level is considered generally a risk factor for the viability of the mechanical structure [54].

2.3.4 URBAN WIND TURBINE REVIEW

Wind is known to flowing following the minimal drag path when interacting with obstacles. The borders of those obstacles lead to a wind speed increase respect the freestream velocity, this phenomenon can be exploited by a wind turbine for power production [55]. The deviation of the streamlines when interacting with obstacles starts much before the reaching of the obstacle and continuous long after the end. So, can be highlighted a region with an elliptic shape inside which the wind flow is turbulent (fig. 2.13).

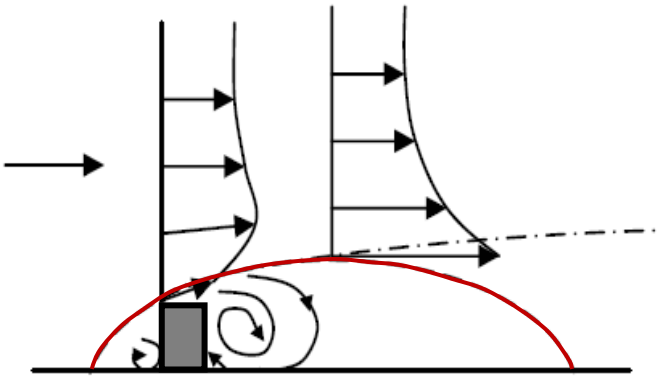

Fig. 2.13 velocity profiles and separation zone (red) of flow field interacting with a bluff body [39]

In a duct through a building, the pressure difference between the upstream and downstream condition makes the air moves towards the lower pressure zone, thus wind flows. At windward facade there is a stagnation zone of flow blocked by building, this cause a local increase of pressure. In contrast, at the leeward side the flowing of the wind generates a low-pressure zone. To enhance this phenomenon building sides can be rounded increasing the pressure difference and guiding smoothly the flow. The existence of the pressure difference between windwards and leeward side is not very sensitive to changes in wind direction, therefore the aerodynamic efficiency of the turbine is not sensitive as well [53]. As the turbine placed inside canyon geometry must be able to operate in two opposite inflow conditions, suitable configurations are: a Darrieus turbine; a Wells turbine or a HAWT with the possibility of 180° pitch of the blades. Wind turbine installed on the roof or along the building facade operates in the speed-up zone, where wind speed can be up to 20% higher than undisturbed velocity, it must be reminded that flows separates at building leading edges with an almost 45° angle [53].

Mertens [37] studied the effect of skew angle γ, which is the angle of the flow respect the roof. This angle is greater at the building windward edge and lower at the downwind zone (fig. 2.14), in accord with the elliptical path of the streamlines already described. The skew angle affects the turbine performance in case of VAWT as well as HAWT. The effect of the angle on the turbine performance are evaluated with equation [56]:

$$\frac{C_P}{C_{P,0}} = \cos^3 \gamma \tag{2.32}$$

Where C_P is the power coefficient of the yawed turbine, $C_{P,0}$ is the power coefficient considering a roof-parallel inflow condition and γ is the skew angle. Mertens found in his study that C_P might vary from 0.96-0.99 of $C_{p,0}$ in case of HAWTs. By contrast, Simão Ferreira et al. [57] showed that in case of VAWTs maximum value of C_P is attained at non-zero skew angle.

Troldborg et al. [58], using an actuator disk approach, showed that effect of roof surface does not seem to play an important role in the wake aerodynamics, the roof roughness is relevant only in the case of a very negative skew angle, i.e. wind towards roof.

Both Micallef et al. [59] in their studies affirmed that to study flow conditions is necessary to consider the turbine presence because the effect of blades rotation change the flow field. Since the mean wind speed in built environment is low, a low start-up torque is essential in order to have a wide range of

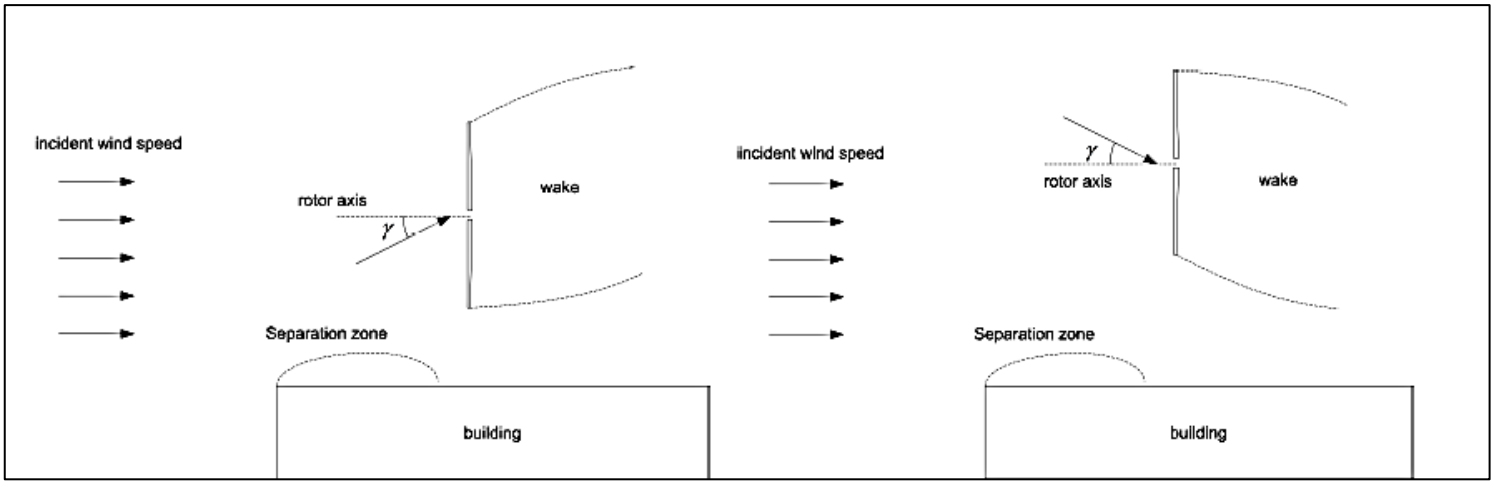

Fig. 2.14 Skew angle orientation on a HAWT mounted on the rooftop of a building [19]

operational conditions. Ebert and Wood [60] showed that in case of HAWTs operating at low wind speed, gusts have a beneficial effect in the starting off the turbine. One of the simplest ways to reduce starting torque issue is the reduction of turbine dimension, thus SWTs can be an appropriate solution to decrease this problem.

Installation of wind turbines in urban environment doesn't need same foundations required for large open-terrain application, but the interaction of turbulence flow with blades generates vibrations that are transmitted to the buildings, hence high-power facilities structure need to be reinforced to avoid any damage. This issue is relevant only for high power production, but it can be simply avoided installing a higher number of turbines with low power, this distribute the loads transmitted to the structure [61]. In addition, when the wind speed changes, the rotor inertia determines a transient process between two steady state angular velocities. In case of a sudden variation of wind speed, a small turbine could be faster in responding, this suggest the use of a SWT in urban environment.

Furthermore, the ability of VAWT pitch mechanism to have a fast response in variation of wind direction is the key factor to work in urban environment maximizing power generation [19]. Moreover, SWTs are favourited because of the small space availability in urban areas.

For these and other reasons, SWTs recently gained renewed attention from international scientific community as one of the actual strategies for the sustainable energy development of built environment. Among the different SWT types, whereas nature of wind flow in urban areas is strongly unsteady and three-dimensional, VAWTs are considered more suitable for the exploitation in urban environment because their ability in capturing the excess of energy inside gusts and turbulence [62]. In case of Savonius rotor turbulence intensity has different influences depending on the wind speed, it enhances turbine efficiency at low wind speed while decrease at high speed [19]. Advantages of VAWTs, compared to horizontal-axis counterpart, are:

- Reduction noises levels due to generally lower peripheral velocity of rotor blades for a given diameter
- Absence of wind track devices such as yaw mechanism
- Ease of architectural integration with buildings thanks to a three-dimensional design

While HAWTs are a common and well-known technology, VAWTs are still under study to completely understand best aerodynamic and installations conditions.

2.3.5 HAWT AND VAWT

VAWT are divided mainly into two categories: Darrieus and Savonius. The former one is usually a lift-driven rotor since most of the torque is generated by means of lift forces, while the latter is a drag-driven rotor. VAWTs are nowadays considered also for large-scale installation both onshore and offshore, but their adoption in urban environment is still under debate. In lift-driven turbine, the variation of bound circulation along the blade gives rise to trailing vorticity, whereas the time variation of bound circulation causes a shed vorticity. The self-interactions of vortices continuously created result in a complex wake cinematic [30]. Ahmadi-Baloutaki et al. [63] performed test on a VAWT model under controlled wind tunnel conditions using different levels of turbulence intensities (up to 10%) by means of turbulence grid. They claimed an improvement in the performance and start-up conditions with high turbulence levels.

Fig. 2.15 (a) Darrieus wind turbine, (b) helical Savonius wind turbine, (c) H-Darrieus wind turbine on offshore location (SeaTwirl)

In urban application it needs to be considered that turbine blades must sustain extreme and unsteady events. Mouzakis et al. [64] calculated that fatigue loading felt by turbine in a complex terrain environment may increase by more than 30%. Carbò Molina et al. [65] showed that power extracted by the VAWT turbine in turbulent wind flow is significantly higher, thanks to the ability of being able to extract excess of energy in gusts and turbulence. In their study a VAWT H-shape Darrieus was tested in the wind tunnel with different turbulence intensity generated with upstream grids. It resulted in an increase of 15% in the power coefficient of the highest turbulent conditions tested (I=9.6%)

compared to the freestream case ($I_u = 0.5\%$). Despite this study, at present it is still not completely clear if VAWTs operate better in turbulent flow than freestream conditions.

Kirke and Lazauskas [66] presented a study about helical Darrieus wind turbine. This shape has a variable pitch angle, which results in a better starting torque. Lift-driven VAWTs are generally not self-starting, this translated into the need of a power supply to make the turbine starts. An improvement on the starting torque conditions can decrease the amount of this energy consumption. Kamoji [67] showed that for a Helical Savonius rotor both power and torque coefficients are higher than common shape. Despite the cost increase, the helical design allows to have a smoothly engaging of the rotor during the rotation. Thus, torque is less fluctuating and loads are less intense.

Sharpe and Proven [43] developed a Darrieus turbine with flexible blades, which allows the installation either vertically or horizontally. Deformation of flexible blades allow the absorption of vibrations instead of their transmission to the structure underneath.

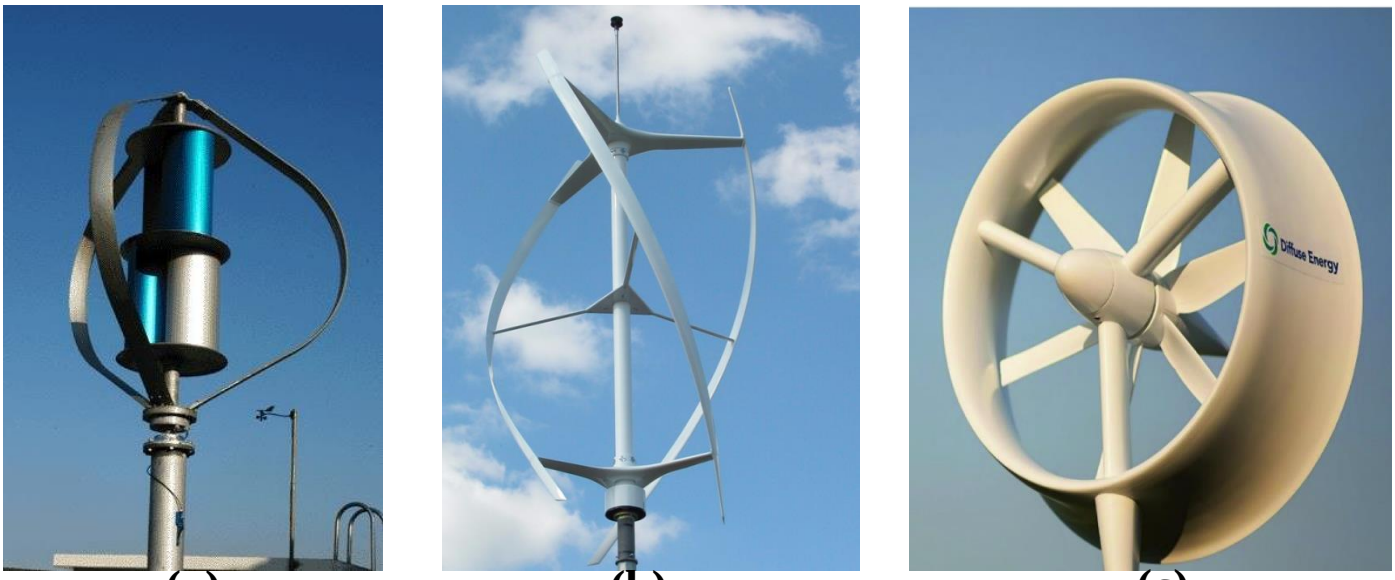

Fig. 2.16 (a) VAWT combination of Darrieus and Savonius rotors by MagLev, (b) Helical Darrieus wind turbine by Quietreviolution, (c) Diffuser-Augmented Wind Turbine (DAWT) by Diffuse Energy

The aerodynamic efficiency of wind turbines depends mainly on the working principle of energy conversion. Lift-driven turbines, such as HAWT and Darrieus, have a considerable high power coefficient, compared with the drag-driven counterpart (fig. 2.2). They make use of airfoil to generate lift force, that produce the torque and the consequent rotation of rotor. Lift based VAWT usually has a high TSR, which result in a fast spin, and has slender blades to minimize centrifugal forces. For lift-driven VAWTs, as the blades are rotating around a vertical axis, the airfoil change continuously angle of attack of inflow condition. This results in a periodic stall during each revolution because airfoil gain energy only when blades are in windward or leeward position. Thus, power and torque have a sinusoidal shape with peaks twice per cycle, in front and back position [68]. Phenomenon of dynamic stall reduces turbine efficiency and induces noise and structural vibrations [69]. Cambering the airfoil

has no significant effect on the performance of the VAWTs because it causes the tangential force increases in one half and decrease in the other half of the total swept region [70]. Several researchers studied the influence of blade number on the rotation of VAWTs, suggesting that a high number of blades help the rotation at low wind speeds. Three-blade configuration for H-Darrieus is considered the more stable [71]. Nazeem et al. [72] investigated with CFD simulation the performance of an H-rotor at different position in two different scenario, one and two bluff bodies side by side upstream the turbine. Compering the results with free stream, it resulted that buildings act as deflectors augmenting wind power downstream. Wind velocity speed up of about 12% and 25% compared to the free stream condition respectively for the single and the double cube configuration, thus power and performance are increased.

The Savonius rotor is a VAWT low speed wind turbine characterized by the simplicity and low cut-in velocity. Saha et al. [73] showed in their study that Savonius rotor is suitable for micro-scale urban power production, even if the power coefficient is generally very low. Savonius turbine has a low power coefficient but has the advantage to be self-starting and to be independent by the inflow direction [33]. Due to its simplicity which implies a very low cost, it can be implemented in regions with extremely low economic resources by using recycled material [74]. Savonius working principle is based on the difference of drag coefficient between a convex and a concave shape. According to Mohamed et al. [75], the addition of a deflector sheet to cover the turbine part which works against the rotation can increase the efficiency of between 5 and 8%. They also concluded that the best number of blades for a Savonius rotor to maximise power coefficient is two.

Main disadvantage of Savonius turbine is the very low power coefficient as shown in fig. 2.2 where are compared power coefficient of different wind turbine types. Thus, drag-driven VAWT needs a support device, such as a power-augmentation guide vane (PAGV), to orient the flow and increase both rotational speed and torque. Otherwise, Savonius turbines can be used as support device in hybrid system [20].

ADVANTAGES and DISADVANTAGES

Comparing Vertical axis wind turbines (VAWT) and horizontal axis wind turbines (HAWT) there benefits and drawbacks on both sides. HAWTs are very sensitive with the wind direction and don't cope well with turbulent flow and buffering. Therefore, HAWTs are suited to be installed in open-terrain with horizontal and parallel flow. HAWTs need a control system to change the yaw system to keep the rotor cross section normal to the incoming flow. In built environment wind direction has quick variation that makes the tracking of direction complex [53]. Inefficiency of yaw mechanism in detecting high and fast variation in time and space results in a high decrease of wind turbine performances. On the other hand, VAWTs have high potential for power generation in urban areas because can be mounted in small places, are independent by wind direction and are less sensitive to turbulence and gusts. VAWTs are less influenced by directional change because, thanks to their geometry, there is not an optimal direction, except for the starting of vertical-axis lift-driven machine. VAWTs are also less noisy, due to a lower TSR, and with a lower visual impact, due to their geometry. VAWTs have also a higher time response, which allows them to rapidly react to the gusts. All these characteristics make VAWT more suitable for urban environment, despite their lower power coefficient.

Several constrains imposed by urban installation can play a relevant role in efficiency of rotor, such as size constrains, noise limitation, visual disturbance, low start-up wind speed. Turbine design in built environment depends on application and constrains case by case. while in common open-terrain applications most of the characteristics are standardized. So, urban installation conditions must be considered during the rotor design project [19].

Power production of wind turbines mainly depends on the mean wind speed, the turbine efficiency and the load factor. Instead, the turbine cost envelops the machine manufacturing, the generator, the additional devices, the foundations, the installation and the O&M costs. Eriksson et al. [76] made a comparison between the three different wind turbines (HAWT, Darrieus and H-rotor) by an economic point of view (€/kWh). They concluded that HAWTs at present appear to be more commercially efficient than both VAWTs, a summary of the result is shown in table 4.

Despite HAWTs are still economically favourable, as all the additional costs are balanced by the high wind power extraction, Grenblatt et al. [77] estimated that VAWTs will dominate the wind energy market within 2-3 decades. This statement relies on the expectation of a huge development of wind market in urban areas and on the fact that VAWTs require less land space than HAWTs.

	H-rotor	Darrieus	HAWT
Blade profile	Simple	complicated	Complicated
Yaw mechanism required	No	No	Yes
Pitch mechanism possible	Yes	No	Yes
Tower	Yes	No	Yes
Guy wires	Optional	Yes	No
Noise	Low	Moderate	High
Blade area	Moderate	Large	Small
Generator position	On ground	On ground	On tower top
Blade load	Moderate	Low	High
Self-starting	No	No	Yes
Tower interference	Small	Small	Large
Foundation	Moderate	Simple	Extensive
Overall structure	simple	Simple	complicated

Table 4 Comparison between H-rotor Darrieus, normal Darrieus rotor, HAWT

Riegler [78] in his research concluded that VAWTs are significantly favourite over HAWTs in application of less than 10kW, since VAWTs can better handle turbulence, have lower noise emissions and costs of both construction and maintenance are strongly lower.

Toja-Silva et al. [33] in their study compared VAWTs and HAWTs, superimposing the turbine structure in a velocity field map simulated by a CFD tool of the interaction of a flow field with a cube. They concluded that installation of HAWT is incompatible with the turbulence condition that characterize the built environment because a high turbulence intensity can bring to the damage of the machine.

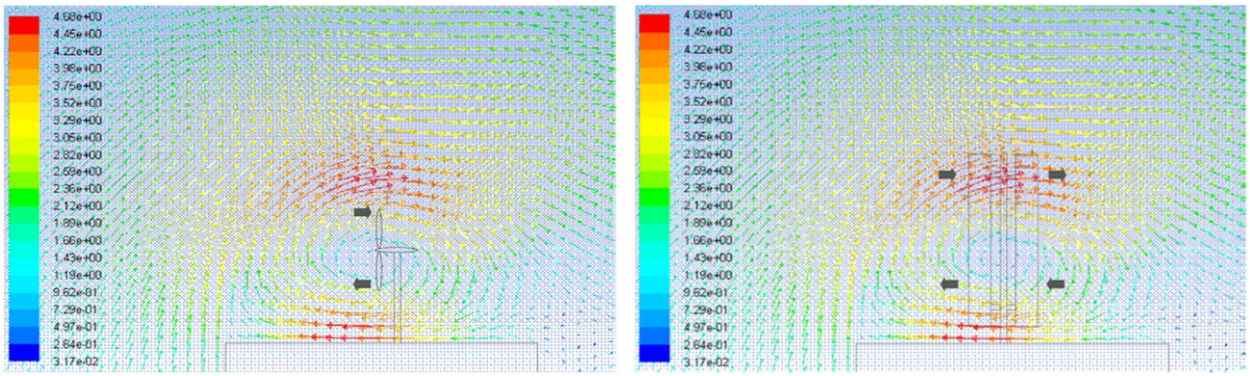

Fig. 2.17 Superposition of HAWT and horizontsl Darrieus wind turbine with flow field generated by an incident velocity of 1 m/s.

VAWTs seems to be the best option for SWT in urban areas due to their ability to harvest wind multi-directionally and to run smoothly even with large wind fluctuations. Moreover, the generator and the gearbox are installed at ground level, hence installation and maintenance operations are simpler and cheaper respect HAWTs, which needs these devices inside the nacelle at several meters above the ground. At present there are four main types of VAWT for urban environment: Savonius (fig. 2.15b), Darrieus (fig.2.15a), Giromill (fig.2.15c), also called H-shape, and Gorlov, which has helical blades (fig.2.16b).

2.4 CUBES INSIDE FLOW

Flow around a cube is a problem of great interest. Studying this allows to better understand mean pressure and velocity field around obstacles in atmospheric boundary layer. This is important for the proper installation of wind turbines in the urban environment. The analysis of the flow field around the three-dimensional bluff body is an essential problem, that can be applied in many areas.

Due to the topology of the urban environment the flow field is complex to be characterized. Generally main parameters for a good description of locations are average wind speed, vertical gradient of velocity and turbulence intensity [39]. A simple cube inside a flow field generate a complex flow with separation zones on the leeward area and vorticities on windward areas (fig.2.17).

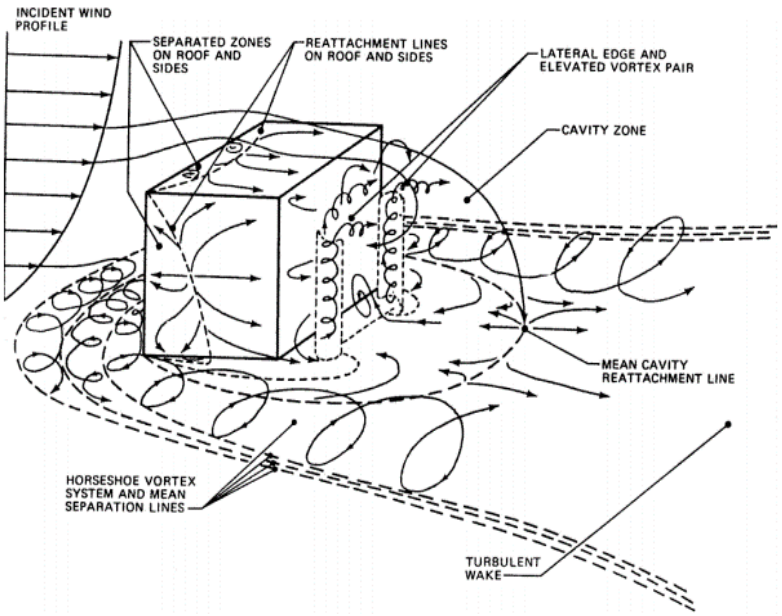

Fig. 2.18 Schematic of separations and vorticities of flow interacting with a cube [91]

Considering the 2D field generated by the interaction of a cube with a parallel flow, it can be assumed a semi-elliptical boundary streamlines that divides the separation and vortical zones from the deflected streamline (fig.2.13). As the streamlines are deflected by the presence of the obstacle, Mertens applied the classical momentum theory approach in bend layers of the flow over the semi-ellipse line, demonstrating that flow has a significant acceleration. It resulted that wind velocity in overspeed region can increase by about 20% compared to the undisturbed wind speed, since the power is linked with the third power of velocity, this acceleration result in a 72% of power increase. Considering the semi-elliptic streamline that divide the two zones, Mertens [39] reported an empirical model proposed by Wilson for the growth of separation zone behind cubical buildings:

$$y = 0.28H^{0.67}x^{0.33}$$

Where y is the vertical height of wake starting from the building roof, x is the horizontal distance in the wind direction starting from the windward edge and H is the smallest dimension normal to the wind of the upwind facade.

Khan et al. [79] studied the wake on an incompressible flow around a cube placed normally to the flow in a wide Reynolds range, $Re \in (500\,, 55\,000)$. The wake was measured with PIV till three cube size downstream the cube. It is stated that for $Re > 10^3$, the wake profile shows a behaviour independent by Reynolds number. Furthermore, the turbulence intensity in the wake region and the recirculation zones are reduce with increasing of Re. Castro and Robin [304] in their study about a cube in uniform and turbulent stream found that for a turbulent upstream boundary layer there is no discernible Reynolds effect with Re_h higher than 4000. Thus, 4000 can be defined the limit for the similarity condition for Reynolds. Re_h is defined as the Reynolds number at the cube height

$$Re_h = \frac{U_h H}{\nu}$$

In their study, Castro and Robins [80] defined also a limit of the ratio between cube height (H) and boundary layer thickness (δ) beyond which both the reattachment length downstream the cube and the characteristic of flow can be considered independent by the Reynolds number

$$\frac{H}{\delta} \leq 0.7$$

This relation is valid for cube fully submerged into the turbulent boundary layer, so that the cube height is lower than the boundary layer thickness.

In the interaction between a flow and a fixed cube. a horseshoe vortex is generated upstream the body due to the blockage of the flow against the front wall. The vortex dimension and intensity depend on the incoming boundary layer thickness δ [80], but the streamwise position was demonstrated by Baker [81] to occur at $x/H = -0.8$ and to be independent by Re.

Moreover, Incident flow separates at the top leading edge of the cube, generating a large three-dimensional recirculation region over the top facade of the cube (fig.2.17). On this recirculation zone a vortex can be observed with the core approximately at 0.7H downstream the leading edge and 0.25H above the surface [82].

Hearst et al. [83] investigated experimentally the influence of turbulence generated in the aft zone of a cube immersed in a turbulent boundary layer by means of Particle Image Velocimetry (PIV) and hot wire anemometry. They observed that windward stagnation point and the leeward reattachment in the wake behind the cube were independent by the incoming profile. Thus, the stagnation point in

windward facade and the reattachment on the wake behind the cube were fixed for all the considered cases at $y_0/H = 0.65$ and $x_R/H = 1.9$ respectively independently by the turbulence intensity. It was also observed a turbulence limit beyond which the wakes are no more influenced by the turbulence increase. They concluded suggesting that a high turbulence level might facilitate the recovery of the wake downstream the cube.

Whereas flows around single bluff bodies have been widely studied, the investigation of two or more bluff bodies has been mainly performed for bidimensional cases.

Martinuzzi and Havel [84] in their study concluded that there are important differences between the flow field generated by a three or a two dimensional study of two bluff bodies in tandem configuration. Martinuzzi and Havel [82] in another work studied the flow around two cubes in tandem position in a thin boundary layer at different bodies spacing (S). The top side of the cube is characterized by a separate shear layer that is generated at the cube top leading edge and it reattaches intermittently. It was observed by Hearst et al. [83] that the increase of the turbulence decreases the intermittency level of the shear layer, thus flow is attached to the cube surface more frequently. For a small separation of the cubes ($S/H < 1.4$), the separate shear layer reattaches on the top surface of the second obstacle. With a small distance the recirculation inside the space in between the two bluff bodies is high and the turbulence level is low. Increasing the distance S, the fluid entering the inter-obstacle region increases, for $S/H > 1.5$ a relevant amount of fluid entering comes laterally. For an intermediate value of the obstacle spacing, $1.4 < S/H < 3.5$, the separated shear layer generated in the first cube impinges on the front side of the second cube. This results in the formation of a shear layer on the front facade of downstream cube. Increasing the distance S, the flow from the sides of the first cube enters inside the blank zone between the cubes increasing the turbulence level. For large distance, the separated layer reattaches on the base plate between the obstacles, thus a new counter-rotating vortex is generated just upstream the leeward cube. The second counter-rotating vortex is recognized starting from $S/H = 4$. With a further increase of the distance S the second cube stops to feel the presence of the upstream cube and starts to have a single cube behaviour [83]. In our experiments the intra-obstacle distance S was fixed at twice the cube height, this allows to place our experiment on the intermediate value of S/H in Martinuzzi and Havel study. Thus, the separated shear layer generated by the upstream cube will not affect the top side of the downstream cube but it will impinge on the front facade.

3 METHOD

The goal of the experiment is to study the behaviour of wind turbine, in this case a VAWT Savonius, on the roof of building in urban environment. To simplify the building is used a cube of 10 cm dimension, to represent the built environment two cube are placed in tandem formation (fig.3.1). The whole system is placed inside the wind tunnel on an acrylic plate much bigger than the cube size in width and length (1.8 x 3.0 m), to avoid the influence of plate edges on the system. The plate is elevated of almost 1 meter from the wind tunnel floor with an aluminium structure not to be affected by the boundary layer of the wind tunnel floor. The leading edge of acrylic plate is sharped to minimize the interaction between wind and plate that can cause a not uniform upstream condition for the system, in this way leading edge divides smoothly the wind upward and downward. Moreover, the system laid far from the leading edge of more than 4 cube heights, this avoid the possible interaction of the cubes with the boundary layer while it is not fully developed.

For studying the wind turbine performance, a rotor with a Savonius design is adopted due to its simplicity, as it must be 3D printed. The turbine is placed at 1.0 cm above the cube roof and the blades are 3 cm high. A more precise description of the turbine geometry is made in the equipment section.

The cube position on the top side we are interested in are the front, centre and back of both cubes, hence there are 6 positions to study, as shown in fig.3.1.

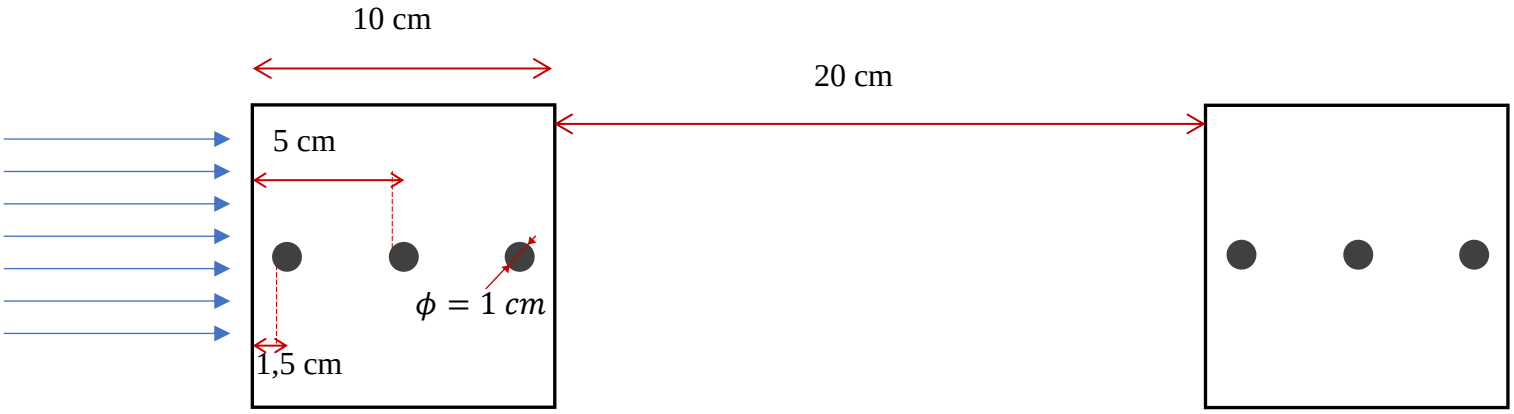

Fig. 3.1 schematic of the experiment configuration

To study the performance in built environment the experiment is mainly divided into two measurements: the PIV, which allows to have a velocity vector map of a target area, and the performance measurement, which is obtained measuring torque and rotational speed of the turbine.

The PIV measurements are described in the subchapter 3.1.1, it consists in the generation of a vector map based on the correlation of fraction of two following frames. Seeding particles are hit by a laser sheet shot from above, the light hitting the particles is reflected towards the cameras placed on the side.

Synchronizing laser and cameras it is possible to have a picture of particles ''frozen'' in the flow. Taking two following pictures in a short time (microseconds) enables to find out the velocity vector field by correlating several sub-parts of frames, for each sub-section is calculated a velocity vector. Thus, smaller section is used more precise is the velocity field, but the correlation become harder. The right size of partitioning is decided by the software based on the PIV system parameters. Since the cameras have a very high resolution, both turbine and cubes are painted with a matt black paint to avoid undesired reflection of the laser that can bring to the saturation of camera pixels. PIV measurements are performed in the darkness, to avoid background light influence. System is made of a laser place above the wind tunnel, which shots downward, and two cameras placed on the side looking perpendicularly to the wind flow direction (fig.3.2). This configuration allows to have a velocity vector map in streamwise direction.

In addition to the six configurations desired, two more cases are performed with PIV measurement. First case considers the plate alone, without any cube. This configuration allows to see how big the boundary layer (BL) is and if it is laminar or turbulent. The characterization of BL is important to evaluate its possible influence on following configurations, by a first PIV acquisition the BL is presumed to be in transitional condition. A transitional BL must be avoided, as it is hard controllable. Therefore, to increase the surface roughness a tripping tape is added at the beginning of the acrylic plate to bring BL in turbulent condition. Turbulent BL is strongly preferred because has a known condition with a controlled BL. The configuration with the only plate is important also to have a reference free-stream conditions, without any blockage effect caused by presence of the cubes. The second case added is made of the plate and both cubes, without the presence of the turbine. This configuration makes us understand the reference flow field to which correlate other configurations. This is important because the presence of turbine influence the flow field, therefore is important to have a reference conditions for a good comparison to understand how turbine affect the flow.

Performance coefficient measurement is obtained by the measurements of torque and rotational speed, because power extracted by wind turbine can be calculated as the product of these two quantities as shown in the following equation,

$$C_P = \frac{P_{conv}}{P_{wind}} = \frac{Q\omega}{\frac{1}{2}\rho A U^2} \tag{3.1}$$

Where Q is the torque at the turbine shaft, ω is rotational speed of turbine, U is the wind speed, A is the cross-sectional area of the turbine and ρ is the air density. The presence of P_{conv} instead of mechanical power or electrical power is explained in chapter 3.2.

The measurement of the rotational speed is performed simply using a photo-transducer and a reflecting tape on the turbine shaft. A photo-transducer is a device made of two components, an IR led, which

emits infrared light, and a transducer sensitive to the light, which gives a voltage output as the light felt at the base surface increases. Placing the photo-transducer pointing towards the turbine shaft, with the wind tunnel on and the turbine spinning, the tape reflects the light emitted by the LED passing in front of the photo-transistor. Thus, counting the time the reflecting tape is passed can be easily calculated the rotational speed of the turbine. A more precise explanation of how photo-transistor works is made in the subchapter 3.1.2.

Torque is difficult to be measured due to the low dimension of turbine. In larger application measurement of this quantity are made with the adoption of a torque-transducer, which works mainly with strain gauges to detect the deformation caused by the application of torque. This is complex to be realized on such a small scale, hence in this small system it is necessary to find out a different solution. Considering the use of a DC motor linked to the turbine shaft, the characteristic of this electro-mechanical link can be exploited to determine the torque induced to the turbine by the wind flow.

In an ideal case the mechanical power generated by the wind due to the interaction with the turbine blades is the equal to the electrical power felt by the DC generator. Thus, the following equation can be written:

$$VI = Q\omega \tag{3.2}$$

Where on the left of the equation there is the definition of electrical power, while on the right is considered the mechanical power, as already seen in equation 3.1.

A DC machine has the advantage to decouple the effect of voltage and current respect to the mechanical quantities, hence we can consider voltage proportional to speed and current proportional to torque. These relations are linear and dependent on a constant given in the datasheet of each DC machine by the constructor [85]. A more precise explanation of DC machine and how the quantities are linked is made in subchapter 3.1.1. As we consider valid these relations, we can measure the shaft torque using a simple current sensor. The DC machine used is a brushed DC motor Portescap Athlonix 10NS61 107C.5, with a nominal voltage of 3V and a stall torque at 0.76 mNm. The specifications of the motor are reported in Table 5.

DATA	SYMBOL	VALUE	DIMENSION
Nominal voltage	V	3	V
No-load speed	n_0	10100	rpm
No-load current	I_0	11	mA
Terminal resistance	R	10.8	Ω
Output max power	P_{max}	0.7	W

Stall torque	T_{stal}	0.76	mNm
Efficiency	η	64	%
Back-emf constant	K_E	0.29	mV/rpm
Torque constant	K_M	2.72	mNm/A
Friction torque	T_F	0.02	mNm
Rotor inertia	J	0.05	$g\ cm^2$

Table 5 Datasheet of DC motor characteristic provided by the manufacturer

Rotor inertia affects the torque during acceleration but, as we consider a steady state operation of wind turbine, inertia effect is not present. The torque constant K_M is the most important property of a DC machine for torque measurement because it relates torque and current with a linear relation.

$$Q = K_M I \tag{3.3}$$

There is a linear relation between voltage and rotational speed too, evaluated by the back-emf constant, K_E, resulting in a similar formula of equation 3.3:

$$V = K_E \omega \tag{3.4}$$

Since, as previously stated, the electrical and mechanical power can be considered the same in an ideal case, the two constants must be the same to corroborate the following identity:

$$VI = Q\omega \frac{K_E}{K_M} \tag{3.5}$$

In fact, can be demonstrate with simple dimensional analysis that the two constants are the same

$$\frac{K_E}{K_M} = \frac{0.29\ mV/rpm}{2.72\ mNm/A} = \frac{60}{2\pi} \frac{0.29\ V/(rad/s)}{2.72\ Nm/A} \sim 1 \tag{3.6}$$

The constants given in the datasheet of the DC machine are considered for the motor mode, but the manufacturer (Portescap) confirms that those values can be considered valid even for the generator mode. The relation between quantities of electric motor are studied in detail in the following chapters.

With the measurement of rotational speed, by means of the phototransistor, and torque, by means of the DC current sensor, the mechanical power can be calculated. To determine the wind power (equation 2.3) is used pitot tube to measure flow undisturbed speed and ideal gas law to calculate air density from pressure and temperature

$$\rho = \frac{p}{RT} \tag{3.7}$$

Where gas constant is $R = 287\ Kj/KgK$. Pressure and temperature are measured respectively with a mercury column and a thermocouple.

The power coefficient is now simply calculated by the equation 3.1 with the ratio between mechanical and electrical power. A normal value of power coefficient for a Savonius wind turbine is in the range of $C_P = 0.1 - 0.3$, due to the small dimensions of the system we expect a lower value. However, since this is a qualitative measurement, the real result will come out from the comparison between the different positions.

3.1 EQUIPMENT

3.1.1 PIV

PIV is an experimental tool which involves a photographic recording of the motion of microscopic particles to provide instantaneous velocity vector in a cross-sectional flow. With enough particles, the entire velocity field of the flow can be determined. Known the velocity field, data such as vorticity, turbulence intensity and strain are easily calculated. By means of a camera, two velocity components are measured, but using a stereoscopic approach could be possible to recorder all three velocities components. The additional use of modern digital cameras and dedicated computing hardware give a real-time velocity map, which is the same output of a CFD tool. Considering a sequence of maps it is obtained a development in time of the flow field with a fixed time step.

Set-up for PIV is quite complex but the advantages of this technique are definitely high; PIV is non-intrusive measurement technique since the only intrusive component are the micro-sized particles inside the flow. The velocity range that is ideally able capable to detect is almost infinity and goes from 0 (stationary condition) to supersonic.

PIV is a system made of a double-pulsed laser, which emits two pulses with a fixe time step Δt. These two pulses passing from two spherical lenses, to control the pulse size, and one cylindrical lens, to expand the beam in one direction, generate a laser sheet. Making the laser sheet covering to the target area, each seeding particles in the flow passing through it will reflect the light. The reflected lights of each pulses will be captured by the cameras in sperate image frames. Synchronizing the laser pulses with the cameras, the light can be detected by the pixels of the camera and, correlating the images captured, can be calculated velocity vector field. With a post process the velocities, the turbulent intensities and other parameters can be easily obtained.

Velocity vectors are derived from sub-sections of target area by measuring the particle-seeding movement between two following pulses with a simple formula

$$\bar{V} = \frac{\Delta \bar{x}}{\Delta t} \tag{3.8}$$

To better correlate the frames, images are divided into smaller subsections called interrogation areas (IA). IA of two following frames are cross correlated pixel by pixel resulting in a signal peak, which identifies the particle displacement, Δx.

$$C(s) = \int\int_{IA} I_1(X) I_2(X) dX \tag{3.9}$$

$C(s)$ is the correlation function that depends on the variable s, which is the displacement. The peak of this function identifies the particle displacement that better link the two frames in the considered interrogation area. A more precise measure of displacement is performed by means of subpixel interpolation. Performing this procedure for all interrogation area of the image a velocity vector map over the whole target area is obtained.

Considering the application of PIV in air flow, seeding particles are typically in the range of 1-5 μm, this value allows to have a good signal peak in cross-correlation, which is the main parameter that evaluates the measurement precision. As rule of thumb, to have a good result each interrogation area has to have particles in a range between 10 and 25.

The set-up of PIV measurement must take into account the side length of interrogation area, d_{IA}, and the image magnification, s'/s. Balancing them with the wind flow characteristic of the experiment allows to have a proper measurement:

$$\frac{\frac{s'}{s}|V_{max} - V_{min}|\Delta t}{d_{IA}} < 5\% \tag{3.10}$$

Δt is decided based on the mean flow velocity and the pixel dimension. The best measurement of PIV is obtained when a tracking particle travels a length equal to several pixels during the time that elapses between two pulses. Delay in time of the second pulse is determinant for a good value of the correlation parameter, time gap too long brings to have some particles leaving the target area during the second pulses, which result in a bad evaluation of velocity vectors. On the contrary, time gap too low determines a particle displacement too short, which can cause a wrong estimation of velocity vector field.

The highest measurable velocity is constrained by the size of IA, if the particles travel further than that length during the time step Δt, correlation of that particle is lost and information about velocity as well. As a rule of thumb we can consider the following equation:

$$\frac{\frac{s'}{s}\mathrm{V_{max}}\Delta t}{d_{IA}} < 25\% \tag{3.11}$$

For a good result is important to set the right setting of power and pulse duration, a high power light source is required to have a good photograph of the light scattered by the tracer particles. Instead, duration of illumination of the pulse must be sufficiently short so that the motion of particles can be considered ''frozen'' during the pulse exposition. It must be also high enough so that scattered light is captured by the pixels of the cameras.

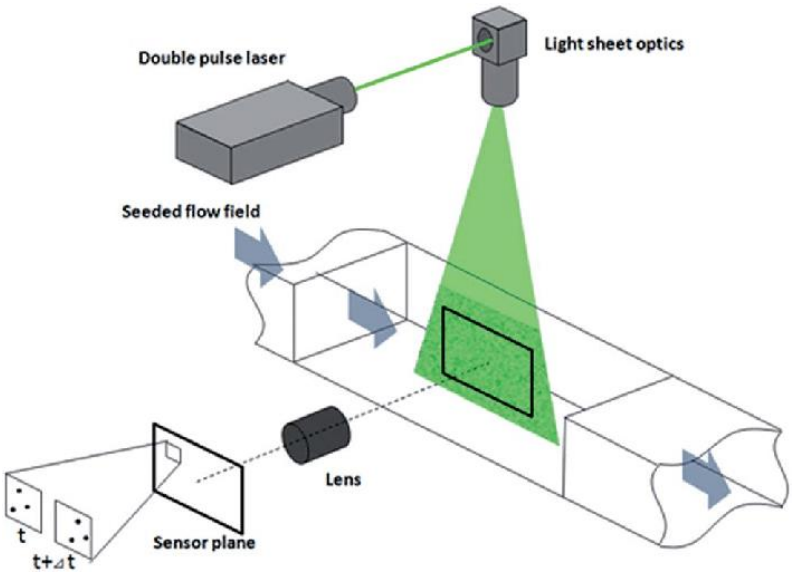

Fig. 3.2 PIV common setup for wind tunnel experiments

3.1.1 DC MOTOR

DC motor is a device which converts electrical power into mechanical work, more precisely it converts current and voltage into rotational speed and torque. It is a widespread technology based on principle of Lorentz Law: ‘’*the current-carrying conductor placed in a magnetic and electric field experiences a force*’’.

DC motor is made of two main components: the rotor, which is the rotating part, and the stator, which is fixed. The rotating part, also called armature, is made of copper coils which are electrically connected to the DC supply. Armature coil is made of two parts: the commutators, which convert the AC induced current in the armature into DC current, and the brushes, which transfer the current from rotor to stator (fig.3.3).

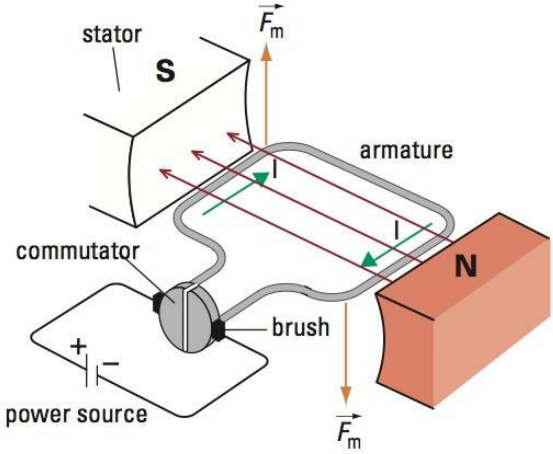

Fig. 3.3 DC motor simplified scheme

Stator is divided into north (N) and south pole (S), this generates a magnetic field which induce a force F into the armature. The force generated by the magnet causes the rotation of the armature, which is then proportional to the magnetic force, as seen in Fig.3.4.

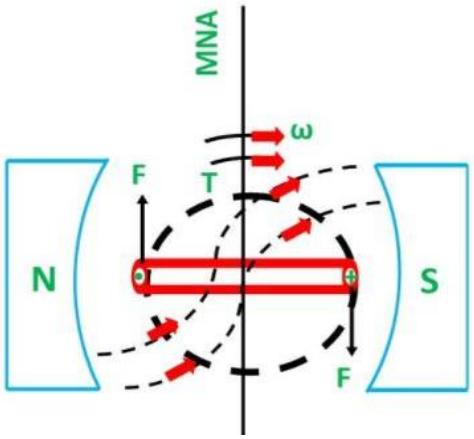

Fig. 3.4 Single coil DC motor operation scheme

The current enters the armature coil through the north pole and moves toward the south pole, therefore the torque induced in the coil become zero when armature is perpendicular to the main field. This zero-torque position is defined in the fig.3.4 with the Magnetic Neutral Axis (MNA). The zero torque means that the motor stops rotating, to overcome this problem the armature is made of several coils radially distributed, therefore, when a coil is perpendicular to the field another one induces the torque and rotor move continuously and uniformly (fig.3.5).

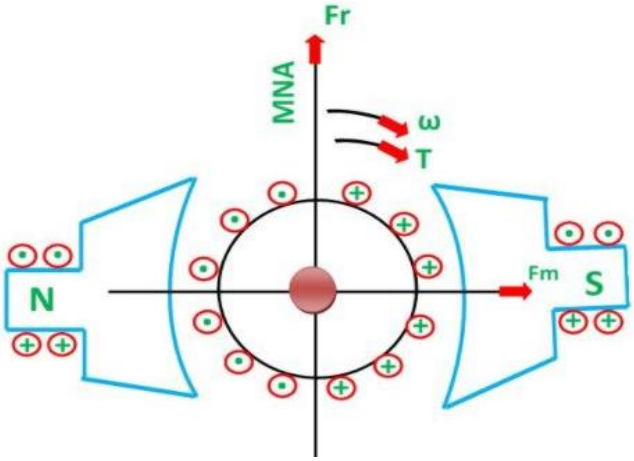

Fig. 3.5 Multiple coils DC motor scheme

CHARACTERISTIC CURVE of a DC MOTOR

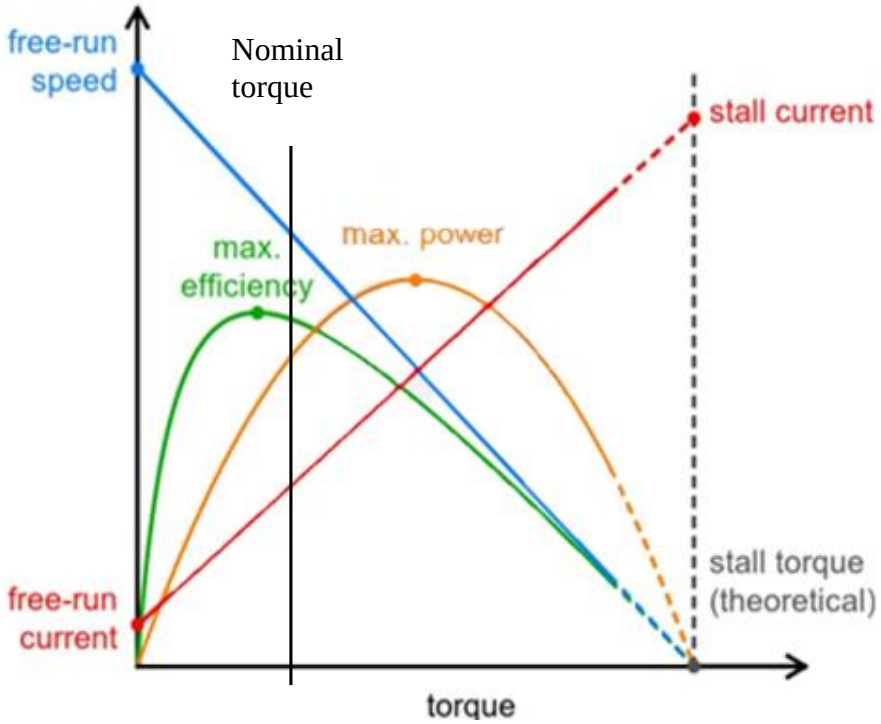

Fig. 3.6 Characteristic curve of brushed DC motor

In fig.3.6 is shown the characteristic curve of a brushed DC motor, with different variables expressed as function of torque. As already seen in the equation 3.3, current and torque are linearly related. In the same way voltage across armature (coils) of motor has an influence on the actual speed (fig.3.7), as already seen in equation 3.4. This means that for a given armature, the speed can be increased by rising the voltage across the armature, this behaviour is at the basis of speed control. By the graph in fig.3.6 it is possible to deduce that speed reach the maximum when the torque produced by the motor is null. Thus, this value is called no-load speed and it is defined as the condition when no load is linked to the motor shaft, which can so spin freely. The other end of the curve identifies the stall torque where the torque is maximum and then there is no speed.

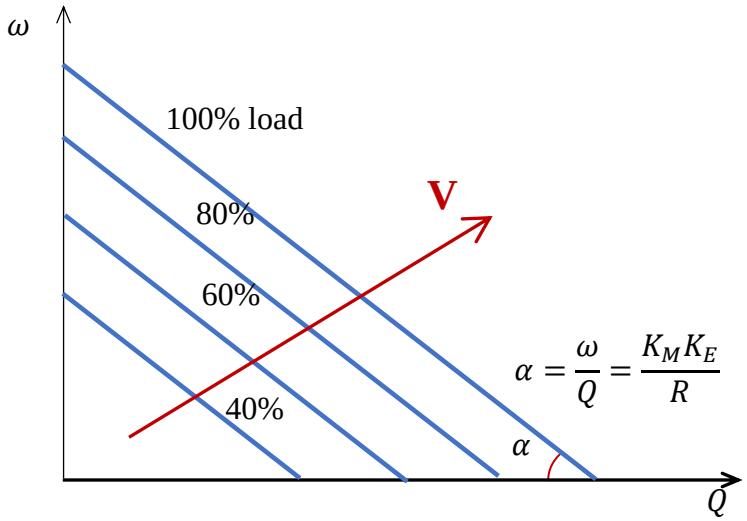

Fig. 3.7 Voltage influence on DC motor characteristic curve

The relation between torque and speed is linear and identifies, as with speed, two values: no-load current, when torque is null, and stall current, which is maximum value. Stall current is considered the starting current as when the motor starts moving the speed is almost null and the torque, and thus the current, is maximum.

Motor is governed by two main equations, the first is the conservation of energy:

$$P_{electrical} = P_{heat} + P_{mech} \tag{3.12}$$

Where P_{heat} is the power lost by the motor as heat and P_{mech} is the useful power provided by the motor. Heat power is mainly lost because joule effect, thus it can be expressed as function of the current and the motor internal resistance R:

$$P_{heat} = RI^2 \tag{3.13}$$

The electrical power, by definition, can be expressed as the product of the current and the voltage

Remembering the expression of mechanical power, already used in equation 3.2, the conservation of energy (equation 3.12) can be rewritten:

$$IV = I^2R + Q\omega \tag{3.14}$$

Where τ is the motor torque, ω is the rotational speed and R is the armature resistance inside the motor. The second main equation of DC motor is the relation that govern the motor voltage:

$$V = IR + L\frac{di}{dt} + V_{emf} \tag{3.15}$$

V is the voltage applied to the motor, L is the inductance of the motor which is related to the instantaneous time variation of current and V_{emf} is the back-emf. This equation results from the second Kirchhoff law applied to the circuit mesh of the DC motor (fig.3.8). In our experiment, as we consider a steady state condition, influence of inductance can be neglected.

Motor characteristic curve, described above, depends on a fixed voltage value. Varying the voltage, the curves that express the relations are scaled. In the datasheet is provided a nominal voltage, which is the value at which other parameters in the datasheet are referred.

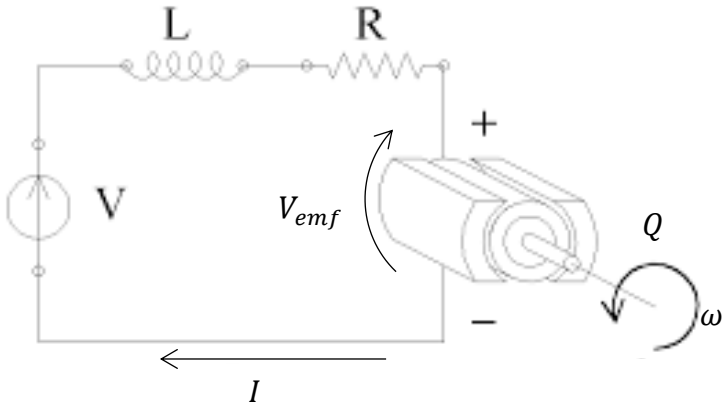

Fig. 3.8 Electric circuit of a DC brushed motor

V_{emf} is the voltage induced by the rotation of the motor armature in opposite direction to the rotation, thus it acts against the applied voltage. V_{emf} is directly proportional to the rotational speed of the motor, faster the motor spins, greater is the back-emf that must be overcome. Thanks to the linear relation with rotational speed, back-emf is defined by the following equation

$$V_{emf} = K_E\omega \tag{3.16}$$

Where K_E is the back-emf constant given in the datasheet, that relates the back-emf to the rotational speed (equation 3.4). As already anticipated in previous chapter, another constant is defined to relate torque and current (equation 3.3), these two constants if expressed in SI units are equals (see equation 3.5). DC motor can be defined by one more constant, K_s, called speed constant, which is simply the inverse of the back-emf constant, but can be useful for further calculation:

$$K_E = \frac{1}{K_S} \tag{3.17}$$

Substituting equation 3.3 that relates torque and current in the energy balance (equation 3.14), it results

$$IV = \mathrm{I}^2 R + K_M I\omega \tag{3.18}$$

As all the power component are dependent on the current, equation 3.18 can be simplified respect the current. Solving then for ω:

$$\omega = \frac{1}{K_M}(V - IR) \tag{3.19}$$

Substituting the current with its torque relation (equation 3.3) and rewriting, it results:

$$\omega = \frac{1}{K_M}\left(V - \frac{Q}{K_M}R\right) \tag{3.20}$$

Adopting the speed constant instead of the torque constant equation 3.17 is

$$\omega = \mathrm{K_S}(V - QK_S R) \tag{3.21}$$

This equation represents the speed-torque curve, thus the no-load speed $\omega_{no-load}$ can be found by setting the torque equal to zero, $Q = 0$

$$\omega_{no-load} = K_s V = \frac{QR}{K_M K_E} \tag{3.22}$$

This expression tells us that no-load speed of a motor is directly proportional to the input voltage. In the same way we, can find the stall torque setting the speed equal to zero, $\omega = 0$, in the equation 3.21.

$$Q_{stall} = \frac{V}{K_s R} = \frac{VK_M}{R} \tag{3.23}$$

From equation 3.19 was observed that relationship between speed and voltage is linear, from equation 3.21 it can be deduced that current and torque are linearly related.

Stall current, also called starting current, can be expressed as function of the stall torque by equation 3.3, it results:

$$I_{stall} = \frac{Q_{stall}}{K_M} = K_s Q_{stall} \tag{3.24}$$

In graph in fig.3.6 the no-load current is not starting from zero, this is due to the friction and inertia that the motor must overcome even in the case of none load linked. Therefore there will always be a current draw with low torque.

To find the equation for power curve observed in fig.3.6, expression of rotational speed in equation 3.21 can be multiplied for the torque:

$$P_{mech} = \mathrm{Q}\omega = \mathrm{Q}[K_s(V - K_s RQ)] = K_s VQ - K_s^2 RQ^2 \tag{3.25}$$

By this equation it is deduced that power as function of torque is a convex parabola as it is dependent on $-Q^2$. To find the maximum power it is derived the power respect the torque and equaled to zero

$$\frac{dP_{mechanical}}{d\tau} = K_s V - 2K_s^2 RQ = 0 \tag{3.26}$$

Solving for the torque Q

$$Q(P_{max}) = \frac{1}{2}\frac{V}{K_s R} = \frac{1}{2}Q_{stall} \tag{3.27}$$

By simple math calculation it is stated that the torque which maximize the power is half of stall torque, which is the maximum value.

The efficiency of a DC motor is simply defined by the ratio between the output power, which is mechanical, and the input power, which is electrical:

$$\eta = \frac{P_{mech}}{P_{el}} \tag{3.28}$$

DC - GENERATOR

A DC machine is an electrical system that converts direct current (electrical energy) into mechanical energy and vice versa. This machine can be used as motor as well as generator, depending on weather the current is provided as input or output. DC motor speed can be controlled by using a variable supply voltage, in the same way generator speed can be varied by changing the load to power. A DC motor can be easily employed as a generator independently by the presence or not of brushes. A brushless motor is more performant but requires a rectifier to pass from AC to DC output, in contrast, brushed machine has directly a DC output due to the presence of commutators, which acts as rectifier converting AC induced voltage into DC.

Working principle of DC generator is based on Faraday's laws of electromagnetic induction: ''*when a conductor is located in an unstable magnetic field, an electromotive force gets induced within the conductor*''.

3.1.2 PHOTOTRANSISTOR

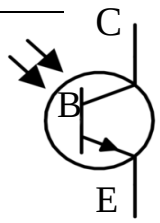

The phototransistor is a device that has the ability to detect the level of incident radiation and consequently change electric current flow between emitter and collector terminals. It is classified as a three-layer semiconductor device, hence it is made by a base (B) which catches the light and passes it down to the emitter (E), which in turn transmits the impulse to the collector (C) in form of current.

The phototransistor is basically the upgrade of a photodiode, since both are light sensing device, the main difference is that in phototransistors the light energy falling on the base region acts as the overall input of the device. So, phototransistor is the combination of a photodiode, which exploits principle of photoelectric effect transforming incident light signal incident into current, and a transistor, which permits the amplification of the current flowing through.

Advantages of phototransistor are high sensitivity, low complexity and low cost, on the contrary it provides a low-frequency response and a low ability to effectively detect small amount of illumination. The operation of phototransistor depends on the intensity of radiation falling at base region. Without incident light there is only a small thermally generated leakage current, I_{CEO}, called dark current, which is typically in the range of nA.

Phototransistor are not sensitive to all light but only to light in a certain wavelength range, usually they are most sensitive to red and infrared part of spectrum. This allows a better working of this transducer in the darkness, where there is no background light that can influence the receiver.

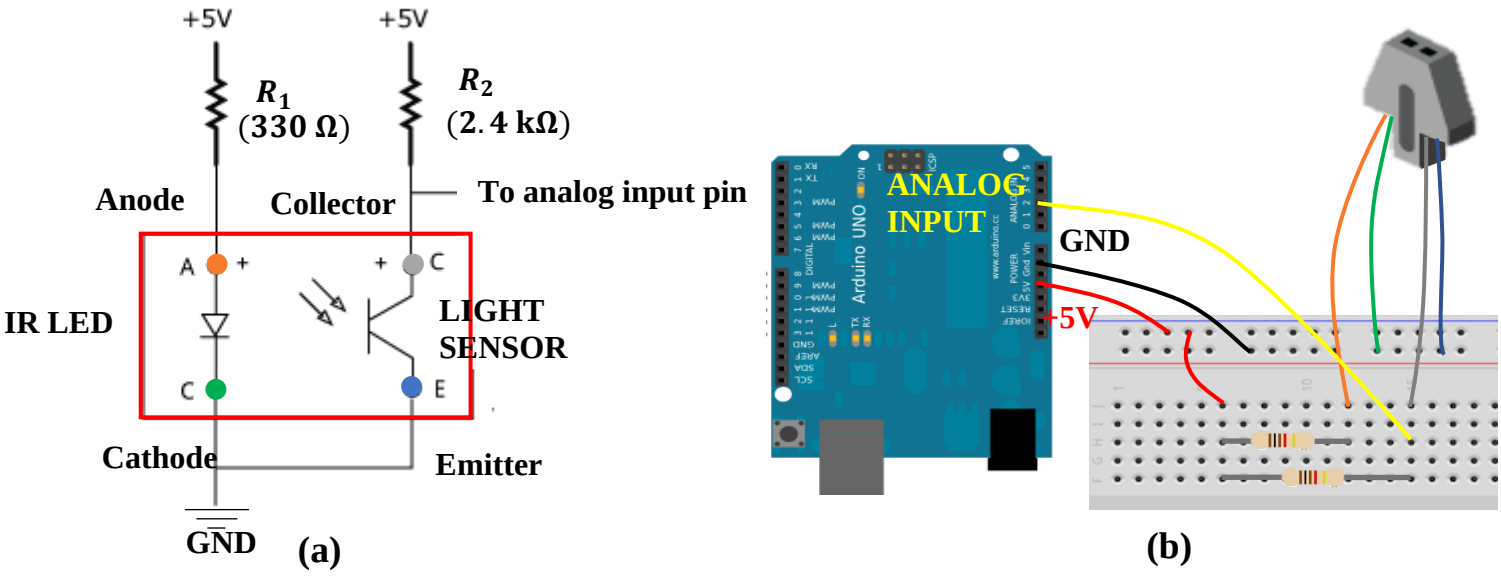

Fig. 3.9 (a) electric circuit of the photo-transistor, (b) scheme of the phototransistor wiring to the arduino board

In fig.3.9 is shown the electrical circuit for the use of the phototransistor (a) and a real scheme of the circuit (b), in our experiment it was used a phototransistor OPB704WZ by TT electronics, which adopts a IR LED of 890 nm wavelength. For the analog read and 5 Volt supply is used an Arduino UNO Rev3 that allows both to power the circuit and to read the sensor value output.

In the electrical circuit, Fig 3.9a, on the left is placed the IR LED, which emits light, and on the right is situated the receiver, which collects light. The red square highlights the electrical part that are placed inside the phototransistor, therefore two resistance are required to be added to complete the circuit. First resistance is used to control the input current value in the diode and the minimum value required is calculated simply applying first Ohm law:

$$R_{min} = \frac{V}{I_{max}} = 125\ \Omega \tag{3.29}$$

Where V is the supply voltage, 5V in this case, and I_{max} is the current limiting sensor, which is equal to 40mA for common LED. Thus, with a resistance lower than R_{min} the current generated is to high and it will break the IR LED. By this formula, we consider a first resistance of 330 Ω.

The second resistance is used as amplification of the current generated for the light absorbed by the receiver, so this value must be high enough to generate a voltage that could be read in output, in our case we consider a resistance of 2.4 $K\Omega$.

Phototransistor is used to detect the light intensity and thus can be used for monitoring the rotational speed of shaft by the only use of a reflecting tape. For a good application of this transistor, is useful to know the optimized distance of the surface with the reflecting tape from the IR LED. The manufacturer in the datasheet provides a clear graph of the phototransistor performances in function of the object distance (fig.3.10), which suggest us to place the object, covered by the reflecting tape, at mostly 5 mm.

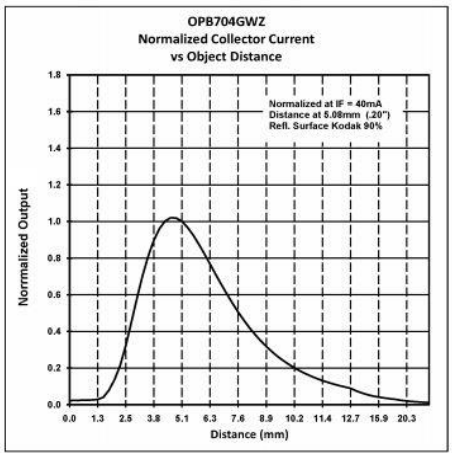

Fig. 3.10 sensor output voltage depending on the distance of the reflecting object

3.1.3 CURRENT SENSOR

Current sensor is a device to measure the current running through a wire by using the magnetic field to detect the current and generate a proportional output. Main advantage of current sensor is to perform the measurement passively, without interrupting the circuit. In our case we adopt the Adafruit INA219 Current Sensor, with the internal 12 bit ADC and a 0.1 Ω current sense resistor, which has a resolution of $0.8mA$ with a range of $\pm 3.2A$. In fig.3.11 is shown a scheme of the wiring of current sensor with the DC motor by means of an Arduino UNO Rev3 board used both to supply voltage to the sensor and to read the DC motor output current value.

Since both motor and Arduino board work with 5V of voltage supply, it can be used a directly the USB port of the computer without adding an external supply to power up the system. In case of a more powerful motor is enough to add a power supply, a normal battery, in between the ground (black wire) and positive pole of motor (orange wire).

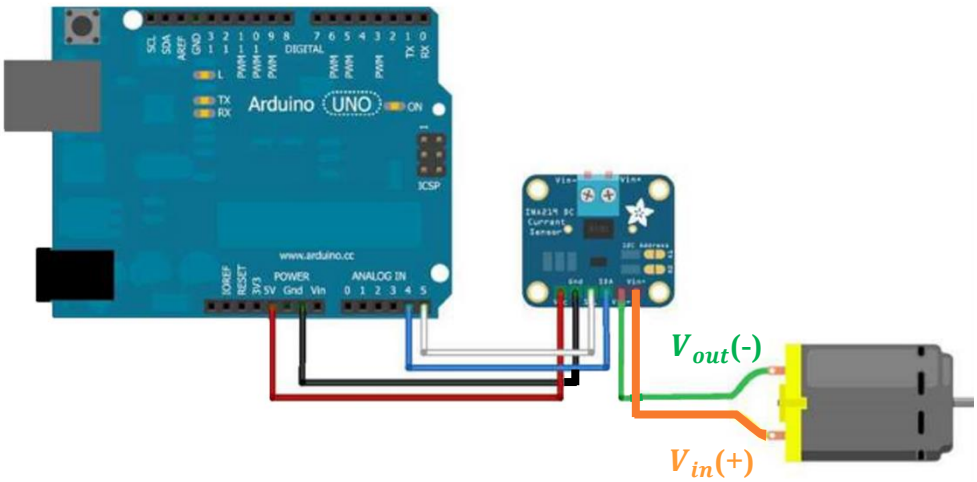

Fig. 3.11 INA 219 current sensor circuit scheme for DC motor current measurement

3.1.4 MOSFET

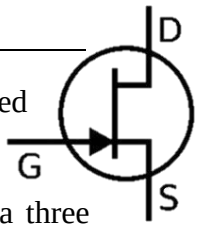

The mosfet (Metal Oxide Semiconductor Field Effect Transistor) is a voltage-controlled device where the potential difference determines its conductivity, thus it is mainly used for amplifying or switching electronic signals with very low power consumption. It is a three terminal device made by three pins: gate (G), drain (D) and source (S); by applying a voltage to the gate pin, the mosfet will start conducting through the drain and source pin.

Most common applications of this transistor are like a switch of a circuit, only applying an input voltage V_{GS} to the gate it is controlled the current across the drain and the source pins. There are mainly two different categories of mosfet, the N-channel and the P-channel, the first category acts as a switch always open until a gate voltage is provided, when it close, by contrast the second category works in opposite way acting as a closed switch until a gate voltage is applied.

Considering a N-channel mosfet, voltage applied to the gate generate a conductive bridge on the substrate of the transducer, causing the increase of conductivity and the consequently drain current (I_D) flowing on it between source and drain. Conductivity depends on the magnitude of applied voltage, hence higher the voltage will let more current pass through the device.

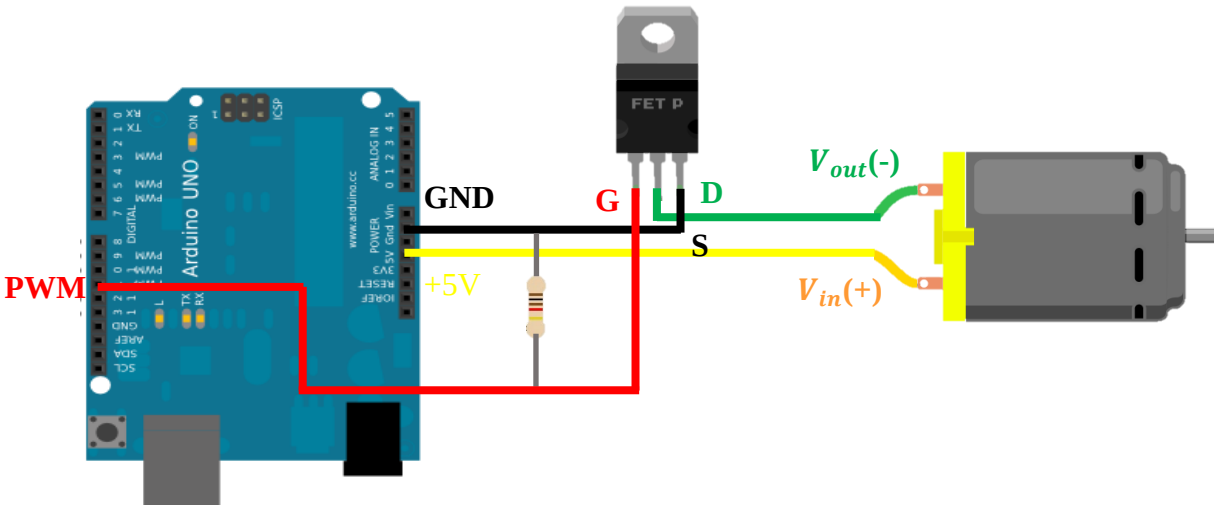

Fig. 3.12 Electrical circuit with mosfet for regulation of DC machine (Mosfet used is IRF540 N-channel by International Rectifier)

In fig.3.12. is shown the circuit wiring for the use of the mosfet to control the current of a DC motor. Gate (G) of mosfet is linked with Source (S) with a 10 $k\Omega$ resistance useful to slow down the turning on and off of the mosfet, this decreases the switching losses without affecting the mosfet properties. A diode can be added between positive and negative pole of DC machine to avoid reverse current, this component is optional.

Mosfet is powered with a PWM (Pulse Width Modulation) pin of Arduino board which allows to use a duty cycle to have an analog signal with digital means. PWM works using digital signal to create a square wave with 1 and 0, where 1 switch the pin on and 0 switch it off. To the value of 1 is associated the potential difference applied by the board (V_cc), while to the value of 0 is related a 0V. The rapid alternation of on and off configuration of the pin can simulate the values in between the full potential difference (V_{cc}) of the board (usually 5 or 3.3V). Therefore, the regulation of voltage applied is performed setting the portion of time that signal is on, duration of ''on time'' is called pulse width. If the switching on and off is fast enough a device can feel a steady signal with a value between 0V and V_{cc}, like an analog input. For a more clear understanding, with a V_{cc}=5V and a duty cycle of 75% the device will receive a square signal where 75% of time is on, thus value is 1 and the voltage is 5V, and the remaining time is off, thus value is 0 and voltage is 0V. As the frequency of switching on and off is at 500Hz the device feels like a constant signal at 3.75V (75% of V_{cc}). Arduino works with 8 bit for the input pins, hence the PWM can use the values between 0 and $2^8 - 1 = 255$, where 255 is 100% of duty cycle and pin always on, while 0 is 0% of duty cycle and pin always off. In this case PWM allows to use values between 0 and 5V to control the mosfet operation and regulate the current flow in the DC machine, more details on the section 3.3 (speed regulation).

3.1.5 PITOT TUBE

Pitot tube is the simplier and more common technique for a puntual measure of flow speed. It is made of a slender tube that has two holes on it: the front hole is placed in the airstream to measure the stagnation pressure (also called total pressure), while the side hole is placed a bit back and measures the static pressure. By measuring the difference between these two pressure it is obtained the dynamic pressure which is related to the speed. Stagnation pressure indicates the pressure of fluid including the effect of velocity. Dynamic pressure is the pressure compenent due to the only fluid velocity. To calculate the vlocity by means of the pitot tube can be easily solved the equation :

$$p_T = p + \frac{1}{2}\rho V^2 + gz \tag{3.30}$$

Where p_T is the total pressure, p is the static pressure, gz is the gravitational component that in wind tunnel experiment can be considered negligible. The pitot tube allows to measure the pressure difference $\Delta p = p_T - p$ and with a simple calculation can be find the airflow speed:

$$\mathrm{U} = \sqrt{\frac{2\Delta p}{\rho}} \tag{3.31}$$

The only parameter that is required to be known is air density, which can be easily calculated considering pressure and temperature with the law of ideal gas as already seen in equation 3.7.

Pitot tube has very simple construction and can be easily used in most of the system. In a wind tunnel experiment, with interaction between objects, pitot tube allows to know undisturbed flow speed if placed far from any possible disturbing object and perpendicular to the cross section of the tunnel

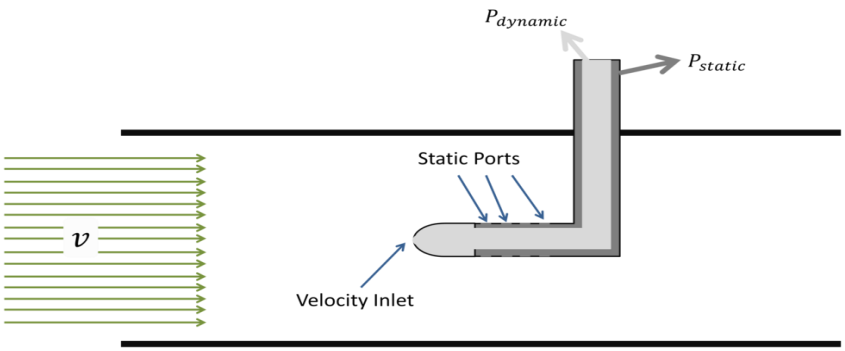

Fig. 3.13 Pitot tube scheme

(fig.3.13). Density of air is considered constant in these experiments since the flow speed is much lower than sonic speed (M<<0.3), therefore Bernoulli equation describes the relation between pressure and velocity along a streamline (considering negligible the potential energy).

3.1.6 TURBINE

Turbine is the main component of the whole system and is 3D-printed, due to the small size. Since the purpose of this experiment is qualitative and not quantitative, the turbine design adopted has been the VAWT with Savonius design due to its simplicity. Savonius VAWT turbine is made of two half-cups link together in opposite direction (fig.3.14a). A small gap can be present in the overlap allowing the flow to pass from one to the other half-cup, this increases the performance in terms of power coefficient but decrease the cut-in speed ability [86]. Turbine is covered with a sprayed layer of matt black paint to avoid undesired reflections during PIV measurements (fig.314c).

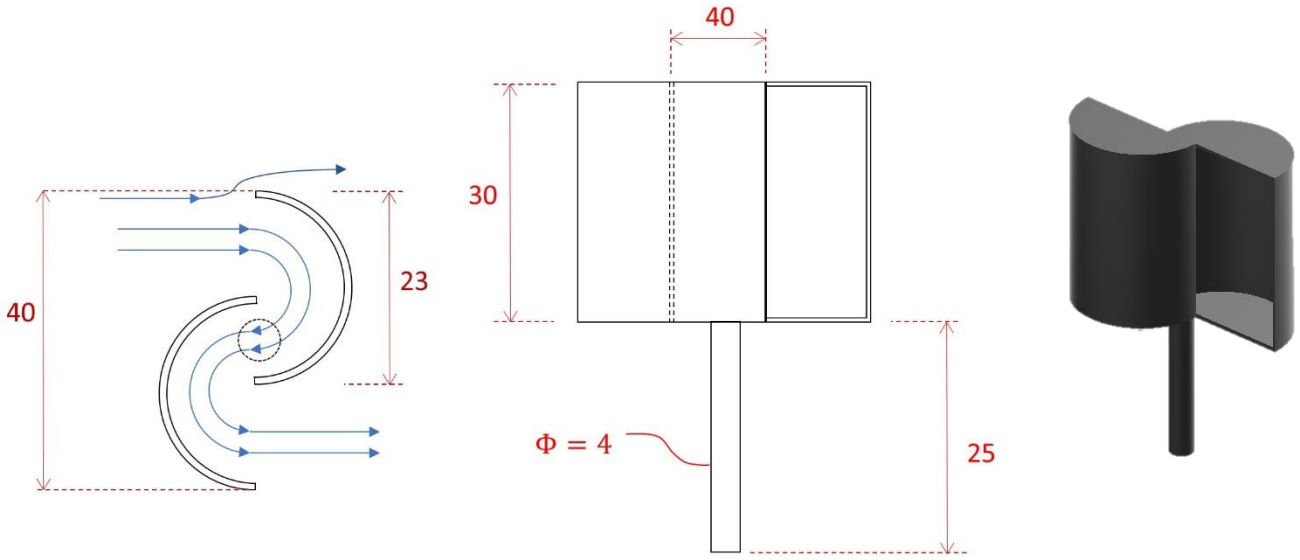

Fig. 3.14 a) turbine section from up; (b) turbine section from side; (c) turbine CAD

Geometry of the turbine is chosen based on the cube dimension. The turbine is lifted of 10% of the cube height (H) from the top of the cube, and has a diameter corresponding to 40% of H.

3.1.7 PLATE AND CUBES

Plate where the system is placed is made of polyacrylic material, which is transparent, strong and flexible. This material allows to easily work on it, making holes and cuts, and to use PIV laser without any undesired reflection.

Buildings are modelled as simple cubes and are painted with matt black paint to decrease the reflectivity on the cube upper face, this is important to minimize the reflection of PIV laser. Reflectivity can be minimized by increasing transmissivity, such as using transparent material like for the plate, or absorptivity, such as adding a layer of black paint.

A low reflectivity is important because laser can be reflected toward the camera lens and damage them, since the pixels have a light saturation level that can't be overcome. All the system is modelled in fig.3.15 below.

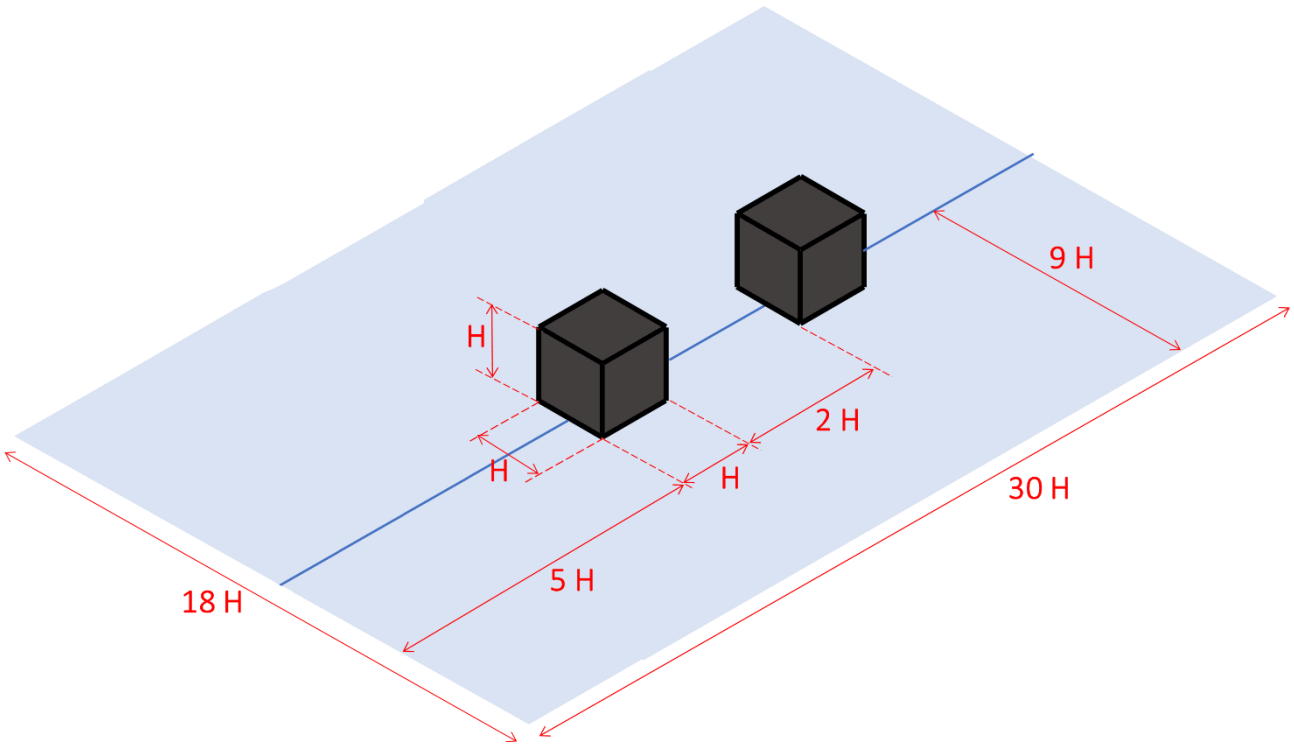

Fig. 3.15 System dimension related to the cube height H

3.1.8 WHOLE SYSTEM

Bearing is a common component in system with rotational and stator part. In this kind of system it can be useful the use of a bearing to keep the shaft in position and avoid the shaft to wobble, moreover, bearing is important to absorb axial load. Due to the small size of the system and the low magnitude of forces, the presence of a bearing could highly affect the torque measurement due to the additional friction. Thus, as the turbine is considered rigid enough to sustain axial loads of wind, the bearing is not used.

The whole system is made by all the components described in the previous sections, cubes are placed on an acrylic plate and fixed with some screws, they are previously drilled in 3 different positions on the top side to allow the turbine shaft pass through. Inside the cubes is positioned the DC motor (fig.3.16), which is linked axially with the turbine with an interference fit. Inside the cube is also placed the phototransistor looking directly at the turbine shaft where a reflective tape is stuck. The cables of all electrical components are brought outside the wind tunnel where are linked to the Arduino UNO board, which is in turn powered by the computer. Above the cubes, outside the wind tunnel, is laid down the laser for the PIV measurements, the cameras are instead placed on the side of the wind tunnel. Each camera has a target area on the laser sheet of 20x30 cm, so using 2 cameras can be ideally reached a target area of 40cm long; since the cameras need a overlapped region to merge the frames, it is reached a target area of 38x30 cm. Downstream cube is placed 2 cube height far from the back of the first cube (fig.3.1), to have a good idea of the flow field it is important to acquire also part of the zone upstream the first cube and downstream the second. By this consideration, the area required to be acquired must be at least 1 meter long, it is then necessary to make three different acquisition in three different position to acquire the whole field we are interested in. To acquire different position, instead of moving PIV laser and cameras, is moved the whole system by only moving the acrylic plate where system is laying.

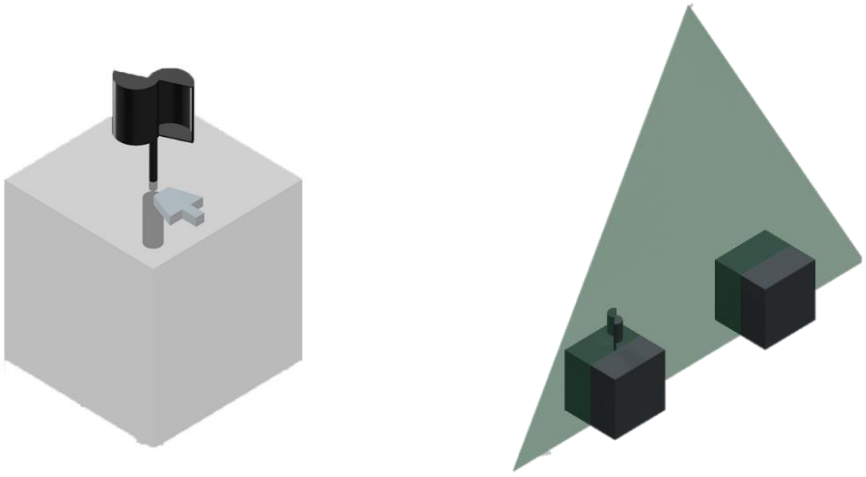

Fig. 3.16 Representation of the system assembled, the green triangle represents the laser sheet shots from above

3.2 POWER EXTRACTION

Wind tunnel experiments are considered one of the most important method for the study of aerodynamic performance of wind turbines and wake evaluation [309]. Wind tunnel experiments allow to simulate different scenarios under controlled conditions, thus, keeping some variable fixed it can be understood the influence of some parameter to the flow characteristic and wind turbine performance.

Reynolds number in wind tunnel flow is inevitably different from the one in the ABL, therefore miniature turbines used for experiments have a poor performance compared to the large-scale counterparts. In general, wind turbine performance is quantified by two main coefficients that normalize torque and power to the wind energy content, as already described on previous sections.

Size of miniature turbines must be much lower than wind tunnel cross sectional area in order to avoid the influence of the wind tunnel walls that can interfere with the model, which is known as the blockage effect. Generally, it is relevant when the blockage is more than 5%, in these experiment in the most conservative calculation it results 3.8%. However, an excessively small miniature turbine worsens the scaling effect due to the different Reynolds number ($Re_c = \rho d U_{rel}/\mu$) between ABL and wind tunnel flow.

Sunda et al. [310] showed that common airfoil suited for high Reynolds number, have a very poor performance in low Reynolds number conditions, in their study are suggested some characteristic that characterize airfoil for low Re: a small thickness, about 5% arc camber and a sharp leading edge.

The power coefficient (C_P) is useful for the evaluation of the turbine efficiency, which is mainly the ability of the machine to extract power from the wind flow.

Although some research tried to improve the efficiency of miniature turbines, in all the prior wind tunnel studies performances were inferior in comparison on their large-scale counterpart. The power extracted by the turbine P_{mec} is constituted by the turbine shaft Q_{sh} and the rotational speed Ω. This mechanical power, by means of the generator coupled with the turbine, is then converted into electrical power P_{el}, characterized by voltage and current.

To calculate the mechanical power, it is necessary to have both variables, torque and rotational speed. Despite the rotational speed of the turbine can be easily measured in every condition due to the simplicity of the measurement and to the several different methods available. The torque is a bit more complicated. Only few studies in literature were able to directly measure the shaft torque of miniature wind turbine (d<50cm) [103] because such low values have a very low accuracy in the measurement.

Electrical power (P_{el}) is always lower than mechanical power (P_{mech}) in energy production due to the friction and electrical losses, respectively P_f and P_j (fig.3.17). Thus, the power balance is expressed by the equation:

$$P_{mech} - P_f - P_j = P_{el} \tag{3.32}$$

As P_{el} is affected by the generator efficiency, it can lead to a wrong understanding of the wind turbine performance [33]. Friction losses are caused by the contact of rotating parts with static ones, this mainly occurs in bearings, if present, and in the generator. Electrical losses depend on the internal resistance of generator that includes the resistance of both armature and brush contact of commutators, according to the equation 3.33

$$P_j = RI^2 \tag{3.33}$$

To split the power balance (equation 3.32) into two different equations, the converted power has been defined as the intermediate step between mechanical and electrical variables. By means of this new component equation (power balance) is then redefined:

$$P_{mech} - P_f = P_{conv} \tag{3.34}$$

$$P_{con} - P_j = P_{el} \tag{3.35}$$

Hence, P_{conv} is the converted power after the decrease of the mechanical losses caused by friction, otherwise it can be considered as the electrical power content that is decremented by the electrical losses.

In general, power related to mechanical system can always be expressed as the product of torque (τ) and rotational speed (ω). In case of constant rotational speed equation 3.34 can be rewritten in torque terms

$$Q_{sh} = Q_{em} + Q_f \tag{3.36}$$

Where Q_{em} is electromagnetic torque, which is the torque fed into the generator, and Q_{sh} is the shaft torque, which is defined as the torque generated at the turbine shaft by the wind.

The same argument can be done for equation 3.35 since the electrical power can be always defined as the product of potential difference and current. With a constant current equation 3.35 can be rewritten in voltage terms:

$$V_{ind} = V + V_R \tag{3.37}$$

Where V_{ind} is the voltage induced by the converted power,V is the output voltage and V_R is the voltage dissipated by the resistances, hence V_R can be defined by Ohm's law:

$$V_R = RI \tag{3.38}$$

Terminal voltage V is always lower than induced voltage V_{ind} because electrical losses are a dissipative component that decrease the output.

As already seen in the previous section, induced voltage V_{ind} and electromagnetic torque Q_{em} are both linked to the DC machine characteristic because both are produced by the motion of armature inside the generator. Thus, both variables can be expressed as a function of the related coefficients. Both equations are recalled below with the aim to facilitate the reader in following the mathematical passages.

$$V_{ind} = K_E \omega \tag{3.39}$$

$$Q_{em} = K_M I \tag{3.40}$$

Where K_E is the back-emf constant and K_M is the torque constant.

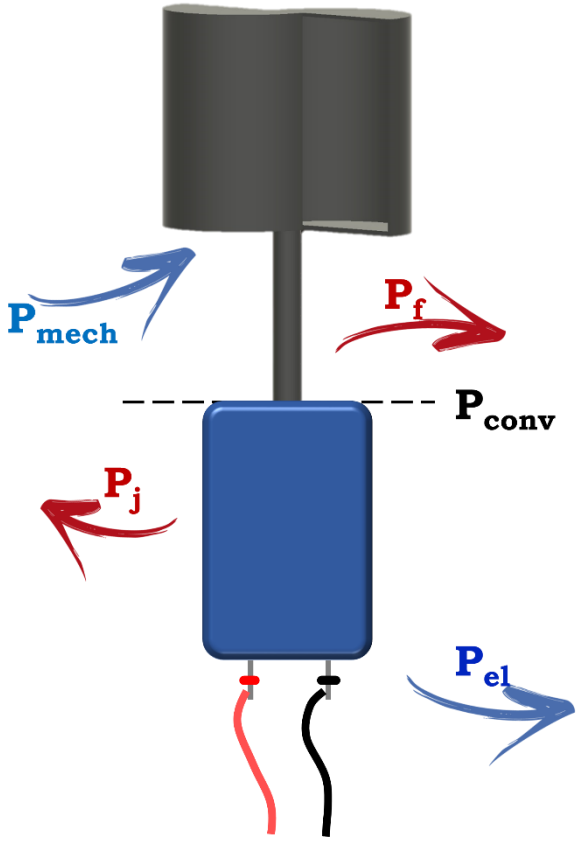

Fig. 3.17 Schematic of power extraction from a Savonius VAWT, losses are marked in red

As the friction torque is dependent by the rotational speed, to estimate the shaft torque it is required to model friction torque. Several models are available in literature, Bastankhah and Porté-Agel[103] considered a linear relation between Q_f and ω, therefore the friction torque can be described as a linear function

$$Q_f \approx \alpha\omega + \beta \tag{3.41}$$

Coefficients α and β can be estimated by the datasheet of DC-machine given by manufacturer (table 5). Usually data provided are in motor mode, but it can be assumed that values are the same for generator mode as well [103]. Considering nominal and no-load conditions, friction torques can be found applying equation 3.36

$$Q_{f,nom} = K_M I_{nom} - Q_{nom} \quad (3.42)$$

$$Q_{f.no-load} = K_M I_{no-load} \quad (3.43)$$

Equation 3.43 doesn't consider any mechanical torque because the no-load condition is evaluated without any load coupled with the DC machine. By the friction torques the coefficients, α and β, can now be calculated; solving the system considering the values for the specific DC machine used in the experiments, it results:

$$\alpha = 5.12 \cdot 10^{-5}$$

$$\beta = -0.4872$$

This method allows to have a more realistic description of the torque influence; thus, it can be adapted based on the actual rotational speed. The manufacturer in the datasheet provides an average value of the friction torque ($Q_f = 0.02\ mNm$), which can be considered valuable considering the coefficients, $\alpha$and β found.

Bastankhan and Porté-Agel [103] validated the relation expressed in equation 3.41 by the comparison between the shaft torque calculated with the relation and the direct measure of the torque by means of a high precision torque transducer. The dependence of the friction torque only by the rotational speed is demonstrated for three different DC machines.

The operating conditions of a miniature turbine can be unequivocally characterized by the rotational velocity and the generated electrical current, which is linearly linked with the torque by the equation (sopra). As the DC machine efficiency is not linear, the use of electrical power can lead to significant

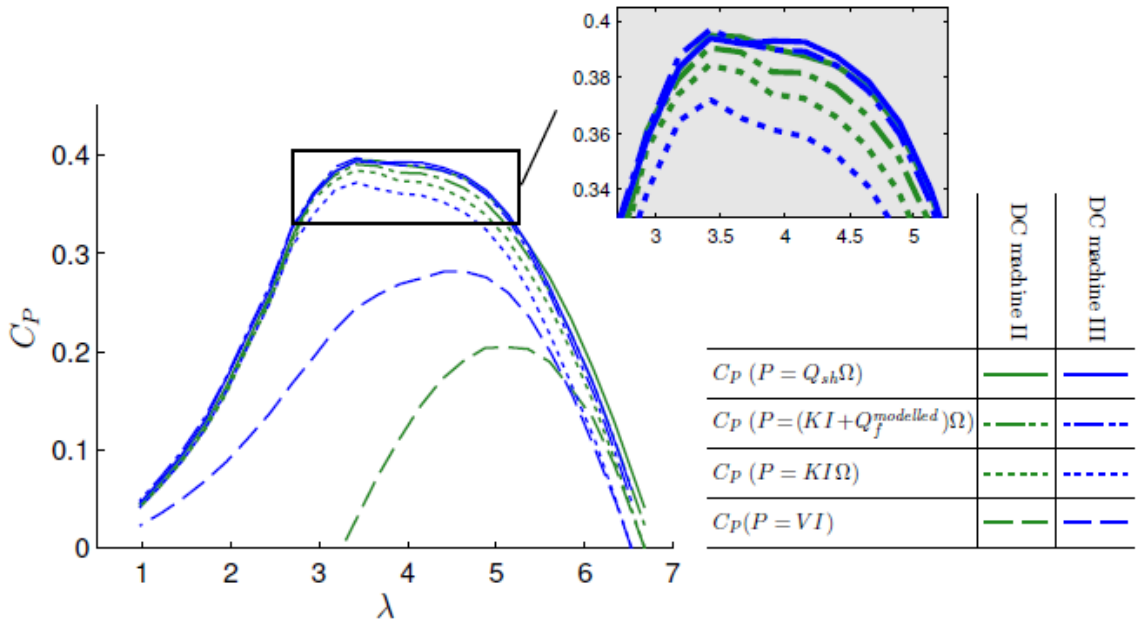

Fig. 3.18 comparison of characteristic curve for two different DC machine with different power definition: mechanical power directly measured (continuous line), mechanical power calculated using friction relation (dashed-dot line), converted power (dot line), electrical power (dashed line) machine [103]

misleading of information about wind turbine characteristics (fig.3.18), thus the use of voltage and current to characterize the power and torque coefficient of turbine is improper. However, the use of the only current to calculate the converted power, avoid the influence of the DC generator efficiency allowing to have a reliable characterization of turbine performance [103]. In fig.3.18 is clear the influence of DC machine efficiency using the electrical power on the calculation of turbine power (dashed line). In contrast, the adoption of converted power lead to lower errors.

An accuracy measure of mechanical power generated by a model turbine is challenging due to the small size, this is of primary importance to quantify the performance of a wind turbine. Torque measurement is complex above all because it is generally an intrusive measurement, that may affect the real value for a so small-scale system.

According to Houck et al. [32] there are four main principles that justify the importance of mechanical power measurement. First, it allows direct comparison among different studies, the use of electrical power considers electrical losses, which are linked to each specific generator, while mechanical power takes only account of turbine. Second, it gives an indication of the ability of the turbine to extract energy from the wind just knowing upstream and downstream velocity, this give a precise characterisation of wind turbine performance. Third, mechanical power is more precise for scaling to large-scale. Last, even if electrical power is attractive due to the simplicity in measuring current and voltage just adding a known resistance as load of the generator, it has many losses source which are hard to control and the efficiency is far to be ideal, so the correlation between mechanical and electrical power is hard to be defined.

3.3 SPEED REGULATION

To study the coefficient performance of turbine is important to be able to vary the rotational speed of turbine (ω), the influence of ω can be performed by mechanical or electrical device. The simplest mechanical way for varying the speed is by means of a friction brake, but this method is hardly predictable and is not suitable to have a good control on the variables. About electrical control methods, there are two ways to change the rotational speed: with a potentiometer, which is a variable resistance, or with a MOSFET, which is a transistor to control the current flowing in a circuit. In the section 3.1.1 (DC MOTOR) is described how torque and speed are linked to current and voltage, thus, to control a mechanical variable (the speed) is possible to act on corresponding electrical variable (the voltage). As current and voltage are linked themselves, the control of speed can be performed varying the current, with a potentiometer, or the voltage, with the MOSFET.

The potentiometer is an electric device, which has the behave of a variable resistance. It allows to control the resistance value to be able to vary the voltage of a circuit. According to the first Ohm law, the resistance affects the potential difference of the circuit without influencing the current, except for a small dissipation due to joule effect. Hence, for a resistance value R, the voltage drop results:

$$V = RI \tag{3.44}$$

Resistive value of potentiometer can be varied electrically or mechanically, by means of a knob, in a range from 0Ω to the max value with a variation that can be linear or logarithmic. A circuit for the control of motor by means of a potentiometer is shown in fig.3.19 below

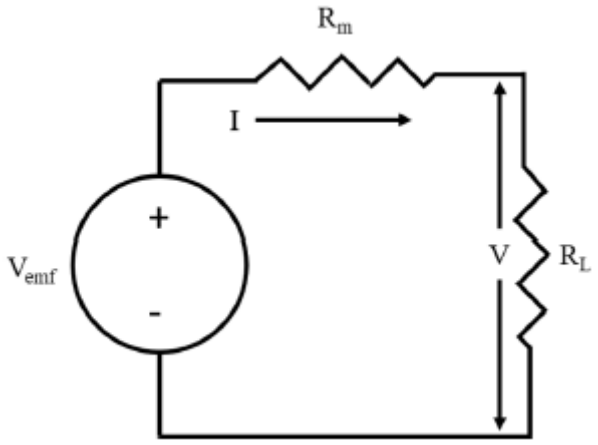

Fig. 3.19 Electrical circuit of a DC generator with a potentiometer for the control of speed, motor is modelled by the back-emf voltage (V_{emf}) and an internal resistance (Rm), potentiometer is represented by the load resistance (RL)

Mosfet has been already treated in section 3.1.4 (Mosfet), it is a transistor that allows to control the current flowing in the circuit. By equation 3.3 it has been defined a linear relation between torque and

current, thus, a variation in the current affect the toque value, which consequently affect the rotational speed.

Mosfet has a characteristic curve which indicates the maximum value of drain-source current (I_D), depending on the gate voltage (V_{GS}) and drain-source voltage (V_{DS}), this value is important not to have a too high power dissipation that can damage the device. In our system the current value is quite small and thus is possible not to pay attention to this specification. To calculate the power dissipated by the mosfet can be applied base electrical formula:

$$P = I_D^2 R_{DS} \tag{3.45}$$

R_{DS} is the internal resistance of the mosfet, which is given by the manufacturer and for IRF540N is 44Ω. Because the values of the current generated by the turbine spinning are in the order of 10mA, the power dissipated by the mosfet is in the order of mW.

The mosfet acts like a partial switch, this allows us to control the current flowing in into the motor and in turn the voltage, which is related to the rotational speed. In fig.3.20 is shown the electric circuit of mosfet configuration for the speed regulation of DC generator. The mosfet gets an analog input voltage

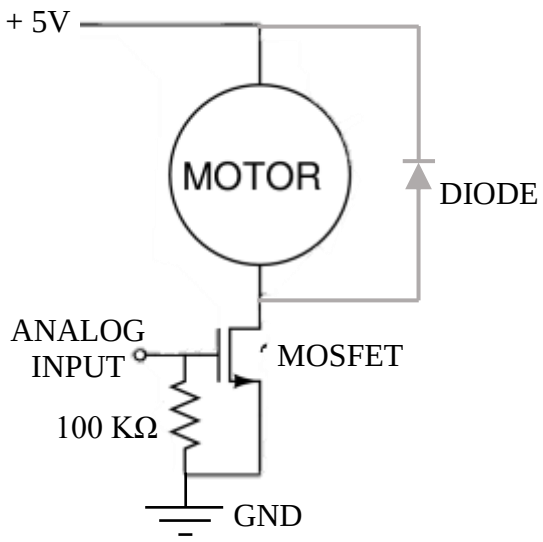

Fig. 3.20 Electric circuit of a MOSFET configuration for the regulation of DC machine speed

from Arduino (5V) which regulates its conductivity, this allows to control the current flowing in the circuit. For our purpose, since it is considered a steady state condition of the turbine, the inductance can be neglected, therefore DC machine is represented only by the back-emf (V_{emf}) and by the internal resistance (R_m).

An optional flyback diode can be placed in parallel to the DC machine to prevent large voltage spikes when the motor is switched from on to off. Since the N-channel MOSFET includes itself a diode which helps to handle the spike, this component is redundant in our circuit. For larger application where

voltage spikes can be considered more relevant, diode presence plays an important role because it is able momentarily to carry the full current of DC machine, which is provided every time motor is switched from on to off.

Till now it has been considered each component individually, but to understand how to operate a speed regulation the whole system must be considered. Our system is quite simple because it is made by the only coupling between wind turbine and DC machine. The spin of the turbine due to the interaction with wind flow makes the DC machine shaft spins, thus it is generated a proportional back-emf voltage. In this configuration DC machine is acting as a generator since the turbine is moving the rotary part of the DC machine, hence current and voltage are outputs of the system.

In fig.3.21 a qualitative representation of the power and torque curve for a Savonius turbine [87]. It is evident that the torque curve has the maximum value at very low speed and, from that point on, the curve has almost a linear dependence. Instead, the power curve is mostly the same of other wind turbines with a parabolic shape.

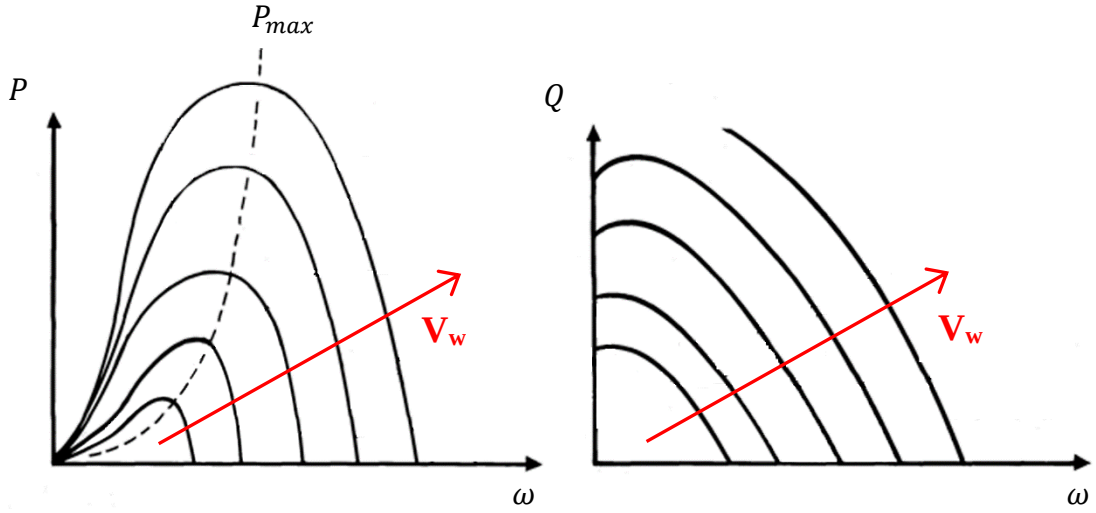

Fig. 3.21 Power and Torque curve in function of turbine rotational speed at different wind speed (Vw), dashed line is the line of best efficient points

Characteristic curve of power and torque are usually represented using non-dimensional coefficient. The power is evaluated with the power coefficient:

$$C_P = \frac{P}{\frac{1}{2}\rho A V_w^3}$$

In the same way torque is evaluated by the torque coefficient:

$$C_m = \frac{Q}{\frac{1}{2}\rho R A V_w^2}$$

In section 3.1.1 8(DC MOTOR), where characteristic curve of DC machine was treated, it has been described the linear relation between torque and rotational speed of the motor. As the turbine is coupled with the DC machine working as a generator, which acts as a resistive load, torque-speed relation is linear (fig.3.22, red line). In case of DC machine working as a motor the turbine is dragged, therefore it is seen by the motor as a load. This is the explanation why the rotational speed is inversely proportional to the torque in DC motor, while it is directly proportional in DC generator.

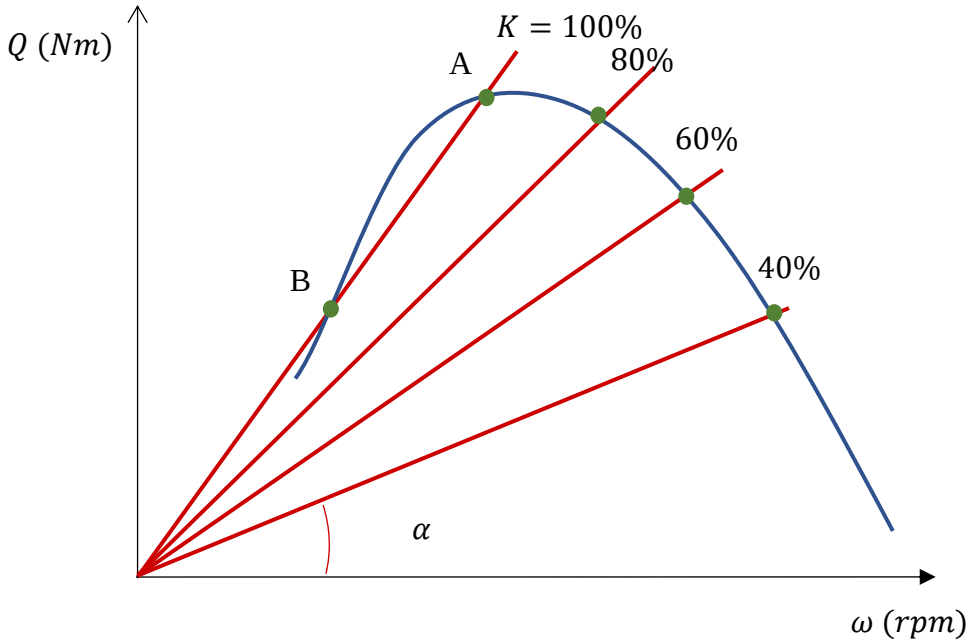

Fig. 3.22 characteristic curve of coupling between a DC generator (red line) and a Savonius wind turbine (blue line) with different mosfet parameter K.

To study the operating point of the system it is necessary to consider both characteristic curves of turbine and generator because operating point must belong to both curves, overlapping the two curves (fig.3.22), are highlighted two operating points.

In fig.3.22 a representation of what it is expected to be a coupling between a turbine (blue line) and a generator (red line), the graph is plotted with torque and rotational speed, even if it can be used non-dimensional value, tip speed ratio (λ) and torque coefficient (C_m). The use of non-dimensional variable is more correct for a correlation between different machines, but since in this graph wind speed, turbine geometry and fluid are kept constant, it is suitable to use dimensional variables. The turbine curve (blue line) can be considered fixed because it depends on the machine, which is the same for all the experiment, and on wind speed of the wind tunnel, which can be consider roughly constant.

The resistant torque generated by the DC generator, represented by the red lines, can be varied allowing to move the operating points and change rotational speed of wind turbine. To understand how to change the slope of resistive load must be analysed the behaviour of mosfet or potentiometer.

Hereinafter only mosfet method is explored because it is the method chosen in this experiment, but, from the circuit in fig.3.19 of the potentiometer configuration, the same calculation can be made arriving to the same conclusion.

From the mosfet circuit in fig.3.20, applying Kirchhoff's voltage law at the mesh can be written:

$$V_{emf} = IR_m \tag{3.46}$$

Using equation 3.16 of the section 3.1.1 about DC machine equation 3.46 can be re-written as

$$KIR_m = K_E\omega \tag{3.47}$$

K is a parameter that evaluates the MOSFET regulation. Since the mosfet has the property to control the current flowing in the circuit from 100% of the value, acting as a switch in on-state, to 0% of the current value, acting as a switch in off-state, to emulate the mosfet effect it has been consider an additional multiplier of the current K, which has the value in the range from 1 to 0. In our experiments this parameter takes five different values (20%, 50%, 70%, 90%, 100%).

Solving equation 3.47 for the current it results:

$$I = \frac{K_E\omega}{KR_m} \tag{3.48}$$

It can be stated that current has a linear relation with rotational speed. It is important to underline the influence of internal DC machine resistance R_m, which decreases the current value for a fixed rotational speed of the turbine.

The second equation that must be considered is the torque relation. Defining Q_L the load torque, Q_T the total torque and Q_F the friction torque, it can be written:

$$Q_L = Q_T - Q_F \tag{3.49}$$

Load torque will be always lower than the total torque due to all the friction in the system. From equation 3.3 we can re-write the total torque as

$$Q_T = KK_MI \tag{3.50}$$

Making a system with torque balance (equation 3.49), equation 3.50 and the current relation find before (equation 3.48), it is obtained the relation between torque and rotational speed as function of different parameters:

$$Q_L = K\frac{K_MK_E}{R_m}\omega - Q_F \tag{3.51}$$

For the potentiometer configuration a similar equation is obtained

$$Q_L = \frac{K_M K_E}{R_m + R_L}\omega - Q_F \tag{3.52}$$

Where R_L is the variable resistance of the potentiometer.

By the equation 3.52 it follows that the torque (Q_L) has a linear relation with the rotational speed (ω) with a slope depending on the DC machine constants $(K_M K_E)$, the internal resistance of the motor R_m and the mosfet parameter K:

$$\alpha = \frac{\partial Q_L}{\partial \omega} = K\frac{K_M K_E}{R_m} = slope \tag{3.53}$$

As we can consider the DC machine parameters constant, the only variable that can modify the line slope is K. Increasing the mosfet parameter starting from 0, the current and the slope increase and consequently the rotational speed decrease. Remembering that rotational speed is linked to voltage, with rotational speed decreasing the voltage decreases as well. As the mosfet parameter is limited to 1, the slope has an upper limit that is related to a minimum ω reachable by the system. Since K_T and K_E are parameters related to the DC machine, their product is fixed. By this consideration, the upper limit to the DC machine curve (K=1) is due to the internal resistance of the motor (R_m), a high internal resistance generate an almost horizontal characteristic curve with a low range of variation of rotational speed, vice versa a low internal resistance allows to have an almost vertical characteristic curve of DC machine allowing a huge range of rotational speed variation available.

Looking at fig.3.20, the coupling between turbine and DC generator can brings to two intersections, point A and point B. Both values are possible operating points of the system, but point B is defined as an unstable condition while point A is defined as stable. B is classified as unstable condition because the first derivative of the generator curve is lower than the derivative of the turbine curve, therefore when there is a small perturbation on the turbine that brings to the movement of the operating point along the curve, the generator is not fast enough in changing to follow the operating point. In a so small system instabilities are almost always present, therefore it is quite impossible to stay in an unstable operating point without any control system in aid. Thus, when system is in an unstable condition it moves from B towards a stable point (A) to bring system in an equilibrium condition. A is a stable point because the DC generator has a faster response to perturbation of system since the red line slope (DC machine) is higher than the blue line one (turbine). The impossibility to stay in the unstable point avoids our system to track the right branch of the turbine curve and makes the finding of the peak difficult.

3.4 EXPERIMENTAL MATRIX

For the speed control is desired to acquire some point to be able to understand how is the increment or decrement of speed in function of relative torque measured, thus are used 5 mosfet parameter (K): 20%, 50%, 70%, 90%, 100%. With these values it is possible to have a good truck of the torque-speed curve.

The experiment has three main variables: mosfet conductivity, position on the cube and cube where turbine is mounted. For the PIV measurement only the variables linked to the location of the turbine are considered and the mosfet parameter (K) is kept constant at 100% so all the current can pass through the circuit as the mosfet is absent.

EXPERIMENTAL MATRIX

CASE	MOSFET parameter (K) %	position	cube
1	20	front	1
2	50	front	1
3	70	front	1
4	90	front	1
5	100	front	1
6	20	centre	1
7	50	centre	1
8	70	centre	1
9	90	centre	1
10	100	centre	1
11	20	back	1
12	50	back	1
13	70	back	1
14	90	back	1
15	100	back	1
16	20	front	2
17	50	front	2
18	70	front	2
19	90	front	2
20	100	front	2
21	20	centre	2
22	50	centre	2
23	70	centre	2
24	90	centre	2
25	100	centre	2
26	20	back	2
27	50	back	2
28	70	back	2
29	90	back	2
30	100	back	2

Table 6 Experimental Matrix

3.5 ACQUISITION TIME

The time of acquisition T is an important parameter of every experimental test. A too short time can cause a lack of convergence, which can lead to wrong results. It is also important to avoid the collecting of data during transient operation, which characterize most of the system at the starting condition.

Generally, T is considered based on some relevant frequency of the system. In this experiment to find a good period of acquisition a long measurement of 10 minutes is performed. The measure is then split in bins. So, from a 10 minute long measure 10 bins of 1 minutes, 20 bins of 30 seconds, and so on can be extracted. This procedure is made for both rotational speed and current. Evaluating data of different bins separately we can obtain an estimation of the error caused by a reduced acquisition time. In fig.3.23 the errors are shown in percentage of each bins (magenta dots) and the average error (red dots). As for the experiments it has been used a time acquisition of 1 minute, we can assume that this bring an error of less than 3% for both the current and the rotational speed.

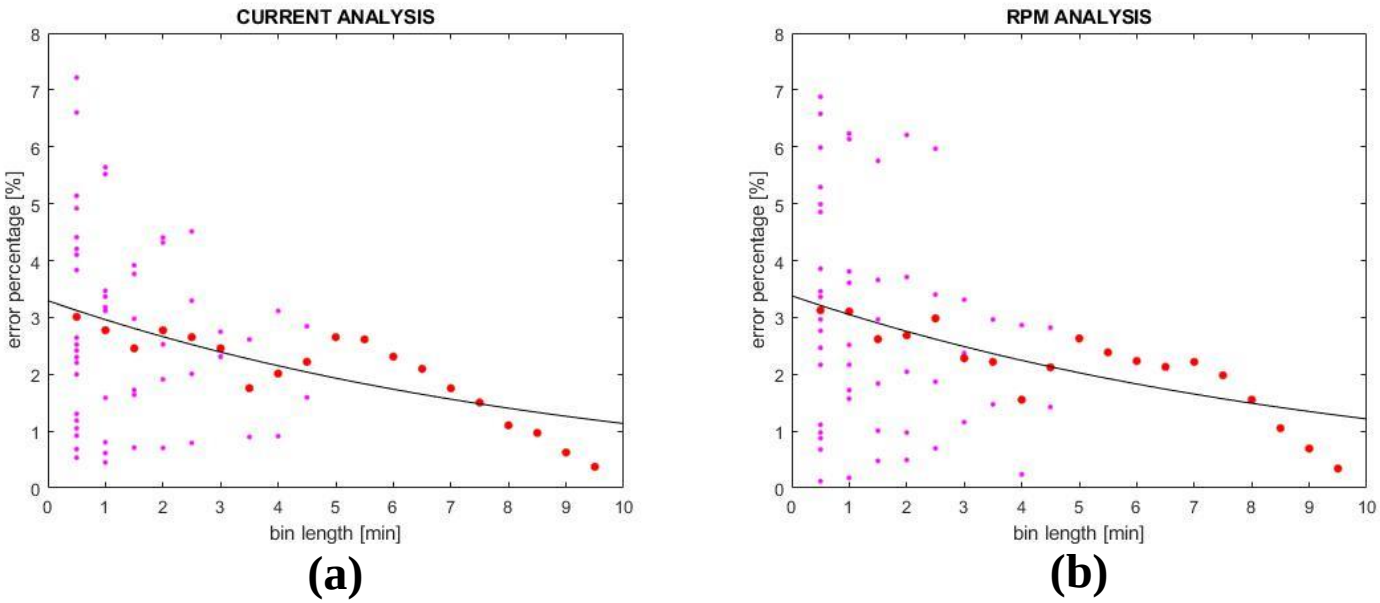

Fig. 3.23 long measure analysis of current (a) and RPM (b) showing for each bin the error in percentage (magenta dots), the average of errors (red dots) and the interpolation of data (black line)

Even if a long measure can lead to a lower error, the aim of these experiments is not to get an exact value, but it is to have comparable value. As the goal is qualitative, instead of quantitative, an acquisition time of 1 minute can be sufficient to have a good estimation of the quantities for a comparison.

4 RESULTS

For each configuration is measured the PIV flow condition. PIV allows to obtain a velocity vector map of both component of velocity: the horizontal component, U $[m/s]$ (called streamwise velocity), and the vertical velocity, V $[m/s]$. In addition, Turbulent Kinetic Energy, TKE $[m^2/s^2]$, and vorticity, ξ $[1/s]$, are calculated. Vorticity is expressed as function of gradient of velocities:

$$\xi = \frac{\partial V}{\partial x} - \frac{\partial U}{\partial y} \tag{4.1}$$

This value is mathematically defined as the curl of velocity and it describes the local rotation of a fluid. Turbulent Kinetic Energy is the kinetic energy content inside the turbulence, this value is representative of the excess of energy discussed at length in theory chapter. TKE is opposite to Mean Kinetic Energy, which is the energy content related to the mean flow speed.

For each configuration it is calculated output power by the measure of rotational speed and torque. By means of the MOSFET the rotational speed is varied to try to define the power curve of the turbine. Despite it is widespread that wind turbine can easily exploit MKE, the ability to harvest TKE is still under investigation.

To calculate the charcateristic curve of the turbine the power is firstly calculated, by means of torque and rotational speed, and then the power cofficient is find as ratio of the mechanical power and the wind power.

The calculation of the rotational speed is made by simply counting the times the reflecting tape stuck on the turbine shaft is passed in front of the photo-transistor. The torque is instead derived by the current measured, according to equation 3.36 ($Q_{sh} = Q_{em} + Q_f$). The friction torque is given by the manufacturer, while the emf torque is calculated by equation 3.40 ($Q_{em} = K_M I$). Therefore mechanical power is obtained by multiplying the shaft torque for the rotational speed.

To calculate the tip speed ratio TSR, instead of using the freestream speed, it has been used the real velocity upstream the turbine, which is considerably lower than the undisturbed speed. To find the real velocity felt by the turbine for each case it has been made an average over the height of the turbine of the streamwise velocity upstream the rotor thanks to the PIV measurements. Thus, to calculate the power coefficient is not used the common formula of the ratio between mechanical and wind power. It is obtained C_P by the product of the torque coefficient C_m and the tip speed ratio TSR.

4.1 PLATE

The PIV measurement of the only plate is important to define the boundary layer of the flow without the influence of the cube presence.

The boundary layer thickness is defined by literature as the distance from the plate at which the flow velocity is 99% of the free stream condition. By this definition in fig.4.1profile velocities at different position are overlapped to the flow resulted by PIV measurement. It is also marked the position of Boundary Layer thickness (dashed line). As it is shown in fig.4.1 the boundary layer is lower than half of the cube height. In fig.4.2 the velocity profile of the freestream is reported, where it is pointed out the boundary layer thickness (dashed line). In this first case the thickness of BL has been measured at 35% of cube height.

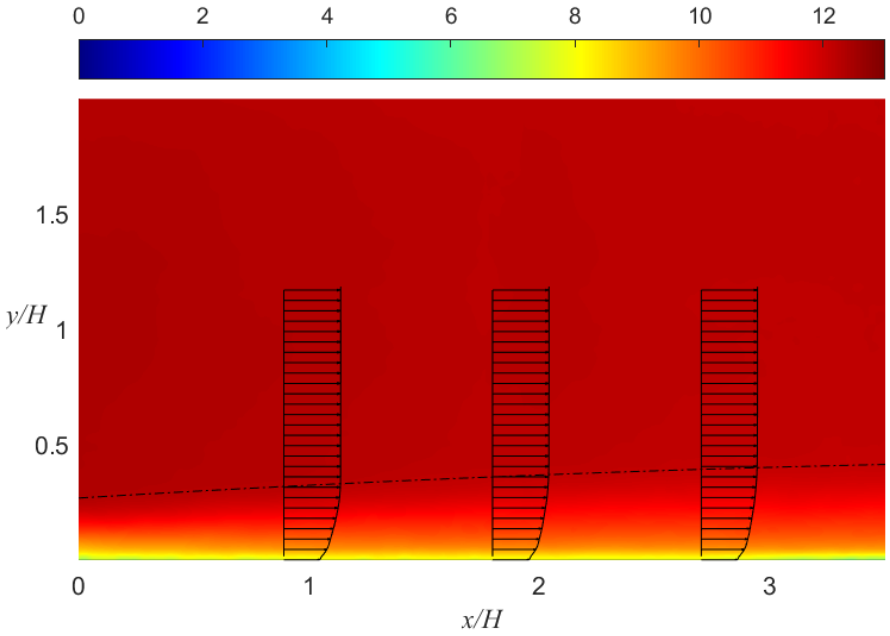

Fig. 4.1 Boundary layer thickness (dashed line) in free stream configuration with three profile velocities at different position

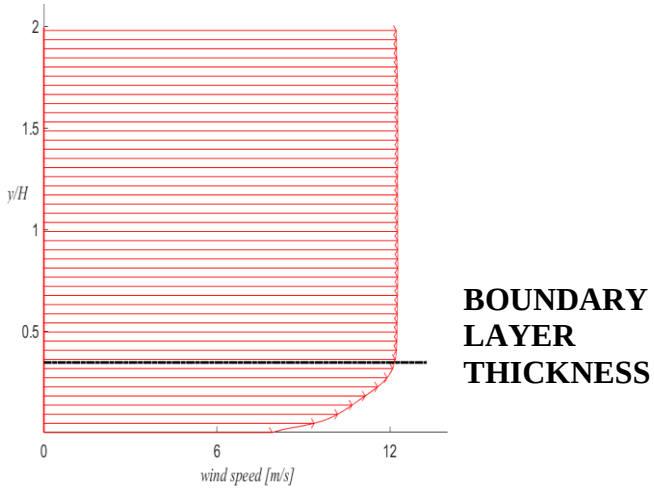

Fig. 4.2 Velocity profile of plate configuration

4.2 CUBES

The cubes configuration is important as the plate to understand how the flow behaves. This can be useful as comparison for the turbine cases. The flow field upstream the first cube has the same profile velocity saw in the plate configuration (fig.4.2). At the top side of both cubes, in the location where the turbine has been planned to be placed, the velocity profiles of half cube height above the cube top surface have been plotted in fig.4.3.

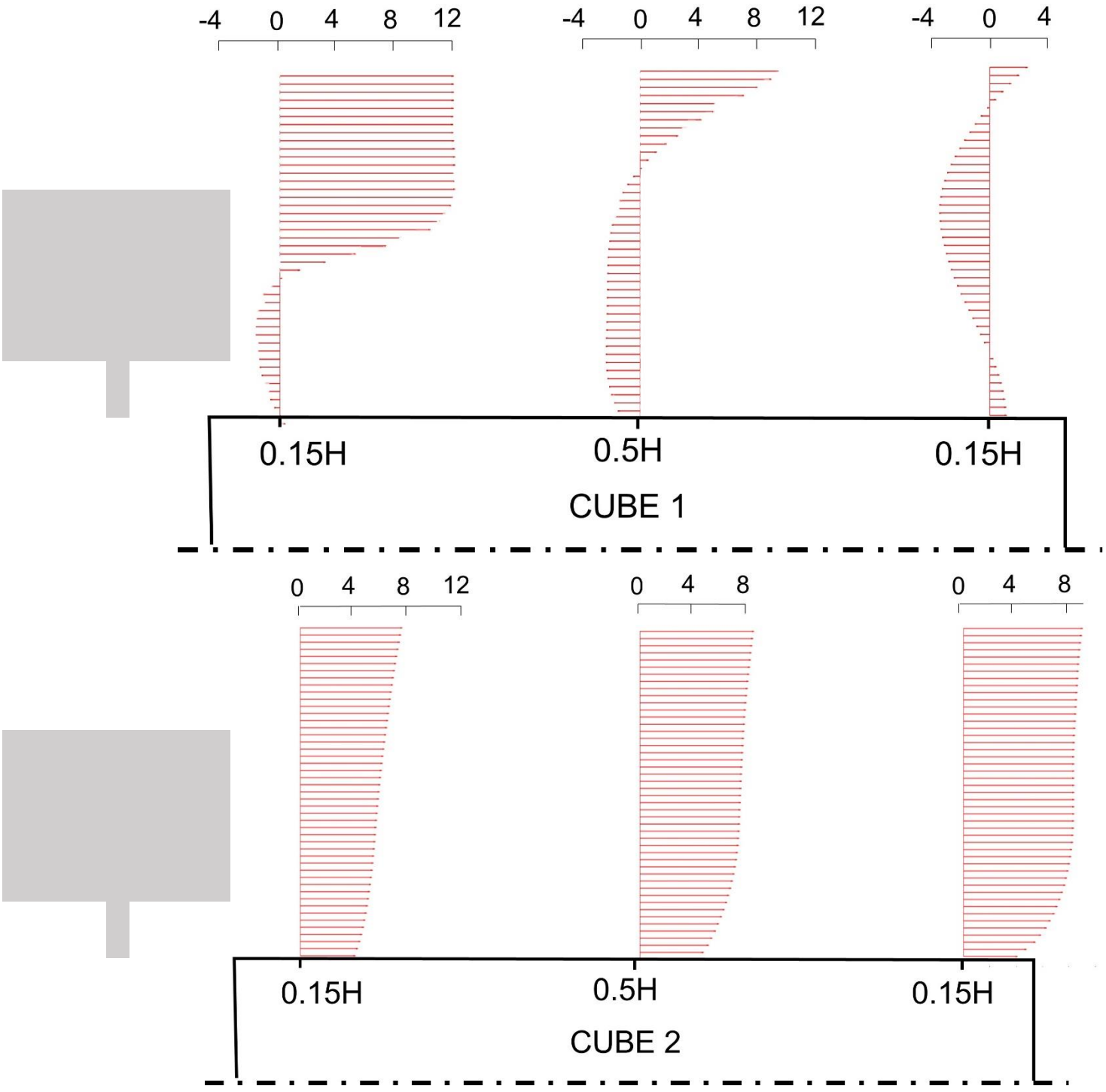

Fig. 4.3 Velocity profiles expressed in m/s in the position where wind turbine will be placed.

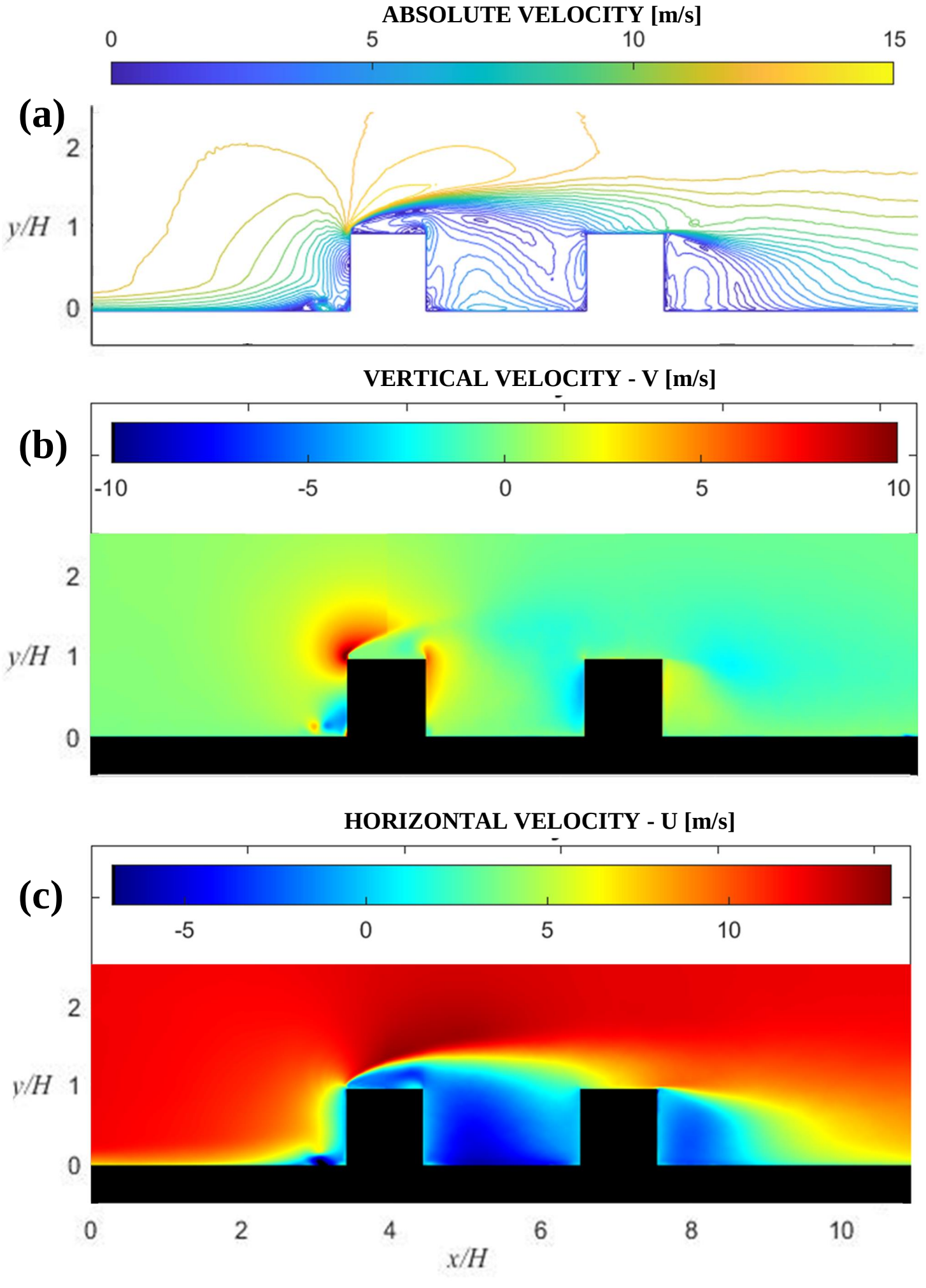
ABSOLUTE VELOCITY [m/s]
0
5
10
15
(a)
2
y/H
1
0
VERTICAL VELOCITY - V [m/s]
(b)
-10
-5
0
5
10
2
y/H
1
0
HORIZONTAL VELOCITY - U [m/s]
(c)
-5
0
5
10
2
y/H
1
0
0
2
4
6
8
10
x/H

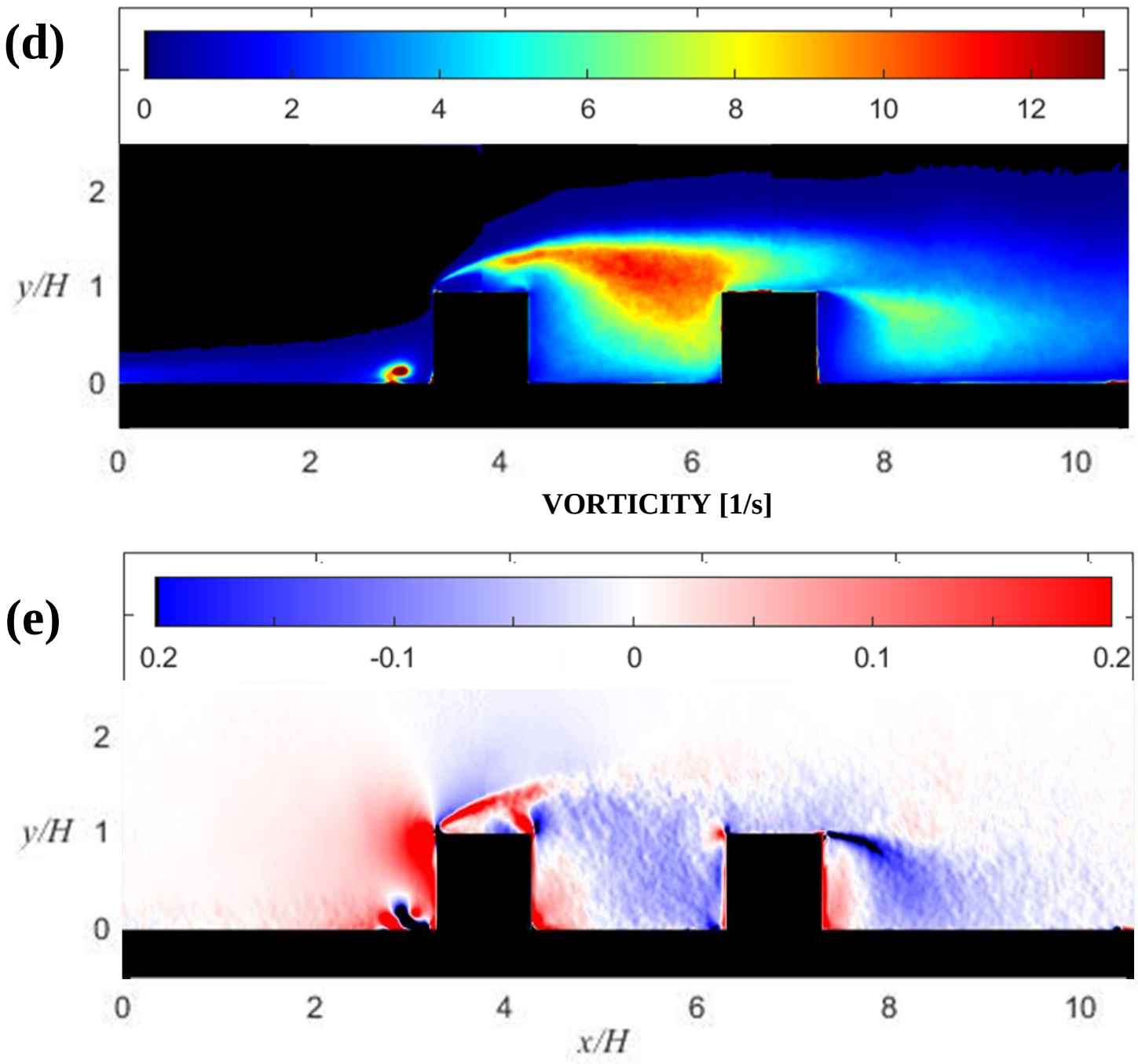

Fig. 4.4 PIV images of cubes configuration of absolute velocity (a), wall-normal velocity (b), streamwise velocity (c), Turbulent Kinetic Energy (d), vorticity (e)

By the velocity profile in fig. 4.3, it is understood that next to the roof of the first cube the flow is reverse and this reverse condition increases going towards the back of the cube. On the other cube, the flow is highly positive in streamwise direction and it accelerates going toward the leeward zone of the cube. This velocity profile suggests that the best location for the upstream cube is the front one, where the reverse condition is lower, while for the downstream cube the best position is the back one, where the flow is faster.

The cube configuration is very important since it is the comparison for all the other cases. The analysis of the velocity profile above reflects the PIV result of the streamwise velocity (U) in fig.4.4c. On the

top of the upstream cube a recirculation bubble is graphically visualized, where there is a high turbulence which result in a reverse flow. At the front of the first cube a stagnation zone due to the blockage effect of the first cube appears. Herast et al. [83] in their study found that the core of the stagnation point is fixed at $y_0/h = 0.65$. In fact, as it is shown in fig.4.4b, almost at that position on the front facade, the vertical component of the velocity passes from being directed downward, in the first half of the front facade, to being directed upward toward the leading edge of the cube, in second half. The vertical velocity reaches almost the streamwise freestream velocity at the leading edge of first cube, where a large separation zone starts to be generated (fig.4.4c). A separated shear layer is generated by the presence of this separation region, it starts at the leading edge of upstream cube and reattaches in the middle of the top of downstream cube. This reattachment of the separated shear layer is the cause of the acceleration of the flow on the top of the second cube, as described by the velocity profiles in fig. 4.3. The recirculation bubble is mainly characterised by reverse flow (fig.4.4c) and by an almost absent vertical component of velocity (fig.4.4b). Above this zone, an overspeed region occurs (fig.4.4c), where the speed reaches an increase of more than 10% of the freestream velocity.

The vorticity images differentiate between the positive vorticity in red, which is counter-clockwise, and the negative vorticity, which is clockwise. In the inter-cubes space, a strong recirculation zone characterized by a horseshoe vortex is graphically visualized (fig.4.4e). This vortex has a clockwise direction, as deduced by the vorticity representation and by the the high vertical component upward on the back of upstream cube and a downward vertical component on the front of the downstream cube (fig.4.4b). Same phenomenon with lower intensity can be visualized on the leeward zone of the second cube, where the wake of the cube causes a second clockwise horseshoe vortex. By the leading edge of the windward cube a region of high Turbulent Kinetic Energy (TKE) is generated following the separated shear layer path (fig.4.4d). This high TKE zone enlarges going backward till the impingement on the leading edge of the downstream cube. A smaller TKE region is generated starting by the trailing edge of the aft cube. A strong vorticity region occurs in front of the upstream cube where the freestream crashes against the front facade (fig.4.4e). A second strong region is present sudden after the trailing edge of the downstream cube- This region can be due to the interaction of horseshoe vortex behind the second cube with the flow coming from the top of that cube. The interaction of two different flow field can generate turbulence and thus, vorticity. On the top of the windward cube, inside the recirculation bubble, the vorticity is messy and cannot be clearly distinguished, this reflects the high turbulence level in that zone. Above the recirculation bubble, in the over-speed region, the vorticity has a low intensity. This can be considered a favourable factor in the plan of a possible exploitation of the wind energy in this region.

The cubes configuration here described is the reference case for all following configuration where turbine will be added. The turbine is expected to have a high influence on the flow due to its size, which is relevant compared to the cube height, and due to the blockage effect. The blockage effect is a typical phenomenon generated by the rapid deceleration of the flow caused by the presence of one of more obstacles. This mass of fluid at very low velocity affect the flow upstream changing the incoming flow. This effect is strongly relevant in turbines where the inflow conditions set the power felt by the rotor, thus a change in the incoming flow change the power extraction. This phenomenon depends on many factors, such as the rotor cross sectional area, the wind speed and the turbulent intensity. In these experiments there are three obstacles (2 cubes and the turbine) that produce three different blockage effect, in addition every obstacle generates a wake downstream. The interaction of all these phenomena cause a complex fluid and this explains the challenge of the understanding and prediction of flow field in urban environment.

In the following section the two cubes are analysed separately and each position is explained individually by means of the PIV images.

4.3 FIRST CUBE

Since the first cube doesn't have any obstacle upstream, the turbine behaviour should be more predictable than the downstream cube. As we can deduct from the fig.4.3 of the velocity profiles and from the PIV images of the cubes configuration (fig.4.4), the front position looks the best among all the three possible locations on the upstream cube. As previously described, the fig.4.3 shows an increase in the reverse flow at the roof of the cube going towards the trailing edge. In case of VAWT wind turbine, for us Savonius design, the reverse flow is not necessary a drawback since the machine is axis-symmetric and thus it can get the flow from every direction. Despite this consideration the turbulence and the vortices can have a great impact on the performance of the turbine.

The result of the positioning of the turbine on the first cube is the reduction of the TKE region downstream the first cube (fig. 4.5 - 7). This region increases moving the turbine on the back position, even if it remains lower than the cubes case. The effect of the presence of the turbine is seen also in the vorticity images, however in this case every position has a different influence in the vorticity field. The front location (fig.4.5) shows that the vorticity that characterizes the recirculation bubble seems to be moved up by the turbine presence. Considering the middle position (fig.4.6), the turbine interrupts the generation of the separation bubble and in turn of the vorticities inside, hence the vorticity field looks less strong than the previous case. Looking at the fig.4.7 about the location on the back of the cube, as the turbine is completely submersed inside the separation zone, its influence on the vorticity is almost irrelevant.

Locating the turbine on the first cube doesn't have relevant effects either on the wake downstream the second cube or on the size of the recirculation in the intra-cubes space. Even the velocity profiles are considerably unchanged respect the reference case. As the turbine on the first cube is in the recirculation zone for all the three cases, despite the front case is not fully immersed, the turbine rotation doesn't influence too much the turbulent conditions that characterize downstream region.

The plots of the power, the torque and the rotational speed reflects the considerations made above about. The location on the back of the first cube, which present the worst flow condition, has very poor performances compared to upstream cases. The front and centre location are almost comparable under all aspects, as they manifest the same power, torque and rotational speed. This leads to an interesting result because by the initial consideration of the cubes configuration the most promising location was seemed to be the front one as it wasn't fully immersed in the recirculation bubble. The power measurement instead reveals that the centre location is promising as well. This enforce the importance of using different methods of analysis to study a so complex flow field.

CUBE 1 - FRONT

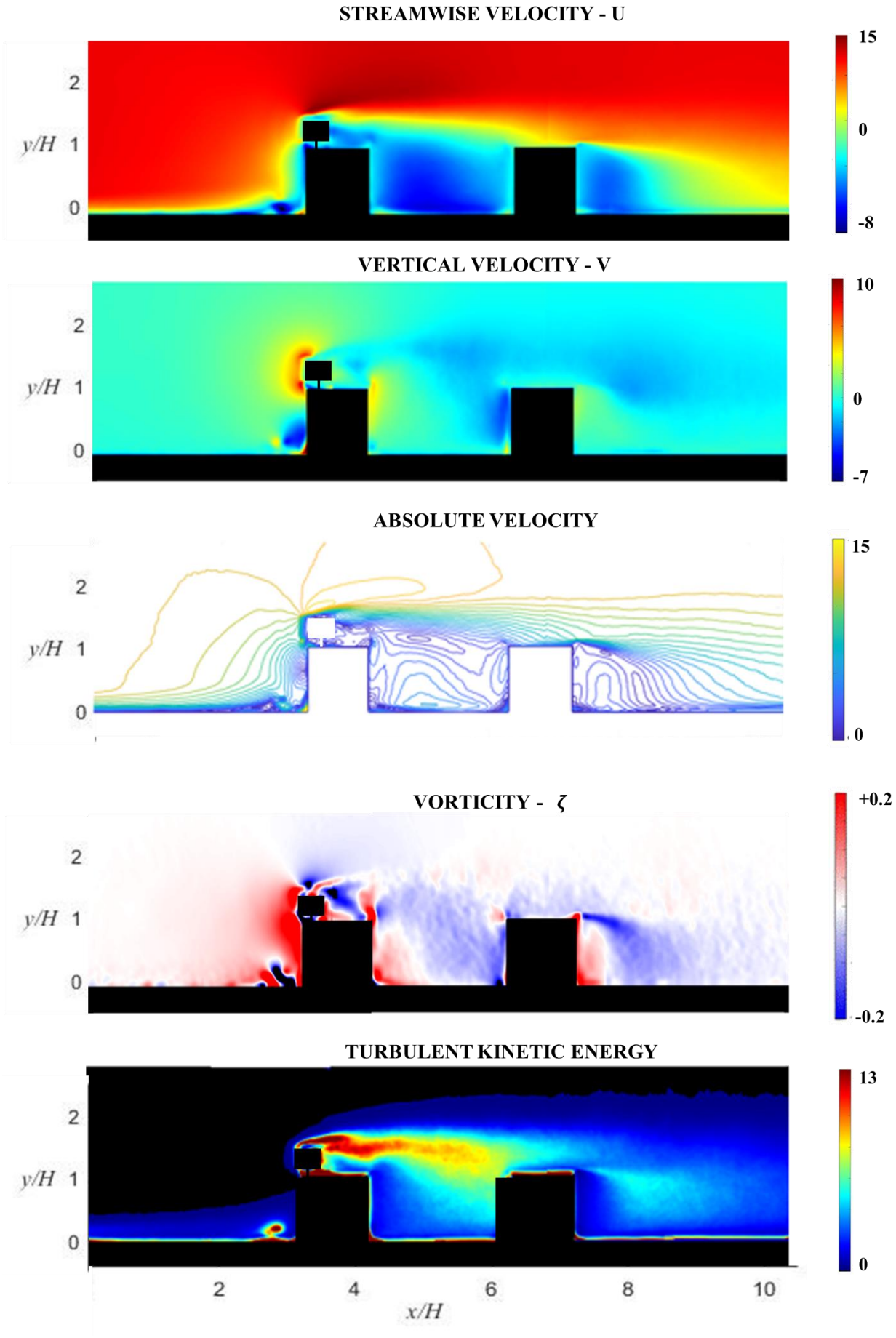

Fig. 4.5 PIV images of turbine located on the UPSTREAM cube in the FRONT position

CUBE 1 - CENTRE

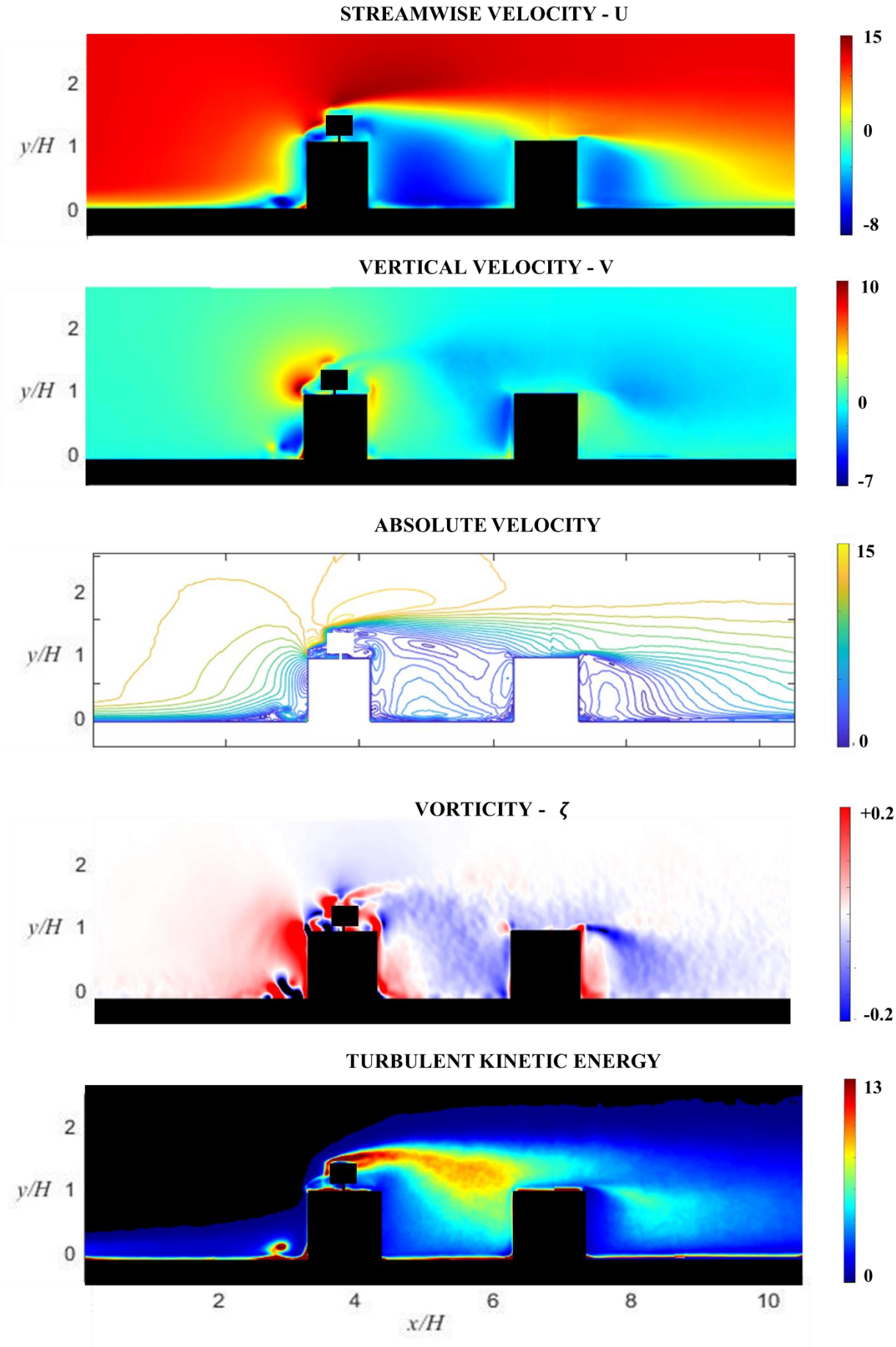

Fig. 4.6 PIV images of turbine located on the UPSTREAM cube in the CENTRE position

CUBE 1 - BACK

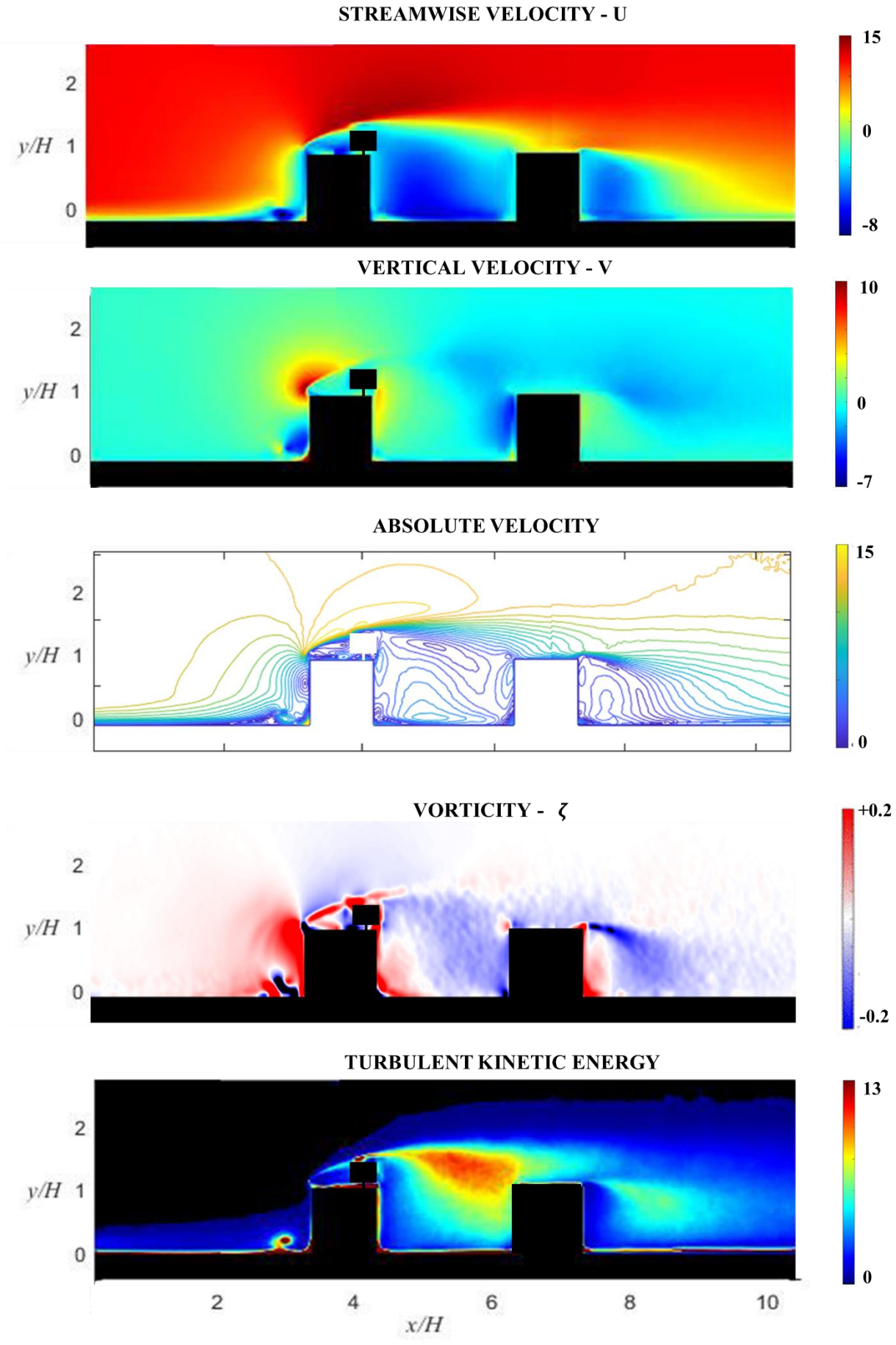

Fig. 4.7 PIV images of turbine located on the UPSTREAM cube in the BACK position

FRONT LOCATION (fig.4.5)

The overspeed zone where flow is accelerated is moved up and thus the reattachment of the separated shear layer on the top of the second cube is shifted more on the back. A big zone of high vertical component of velocity occurs upstream the rotor since it is partially out of the recirculation bubble, this can be the reason of the moving up of the overspeed region. As the turbine is in between the limit of the recirculation bubble, the vorticity region is messed up and enlarged by the rotor.

The TKE region is shrunk compared to the cubes configuration, this can suggest that the turbine somehow extract some turbulence energy from the flow. Otherwise it is possible even that the turbine presence decreases the turbulence presence of the flow due only to the interaction with the obstacles. Both options result in a positive effect of the turbine on the flow that is the decrease in turbulence.

Without the turbine the upstream cube manifests a small vortex at the base of the front facade. This cube is very small but this zone represents in our model the zone where people walks, thus is important to keep an eye on it. Placing the turbine on the front position of the upstream cube, this vortex is enlarged because the flow on the front facade is modified. We can't state if this change is positive or negative but it will surely affect the people comfort on the ground.

CENTRE LOCATION (fig.4.6)

The turbine positioned on the central position is probably the most interesting of all. As seen by vertical velocity image (fig.4.6), the turbine is completely inside the recirculation bubble, thus the graph of V_y is not affected. In contrast the image of horizontal component of velocity is strongly different compared to the reference case, the recirculation bubble seems to be kept low by the turbine presence. We could state that the rotor delays the formation of the separation bubble, however downstream the turbine the separation zone returns to be large as the rotor height. Hence, the recirculation bubble is smaller upstream the rotor and larger downstream (compared to the reference case). This is a promising result because the rotor performance is mostly influenced by the incoming flow conditions.

Looking at the absolute velocity graph, the inter-obstacle horseshoe vortex is enlarged. This is related to the higher separation zone generated on top of the first cube, which results in an addition of low speed flow on that recirculation region.

Vorticity is messy both upstream and downstream of the rotor with positive and negative vortices. We can graphically see that upstream the rotor on the upper part a big positive vorticity region is present, in contrast on the lower part a strongly negative vorticity zone occurs. This condition of the flow is

quite strange and complex, thus the positive influence of that to the turbine performance can be defined only by the power measurement. The measurements show a power extraction of central position as high as the front position. Therefore we can conclude asserting a positive influence of this complex high vorticity configuration on the turbine performance.

BACK LOCATION (fig.4.7)

With the turbine mounted on the back position of the upstream cube the flow field is mostly unchanged respect the reference case of the cubes. In this configuration the turbine is completely submersed in the recirculation bubble and its influence on the rest of flow field is minimal. The only aspect of the PIV which varies is the dimension of the TKE region, which slightly decreases. As we expected, in this location the power extraction is very poor. It is still not clear if turbine is able to harvest turbulent kinetic energy, but even with the improvement of this ability, the flow field is too messy with too high fluctuations and turbulence to be somehow a possible option.

4.4 SECOND CUBE

As the position of the second cube is downstream of the first one, the flow field of windward cube is mostly unchanged by the addition of the turbine on the top of second cube. The presence of the turbine generates a vorticity in the proximity of the rotor and a high density TKE on the wake. The vorticity increases moving the turbine on the back of the cube, next to the trailing edge. The explanation is obvious in this cube, just looking at the velocity images. Farther from the leading edge of the cube, the effects of the upstream cube are lower. More precisely the effect of the separated shear layer detached by the front edge of the upstream cube and the large horseshoe vortex generated in between the cubes have high influence on the turbine located on the second cube. Thus, the back position is the less affected by these phenomena. The front and centre position on the second cube can be still considered in the wake of the upstream cube. The front position is directly impinged by the TKE region and by the separated shear layer generated by the upstream cube, thus the performance of the turbine is strongly decreased (fig.4.8). Moving the location of the turbine backward, the performance increases because the reattachment of the separated shear layer brings favourable flow conditions. These considerations are confirmed by the power measurements, which show an increase of the extracted power moving the turbine on the leeward part of the cube (fig.4.12).

As reported in fig.4.11, the profile velocities on the second cube are highly influenced by the presence of the turbine. This can be related to the absence of a large separation bubble as it occurs above the first cube. The turbine placed in front of the second cube causes a speed decrease on the back zone, this is a common result of the wake of the turbines. More interesting is to see in fig.4.11 that for both centre and back position even the upstream profile velocities are decreased by the turbine presence. That is a combination of both the Savonius rotor design and the low speed of the flow. Looking at the profile velocity next to the trailing edge when the turbine is located at the centre, it is graphically visualized a high reverse flow at the top facade of the cube. This is due to a very thin separation zone generated at the top of the cube, which can be visualized zooming the image.

CUBE 2 - FRONT

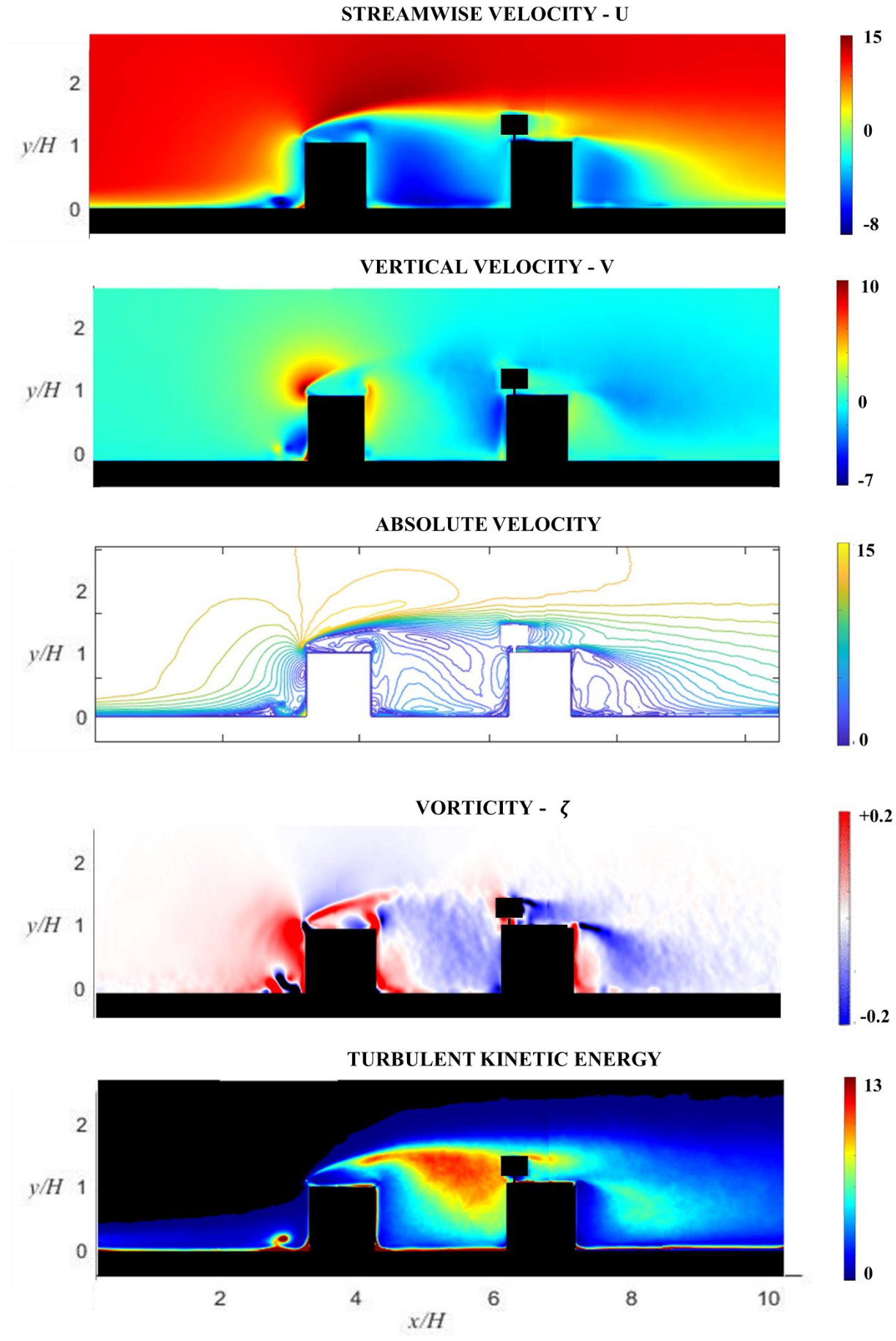

Fig. 4.8 PIV images of turbine located on the DOWNSTREAM cube in the FRONT position

CUBE 2 - CENTRE

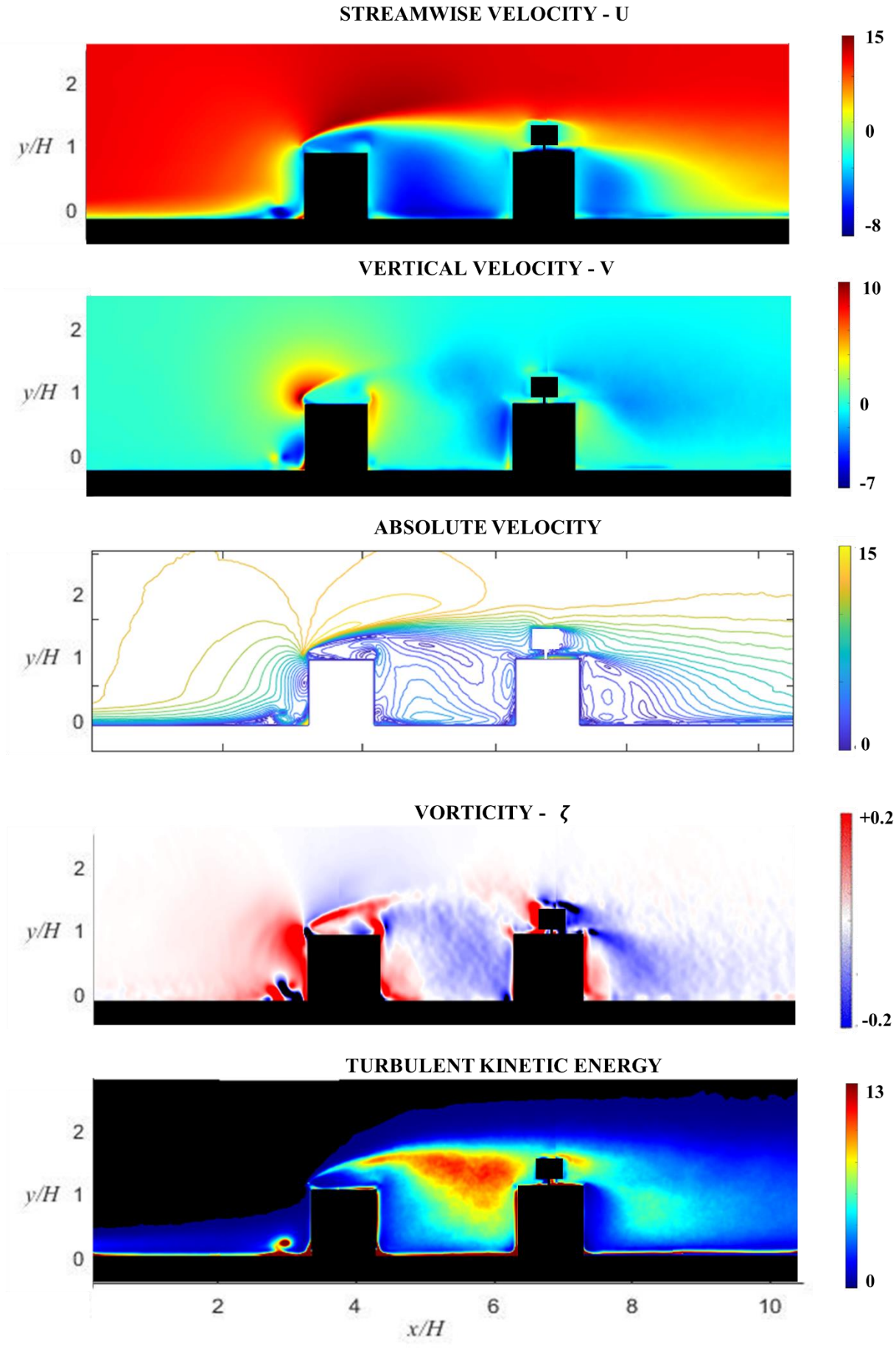

Fig. 4.9 PIV images of turbine located on the DOWNSTREAM cube in the CENTRE position

CUBE 2 - BACK

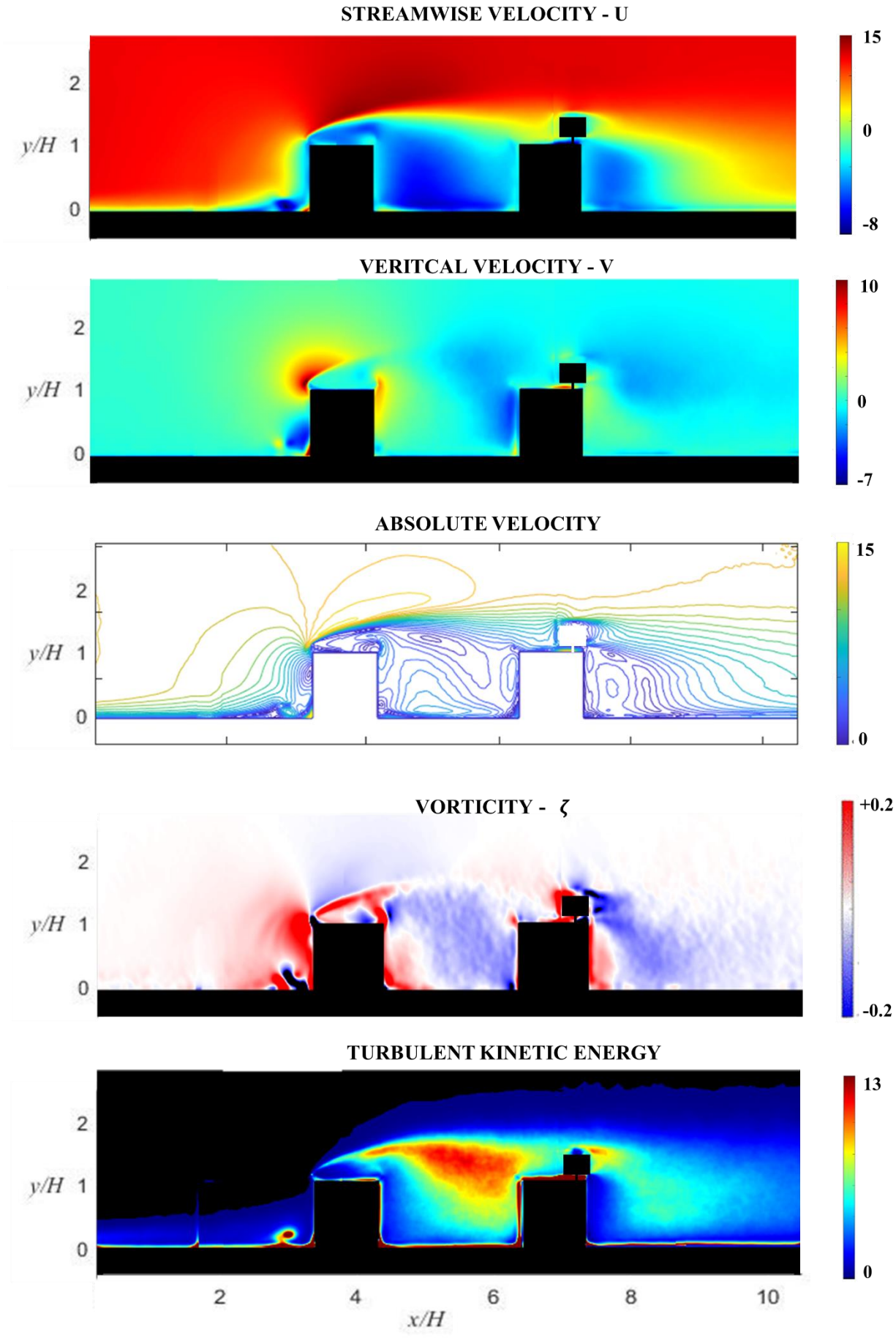

Fig. 4.10 PIV images of turbine located on the DOWNSTREAM cube in the BACK position

FRONT LOCATION (fig.4.8)

The front turbine is directly impinged by the TKE region that characterizes the wake of the upstream cube. The turbine is located at the top of the facade, where there is high effect of the horseshoe vortex in between the cube. Even if the turbine is located on the front edge of the cube, it influences the horseshoe vortex on the wake of the cube, which results enlarged compared to the cubes configuration. This, as previously cases, is due to the interaction of the rotor with the flow. The turbine, extracting power, decreases the flow field velocity as explained in section 2.1 (wind energy); this deceleration of the flow increases the low momentum fluid which in turn increases the recirculation region. Thus, the wake of a wind turbine will present always slower fluid than upstream, low velocity results in lower momentum, hence the flow is more sensitive to interaction with obstacles or other stream-tubes. This explains why the low momentum flow is often related with turbulence and vorticity.

CENTRE LOCATION (fig.4.9)

The turbine located in the central position of the downstream cube can be considered in the borderline of the wake of the upstream cube. This is the position where the separated shear layer generated at the leading edge of the upstream cube is reattached on the roof of the second cube. Moreover, here the high TKE region generated by the first cube presence starts to vanish. All these aspects made this location a better solution then the front one, in fact the power extracted here (fig.4.12) is higher than the one extracted next to the leading edge.

BACK LOCATION (fig.4.10)

The back turbine can be considered slightly influenced by the wake of the upstream cube because is farther than others. It has less turbulent flow condition of other cases on the same cube and this is reflected in the power extraction which is higher. The horseshoe vortex downstream the aft cube is increased by the presence of the turbine because the addition of low momentum flow. Therefore, the best condition for a cube in the wake of an upstream cube is next to the trailing edge. This result is clearly observed with a simple comparison of the PIV images and it is validated by the power measurements. The low momentum flow that characterize the wake of the upstream cube influence the frontal positions (front and centre), while in the back position the flow gains speed.

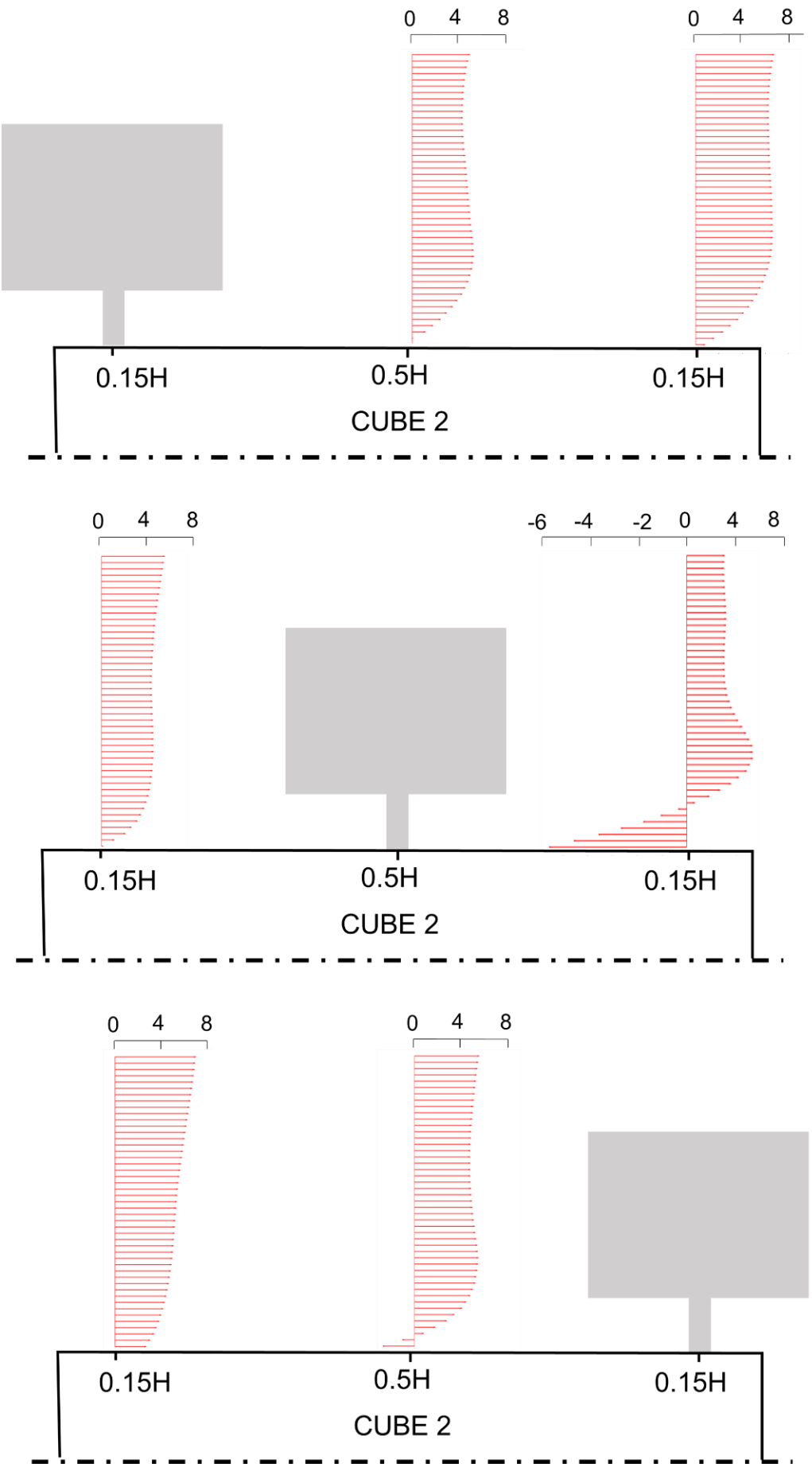

Fig. 4.11 velocity profiles of the turbine located on the different positions on the downstream cube

4.5 POWER COMPARISON

In fig.4.12 it is shown a comparison between the six different locations and the power output of the turbine. For clearness, the torque and the rotational speed measurements are drawn near the power. All the three variables identify the same results, in the upstream cube the best locations are both the front and the centre one, in the downstream cube the performances increase going towards the back of the cube.

As already discussed, the central location of the upstream cube reaches a so unexpected power output because the rotor presence causes a delay in the formation of the recirculation region above the cube. Considering the lower wind speed just upstream the rotor felt by the turbine in the central location, we can establish that this location is a bit more efficient than the frontal one. The strong inefficiency of the back location is predictable and unavoidable.

Considering the downstream cube, the situation is less evident, however there is a clear indication of the increase in power extraction of the turbine moving toward the back. The back location, which is the best of the aft cube, has a much lower power compared to the best location of the upstream cube. On the other hand, the worst location of the aft cube (front) extracted more power than the worst location of the upstream cube (back). This is a significant result since the choice of trying to locate the turbine on the front/centre location of an upstream cube is followed by the risk to bring the turbine in a very low efficient location. In contrast, locating the turbine on a cube behind another obstacle doesn't allow to reach high power extraction but in the worst scenario the efficiency is not so low.

To have a proper understanding of these values the turbine is made spinning in freestream conditions. The turbine is then placed in the wind tunnel much above the plate, to avoid the boundary layer presence, and without any obstacle upstream or downstream, to avoid blockage effect. In these conditions the turbine produced $60\ mW$ of power and $114.7\ mNm$ of torque with a rotational speed of $5000\ rpm$.

This case is considered the reference case for the power measurements. As it visible by a first look, the power extracted in freestream conditions is much higher than the highest power extracted by the turbine on a cube. Then it could be defined an efficiency related to these experiments which evaluates the power extracted in the different configurations respect the open-terrain condition. With this argument the frontal and central locations on the upstream cube, which are the best, reach an efficiency of 40%, while the location on the back has an efficiency lower than 7%. This give us an indication on the power decrement of the urban environment compared to the open-terrain condition.

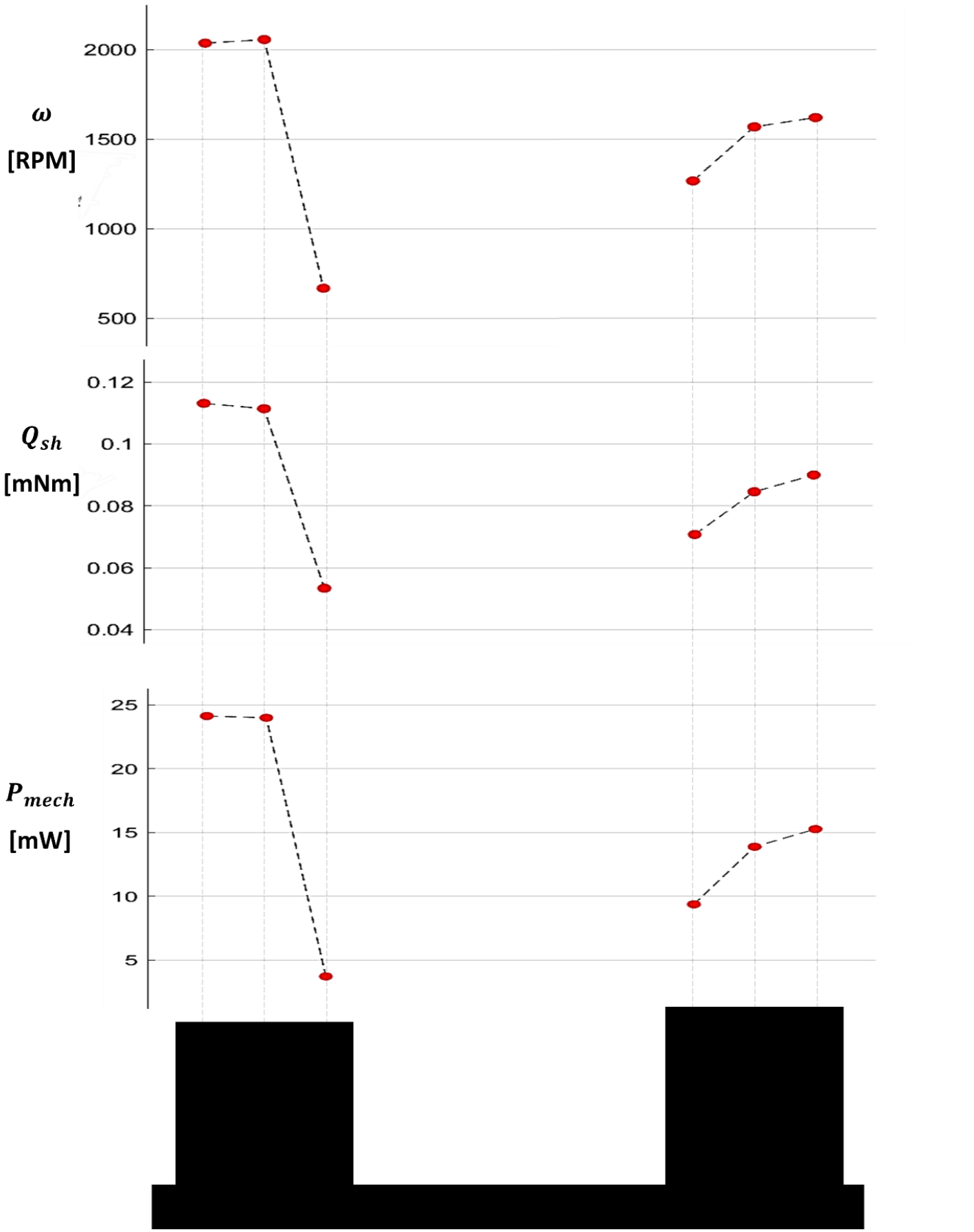

Fig. 4.12 POWER COMPARISON of rotational speed (ω), shaft torque (Q_{sh}) and mechanical power (P_{mech}) at different turbine position

4.6 POWER CURVE

Independently by the turbine location, the characteristic curves of a turbine are fixed considering non-dimensional values (C_P and C_m). To have a good estimation of these curves is important to have a wide regulation of the rotational speed. Unfortunately, the speed regulation of these experiments was quite tight due to the high internal resistance of the motor. Therefore, the use of MOSFET for the speed variation allows only to go to higher rotational speed, measuring the left branch of the power coefficient curve. To also explore the left branch, which is determinant to be able to determine the maximum efficiency point, a speed regulation by means of a voltage supply is required. This allows to increase the slope of the DC machine curve, and thus to reach lower ω.

Despite this consideration the power curve was extrapolated with the small amount of values available. Since the values are all concentrated at high TSR, this curve is a rough estimation of the real curve. Knowing that the power curve is generally a negative parabolic curve, by means of a quadratic fit it is obtained the C_P curve shown in fig.4.13.

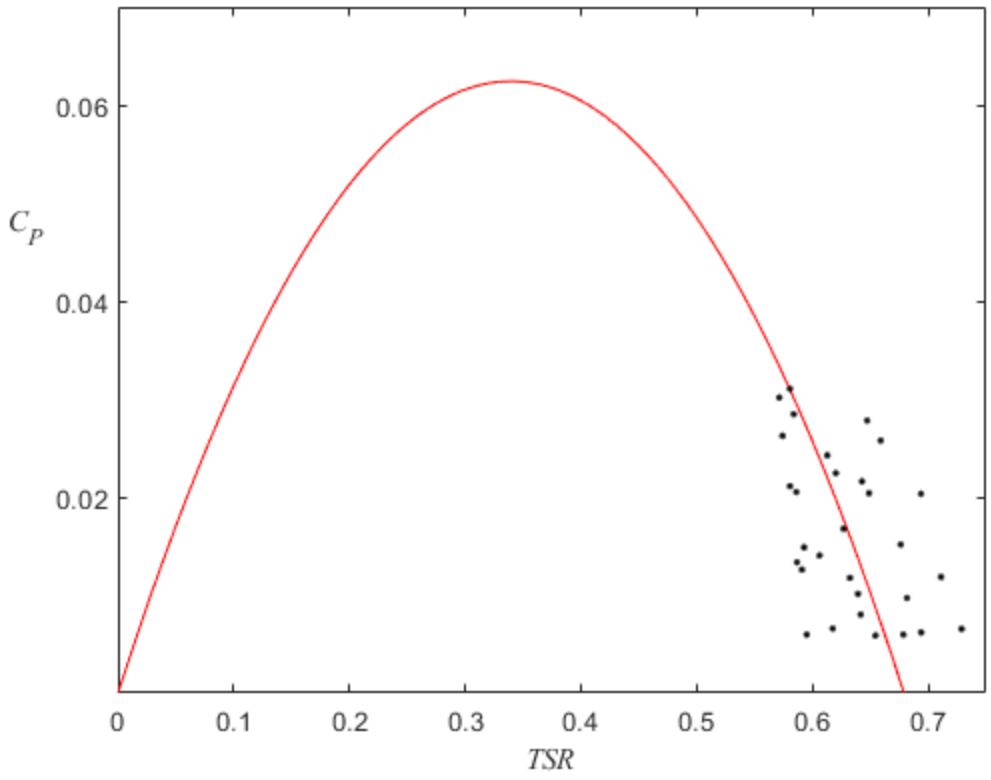

Fig. 4.13 Cp curve extrapolated by data obtained with speed regulation

As the TSR is defined as the ratio between the inflow velocity and the rotational speed at the blade tip, the inflow condition is calculate averaging the velocities just upstream the turbine. This value is much lower than the freestream value due to the flow interaction with obstacles which makes the fluid decelerates. By this consideration, the power coefficient, such as the torque coefficient, can be defined

using the freestream velocity, which is the most common option, or using the real inflow velocity that the turbine feels. In fig.4.13 I adopted the first case because it allows to compare results with other studies. Still, the use of this second coefficient allows to give a real description of the turbine performance. The average velocities used to calculate the TSR are reported in the table below

	CUBE 1			CUBE 2		
	FRONT	CENTRE	BACK	FRONT	CENTRE	BACK
$V_{in}[m/s]$	7.35	7.54	2.35	4.12	5.36	5.24

Table 7 Average velocity upstream the rotor

As the turbine on the centre position on the first cube produce almost the same power of the front one with a lower inflow velocity, it is possible to deduce that the position more efficient is the centre one. As already discussed, this efficiency of the central position is related to the delay in the recirculation bubble formation due to the rotor presence.

For the turbine three different efficiencies can be defined. The first and most common way to define the turbine performance is the ratio between the power extracted and the freestream wind power which is related to the far upstream wind speed (C_P). The second way to define the performance of the turbine has been described in the previous chapter and it relates the power extracted and the power extractable in freestream condition (η_{II}). The last way to define the turbine performance is consider the power extracted respect the wind power incoming in the rotor (η). This last method is quite challenging since the inflow condition is not clearly defined and it is hard to be calculated. Furthermore, it is not clear how a variable velocity profile can affect the turbine performances. One more issue is associated to the acquisition of a 2D flow field while the inflow condition is related to all three spatial coordinates. To simplify the inflow conditions properly it could be considered the flow field in the cross sectional plane, which is perpendicular to the flow direction. Unfortunately, we know just one coordinate of this plane (the vertical direction). Therefore the calculation of the performance with the last way (η) could bring to rough results. Then, it is evaluated the turbine with the C_P value. It has the advantage to be related to the freestream conditions, which are well-known, and it can be compared to the results of other studies.

Despite these considerations about the power coefficient, the tip speed ratio is calculated by using the average of the incoming wind speed just upstream the rotor. This gives a more realistic understanding of how the turbine is working compared to the flow where it is submersed.

As shown in table 7, the upstream average velocity of turbine located in the front or in centre of the upstream cube are comparable, that is the reason why turbine in those positions produces the same power. By this table we can even understand the strong difference of these two places compared to the

back location. In fact, in the back the incoming average wind speed is the 30% of the other upstream cases. As the power is linked to the wind speed raised to the power of three, a so strong deceleration in the inflow condition is reflected in the power measurement.

Looking at the value of the average inflow wind speed for the cases on the second cube, the velocities are quite similar. However, the front case is considerably lower than the others. The velocity averaged upstream the rotor in the central and leeward position are very similar, this is not reflected perfectly in the power measurements where there is a clear distinction between the two cases, as already discussed. This comparison between the wind speed and the power measurements suggests that even if the velocity of the incoming flow is the same for both positions, the one in the back produce more power. Thinking of the considerations made about the PIV images, the turbine located on the central position present more vorticity and higher TKE. These two factors could be the key in the understanding of the gap between the wind speed and the power measurements. The high vorticity and turbulence with the turbine in the centre can cause a lower power available for the extraction with the same incoming wind speed. The more constant and low turbulent flow felt in the back of the cube is more suitable for power extraction.

5 CONCLUSION

The importance to use different methodology to have a complete understanding of the flow field was highlighted in the literature review. The sharing of understanding between real measurements, CFD simulations, wind tunnel tests and meteorological campaign can lead to a fully understand of the flow conditions. Considering an obstacle in the free stream flow, even if the best location could seem to be the nearest to the leading edge in order to avoid the negative influence of the turbulent fluctuations; the location barely inward can lead to good performance as well. The front location is largely affected by a vertical component of the velocity due to the separation of the flow at the cube edge, this could increase the fatigue load on the machine. In contrast, the position in the centre allows to have a negligible effect of the vertical speed. It is still not clear how much power can be extracted from the vertical component of velocity of wind flow by the turbine, this ability is determinant to define the best location. In the case of these experiments, where a Savonius design was adopted, the power produced looks linked only to the streamwise velocity, in fact the velocities values just in front of the rotor reported in table 7 have the same shape in the location positions of the power. This suggests that the produced power is higher where streamwise velocity is higher, without accounting for the wall-normal speed. However, in case of other designs or supported devices, the vertical component can bring to an improvement of the power extraction.

As most of the turbine designs are not suited for turbulent conditions, the worst location is surely on the trailing edge. That location is completely immersed into the separation zone and in a high turbulent condition. The most promising part of the interaction between the wind flow and the obstacles is the overspeed region generated above the separated shear layer. This region is graphically moved up by the presence of the turbine (appendix fig.3-4). However, a higher turbine could be able to reach that zone in order to catch the higher wind energy. This overspeed zone is characterized by an increase in the streamwise velocity of more than 10%, which results in about 60% increase in the power content. As the mean wind speed in urban areas is generally low, this overspeed region can be considered an attractive location for wind energy exploitation.

The ability in the power extraction of the turbine from turbulent conditions is still not fully clear, however if the rotor on the upstream cube is large enough to influence the separated shear layer, it suppresses the Turbulent Kinetic Energy (TKE) generated by the cube (fig.4.4c). On the other hand, the turbine itself generates a wake zone with high TKE, this prevent the use of wind turbines in tandem configuration. In the case of the turbine located on the back position, as it has no influence on the layer that delimitate the recirculation region above the cube, it doesn’t affect the TKE generated by the cube.

Considering instead the turbine location on a bluff body downward of a first obstacle, the turbine location which allows the best power extraction is the farther from the front edge of the body. This consideration is valid for the case of an intra-obstacle spacing of two cube height. Closer or farther cubes distance could lead to different results. In these experiments the fixed distance of 2 cube heigh caused the impinging of the high turbulent zone generated by the upstream obstacle on the leading edge of the second cube. This clearly affect the performances of the turbine on the front location. Even in this aft cube, the turbine on the front deals with a high vertical component of the velocity.

The absence on the second cube of a big recirculation region on the top facade allows to not have any very inefficient location, as for the upstream cube. The performances seem to be affected only by the recirculation generated in the intra-obstacle space and by the wake of the windward cube. Thus, the wake generated by the front cube, where the free stream collides, has a very high influence both on turbine location above itself and on the locations on the downward cube.

This study brings to the conclusion that for a VAWT elevated of $0.1\,H$ from the roof of a building, with a rotor of $0.4\,H$ diameter and $0.3\,H$ height, the best location for the installation is the centre location without knowing the buildings around. This guarantee good power extraction independently by the wind direction and the interference of upstream buildings. If the wind direction is considerably constant, the inner edges of buildings in tandem configuration must be avoided because those locations are near the intra-obstacle horseshoe vortex which decreases the performance. Instead, it is preferable the installation in the outer edges, in this study the front edge of the upstream cube and the trailing edge of the downstream cube. These edges are far from the big turbulence generated in the wake.

It can be stated that to have a fully understanding of the potentiality of a flow field in complex conditions it must be accounted for the influence of the turbine in the flow. On the other hand, to define the most promising location is essential the synergy between a flow field characterization, in this case the PIV measurements, and the direct measurements, in this experiment the rotational speed and the torque.

The improvement of this study can focus on a better characterization of the power curve and the addition of other variable measurements that can help in the understanding of the forces involved, such as axial force, shaft strains, vibrations. These experiments were performed with a 2D PIV, as it can be seen by the images, thus the flow field is defined in a streamwise plane excluding the characterization of the flow in the cross-sectional plane. An improvement in the flow field understanding can be given also with a three-dimensional characterization of the velocity vector map. This can lead to the insight of the transversal vorticities in the high turbulent region. In addition, a three-dimensional characterization of the flow field can help the understanding of the wind turbine installation near the side of the cube.

LIST OF FIGURES

LIST OF TABLES

BIBLIOGRAPHY

[1] J. Kaldellis and D. Zafirakis, “The wind energy (r)evolution: A short review of a long history,” *Renewable Energy,* vol. 36, 2011.

[2] M. Pasqualetti, R. Righter and P. Gipe, “Wind Energy, History of,” *Encyclopedia of Energy,* vol. 6, pp. 419-433, 2004.

[3] IPCC, “Summery for Policymakers in: Global Warming of 1.5°C. An IPCC Special,” 2018.

[4] IRENA, “Global Energy Transformation: A Roadmap to 2050,” 2018.

[5] IEA, “Key World Energy Statistics 2020,” 2020.

[6] GWEC, “Global Wind Report,” 2019.

[7] REN21, “Renewable 2020 Global Status Report,” 2020.

[8] U. Zafar, “Literature review of Wind Turbines,” 2018.

[9] S. Vargas, G. Esteves, P. Maçaira, B. Bastos, F. Oliveira and R. Souza, “Wind power generation: A review and a research agenda,” *Journal of Cleaner Production,* vol. 218, no. 2019.

[10] A. Darwish and R. Al-Dabbagh, “Wind energy state of the art: present and future technology advancements,” *Renewable Energy and Environment Sustainability,* vol. 5, 2020.

[11] H. Díaz, Soares and C. Guedes, “Review of the current status, technology and future trends of offshore wind farms,” *Ocean Engineering,* vol. 209, 2020.

[12] U. Zillmann and P. Betchle, “Emergence and Economic Dimension of Airborne Wind Energy,” Singapore, Springer, 2018, pp. 1-2.

[13] S. Watson, A. Moro, V. Reis, C. Banlotopoulos, S. Barth and G. Bartoli, “Future emerging technologies in the wind power sector_ A European perspective,” *Renewable and Sustainable Energy Reviews,* vol. 113, 2019.

[14] GWEC, “Global Offshore Wind Report,” 2020.

[15] M. Borg, M. Collu and A. Kolios, “Offshore floating vertical axis wind turbines, dynamics modelling state of the art. Part II_ Mooring line and structural dynamics,” *Renewable and Sustainable Energy Reviews,* vol. 39, 2014.

[16] J. I. Marvik, E. V. Øyslebø and M. Korpås, “Electrification of offshore petroleum installations with offshore wind integration,” *Renewable Energy,* vol. 50, 2013.

[17] A. Crivellari and V. Cozzani, “Offshore renewable energy exploitation strategies in remote areas by power-to-gas and power-to-liquid conversion,” *International Journal of Hydrogen Energy,* vol. 45, 2020.

[18] D. Caglayan, D. Ryberg, H. Heinrichs, J. Linßen, D. Stolten and M. Robinius, “The techno-economic potential of offshore wind energy with optimized future turbine designs in Europe,” *Applied Energy,* vol. 255, 2019.

[19] T. Stathopoulos, H. Alrawashdeh, A. Al-Quraan, B. Blocken, A. Dilimulati, M. Paraschivoiu and P. Pilay, “Urban wind energy: Some views on potential and challenges,” *Journal of Wind Engineering & Industrial Aerodynamics,* vol. 179, 2018.

[20] D. Micallef and G. Van Bussel, “A Review of Urban Wind Energy Research: Aerodynamics and Other Challenges,” *Energies,* vol. 11, 2018.

[21] T. Ishugah, Y. Li, R. Wang and J. Kiplagat, “Advances in wind energy resource exploitation in urban environment_ A review,” *Renewable and Sustainable Energy Reviews,* vol. 37, 2014.

[22] A. Arnfield, “Two decades of urban climate research: A review of turbulence, exchanges of energy and water, and the urban heat island,” *International Journal of climatology,* vol. 23, 2003.

[23] L. Wang, D. Li, Z. Gao, T. Sun, X. Guo and E. Bou-Zeid, “Turbulent Transport of Momentum and Scalars Above an Urban Canopy,” *Boundary-layer meteorology,* 2014.

[24] M. Piringer, C. Grimmond, S. Joffre, P. Mestayer, D. Middleton, M. Rotach, A. Baklanov, K. De Ridder, J. ferreira, E. Guilloteau, A. Karppinen, A. Martilli, V. Masson and M. Tombrou, “investigating the surface energy balance in urban areas - recent advances and future trends,” *Water, Air & Soil Pollution,* 2002.

[25] L. Ledo, P. Kosasih and P. Cooper, “Roof mounting site analysis for micro-wind turbines,” *Renewable Energy,* vol. 36, 2011.

[26] Wind Energy Engineering, A Handboook for Onshore and Offshore Wind Turbines, 2017.

[27] J. Kesby, D. Bradney and P. Clausen, "Determining Diffuser Augmented Wind Turbine performance using a combined CFD/BEM method," *Journal of Physics: Conference Series,* vol. 753, 2016.

[28] A. KC, J. Whale and T. Urmee, "Urban wind conditions and small wind turbines in the built environment: A review," *Renewable Energy,* vol. 131, pp. 268-283, 2019.

[29] NREL, "Deployment of wind turbines in the built environment: risks, lessons and recommended practices," 2016.

[30] F. Emejeamara, A. Tomlin and J. Millward-Hopkins, "Urban wind: Characterisation of useful gust and energy capture," *Renewable Energy,* vol. 81, pp. 162-172, 2015.

[31] G. Scelba and A. Consoli, "Gust tracking capability of small direct-drive Wind Turbines," in *2010 IEEE International Conference on Sustainable Energy Technologies (ICSET),* 2010.

[32] L. Lu and K. Ip, "Investigation on the feasibility and enhancement methods of wind power utilization in high-rise buildings of Hong Kong," *Renewable and Sustainable Energy Reviews,* vol. 13, 2009.

[33] F. Toja-Silva, A. Colmenar-Santos and M. Castro-Gil, "Urban wind energy exploitation systems_ Behaviour under multidirectional flow conditions—Opportunities and challenges," *Renewable and Sustainable Energy Reviews,* vol. 24, 2013.

[34] F. Balduzzi, Bianchini, A., Carnevale, E. Antonio, F., Lorenzo and S. Magnani, "Feasibility analysis of a Darrieus vertical-axis wind turbine installation in the rooftop of a building," *Applied Energy,* vol. 97, pp. 921-929, 2012.

[35] A. Al-Quraan, T. Stathopoulos and P. Pillay, "Comparison of wind tunnel and on site measurements for urban wind energy estimation of potential yield," *Journal of Wind Engineering and Industrial Aerodynamics,* vol. 158, 2016.

[36] J. Kaimal, "Turbulence spectra, length scales and structure paramters in the stable surface layer," *Boundary-Layer Meteorology,* vol. 4, pp. 289-309, 1973.

[37] S. Mertens, "The energy yield of roof mounted wind turbines," *Wind Engineering,* vol. 27, 2003.

[38] S. Allen, G. Hammond and M. McManus, “Prospects for and barriers to domestic micro-generation: A United Kingdom perspective,” *Applied Energy,* vol. 85, pp. 528-544, 2008.

[39] S. Mertens and G. Van Bussel, “Small wind turbines for the built environment,” *EACWE4,* 2005.

[40] T. Mucke, D. Kleinhans and J. Peinke, “Atmospheric turbulence and its influence on the alternating loads on wind turbines,” *Wind Energy,* vol. 14, pp. 301-316, 2011.

[41] A. Tabrizi, J. Whale, T. Lyons and T. Urmee, “Extent to which international wind turbine design standard, IEC61400-2 is valid for a rooftop wind installation,” *Journal of Wind Engineering and Industrial Aerodynamics,* vol. 139, pp. 50-61, 2015.

[42] S. Evans, A. KC, D. Bradney, T. Urmee, J. Whale and P. Clausen, “The suitability of the IEC 61400-2 wind model for small wind turbines operating in the built environment,” *Renew. Energy Environ. Sustain,* vol. 2, 2017.

[43] T. Sharpe and G. Proven, “Crossflex: Concept and early development of a true building integrated wind turbine,” *Energy & Buildings,* vol. 42, pp. 2365-2375, 2010.

[44] W. Chong, A. Fazlizan, S. Poh, K. Pan and H. Ping, “Early development of an innovative building integrated wind, solar and rain water harvester for urban high rise application,” *Energy & Buildings,* vol. 47, pp. 201-207, 2011.

[45] W. Chong, A. Fazlizan, S. Poh, K. Pan, W. Hew and F. Hsiao, “The design, simulation and testing of an urban vertical axis wind turbine with the omni-direction-guide-vane,” *Applied Energy,* vol. 112, pp. 601-609, 2013.

[46] F. Ardente, M. Beccali, M. Cellura and M. Mistretta, “Energy and environmental benefits in public buildings as a result of retrofit actions,” *Renewable and Sustainable Energy Reviews,* vol. 15, pp. 460-470, 2011.

[47] T. Bannon, “FAR Part 139 Certificated Airports Shifting Towards Environmentally-Friendly Practices,” *Research Papers,* vol. 194, 2012.

[48] F. Wang, L. Bai, J. Fletcher, J. Whiteford and D. Cullen, “The methodology for aerodynamic study on a small domestic wind turbine with scoop,” *Journal of Wind Engineering and Industrial Aerodynamics,* vol. 96, pp. 1-24, 2008.

[49] S. Zanforlin and S. Letizia, “Improving the Performance of Wind Turbines in Urban Environment by Integrating the Action of a Diffuser with the Aerodynamics of the Rooftops,” *Energy Procedia,* vol. 82, pp. 778-781, 2015.

[50] K. Pope, V. Rodrigues, R. Doyle, A. Tsopelas, R. Gravelsins, G. Naterer and E. Tsang, “Effects of stator vanes on power coefficients of a zephyr vertical axis wind turbine,” *Renewable Energy,* vol. 35, pp. 1043-1051, 2010.

[51] W. Chong, K. Pan, S. Poh, A. Fazlizan, C. Oon, A. Badarudin and N. Nik-Ghazali, “Performance investigation of a power augmented vertical axis wind turbine for urban high-rise application,” *Renewable Energy,* vol. 51, 2013.

[52] C. Stork, C. Butterfield, W. Holley, P. Madsne and P. Jensen, “Wind conditions for wind turbine design proposals for revision of the IEC 1400-1 standard,” *Journal of Wind Engineering and Industrial Aerodynamics,* Vols. 74-76, pp. 443-454, 1998.

[53] S. Mertens, “Wind energy in urban areas: concentrator effect for wind turbines close to buildings,” *Refocus,* vol. 3, 2012.

[54] L. Battisti, E. Benini, A. Brighenti, S. Dell’Anna and M. Castelli, “Small wind turbine effectiveness in the urban environment,” *Renewable Energy,* vol. 129, 2018.

[55] A. Cismilianu, A. Boros, I. Oncescu and F. Frunzulica, “New urban vertical axis wind turbine design,” *INCAS bulletin,* vol. 7, pp. 66-76, 2015.

[56] R. Coleman, A. Fringold and C. Stempin, “Evaluation of the induced-velocity field of an idealized helicopter rotor,” 1945.

[57] C. Ferreira, G. Van Bussel and G. Van Kuik, “Wind tunnel hotwire measurements, flow visualization and thrust measurement of a VAWT in skew,” *Journal of Solar Energy Engineering,* vol. 128, pp. 487-497, 2006.

[58] N. Troldborg, M. Gaunaa and R. Mikkelsen, “Actuator Disc Simulations of Influence of Wind Shear and Ground Proximity on Power Production of Wind Turbines,” 2010.

[59] D. Micallef, T. Sant and C. Ferreira, “The influence of a cubic building on a roof mounted wind turbine,” *Journal of Physics: Conference Series,* vol. 753, 2016.

[60] P. Ebert and D. Wood, “Observation of the starting behaviour of a small horizontal axis wind turbine,” *Renewable Energy,* vol. 12, pp. 245-257, 1997.

[61] M. Grauthoff, “Utilization of Wind Energy in Urban Areas - Chance or Utopian Dream?,” *Energy and Buildings,* vol. 16, pp. 517-523, 1991.

[62] M. Ragheb, *Wid turbines in the urban environment,* 2014.

[63] M. Ahmadi-Baloutaki, R. Carriveau and D. Ting, “Performance of a vertical axis wind turbine in grid generated turbulence,” *Sustainable Energy technologies and Assessments,* 2015.

[64] F. Mouzakis, E. Morfiadakis and P. Dellaportas, “Fatigue loading paramter identification of a wind turbine operating in complex terrain,” *Journal of Wind Engineering,* vol. 82, 1999.

[65] A. Carb Molina, G. Bartoli and T. De Troyer, “Generation of Uniform Turbulence Profiles in the Wind Tunnel for Urban VAWT Testing,” Green Energy and technology, 2018, pp. 27-43.

[66] B. Kirke and L. Lazauskas, “Limitations of fixed pitch Darrieus hydrokinetic turbines and the challenge of variable pitch,” *Renewable Energy,* vol. 36, 2011.

[67] M. Kamoji, S. Kedare and S. Prabhu, “Performance tests on helical Savonius rotors,” *Renewable Energy,* vol. 34, 2009.

[68] M. D'Ambrosio and M. Medaglia, “Vertical Axis Wind Turbines: History, Technology and Applications,” 2010.

[69] A. Buchner, J. Soria, D. Honnery and A. Smits, “Dynamic stall in vertical exis wind turbines: Scaling and Topological considerations,” *Journal of Fluid Mechanics,* vol. 814, 2018.

[70] P. Deglaire, S. Engblom, O. Ågren and H. Bernhoff, “Analytical solutions for a single blade in vertical axis turbine motion in two-dimensions,” *European Journal of Mechanics B/Fluids,* vol. 28, 2009.

[71] A. Sunyoto, F. Wenehenubun and H. Sutanto, “the effect of Number of Blades on the Performance of H_Darrieus type Wind Turbine,” in *2013 international Conference on QiR,* YogYakarta, 2013, pp. 192-196.

[72] A. Naseem, E. Uddin, Z. Ali, J. Aslam, S. Shah, M. Sajid, A. Zaidi, A. Javed and M. Younis, “Effect of vortices on power output of vertical axis wind turbine (VAWT),” *Sustainable Energy Technologies and Assessments,* vol. 37, 2020.

[73] U. Saha, S. Thotla and D. Maity, “Optimum design configuration of Savonius rotor through wind tunnel experiments,” *Journal of Wind Engineering and Industrial Aerodynamics,* vol. 96, 2008.

[74] V. D’Alessandro, S. Montelpare, R. Ricci and A. Secchiaroli, “Unsteady Aerodynamics of a Savonius wind rotor: a new computational approach for the simulation of energy performance,” *Energy,* vol. 35, 2010.

[75] M. Mohamed, G. Janiga, E. Pap and D. Thévenin, “Optimization of Savonius turbines using an obstacle shielding the returning blade,” *Renewable Energy,* vol. 35, 2010.

[76] S. Eriksson, H. Bernhoff and M. Leijon, “Evaluation of different turbine concepts for wind power,” *Renewable and Sustainable Energy Reviews,* vol. 12, 2008.

[77] D. Greenblatt, M. Schulman and A. Ben-Harav, “Vertical axis wind turbine performance enhancement using plasma actuators,” *Renewable Energy,* vol. 37, 2012.

[78] H. Riegler, “HAWT versus VAWT,” *Refocus,* vol. 4, pp. 44-46, 2003.

[79] M. Khan, P. Sooraj, A. Sharma and A. Agrawal, “Flow around a cube for Reynolds numbers between 500 and 55,000,” *Experimental Thermal and Fluid Science,* vol. 93, 2018.

[80] I. Castro and A. Robins, “The flow around a surface-mounted cube in uniform and turbulent streams,” *Journal of Fluid Mechanics,* vol. 79, 1977.

[81] C. Baker, “The trubulent Horseshoe Vortex,” *Journal of Wind Engineering and Industrial Aerodynamics,* vol. 6, 1980.

[82] R. Martinuzzi and B. Havel, “Turbulent flow around two obstacles interfering surface-mounted cubic obstacles in tandem arrangement,” *ASME,* vol. 122, 2000.

[83] R. Hearst, G. Guillaume and G. Bharatham, “Effect of turbulence on the wake of a wall-mounted cube,” *Journal of Fluid Mechanics,* vol. 804, 2016.

[84] R. Martinuzzi and B. Havel, “Vortex shedding from two surface-mounted cubes in tandem,” *International Journal of Heat and Fluid Flow,* vol. 25, pp. 364-372, 2004.

[85] M. Bastankhah and F. Porté-Agel, “A New Miniature Wind Turbine for Wind Tunnel Experiments. Part I: Design and Performance,” *Frede Blaabjerg,* vol. 10, 2017.

[86] J. Kumbernuss, J. Chen, H. Yang and L. Lu, “Investigation into the relationship of the overlap ratio and shift angle of double stage three bladed vertical axis wind turbine (VAWT),” *Journal of Wind Engineering and Industrial Aerodynamics,* Vols. 107-108, 2012.

[87] R. Ricci, S. Montelpare, A. Secchiaroli and V. D'Alessandro, “Flow field assessment in a vertical axis wind turbine,” in *WIT Transactions of Engineering Sciences,* 2010.

[88] I. van der Hoven, “Power spectrum of horizontal wind speed in the frequency range from 0.0007 to 900 cycles per hour,” *Journal of Meteorology,* vol. 14, pp. 160-164, 1956.

[89] E. Aguilar, I. Auer, M. Brunet, T. Peterson and J. Wieringa, “Guidance on Metadata and Homogenization,” 2003.

[90] A. Bernardino, A. Pelliccioli, P. Monti, G. Leuzzi and F. Sammartino, “Performances of parametric laws for computing the wind speed profile in the urban bounadry layer. Comparison to two-dimensional building water channel experiment,” in *18th International Conference on Harmonisation within Atmospheric Dispersion Modelling for Regulatory Purposes,* 2017.

[91] C. Metral, G. Falquet and K. Karatzas, “Ontologies for the integration of Air Quality Models and 3D City Models,” *Computing Research Repository (CoRR),* 2012.

[92] K. Oyundolgor, Z. Gunjee, B. Sosorbaram and N. Chiba, “Wind field synthesis for animating volume,” *International Journal of Virtual Reality,* vol. 10, 2011.